

**Displacement measurements on suspended mirrors
for off-resonant thermal noise detection**

Dipl.-Phys. Volker Leonhardt

2003

**Displacement measurements on suspended mirrors
for off-resonant thermal noise detection**

Vom Fachbereich Physik
der Universität Hannover
zur Erlangung des Grades

Doktor der Naturwissenschaften
– **Dr. rer. nat.** –

genehmigte Dissertation von

Dipl.-Phys. Volker Leonhardt

geboren am 14. Februar 1974 in Hannover

2003

Referent: Prof. K. Danzmann
Korreferent: Prof. M. Kock
Tag der Promotion: 9. Februar 2004
Druckdatum: 12. Februar 2004

Zusammenfassung

Das thermische Rauschen setzt eine Empfindlichkeitsgrenze für gegenwärtige und zukünftige Gravitationswellendetektoren. Es ist von großem Interesse Experimente aufzubauen, welche die einzelnen Formen des thermischen Rauschens messen können. Dadurch sollen die existierenden Modelle verifiziert und die Limitierungen durch das thermische Rauschen verringert werden. Viele Gruppen auf der Welt tragen zur Zeit zu diesem Zweig der Forschung bei.

Manche Formen des thermischen Rauschens führen zu einer Bewegung der Oberfläche der in Gravitationswellendetektoren verwendeten Spiegel, andere resultieren in einer Pendelbewegung der Spiegel. Für diese thermische Pendelbewegung sagen verschiedene Modelle bei Frequenzen außerhalb der Pendelresonanz abweichende Verläufe vorher. Um diese Modelle zu überprüfen ist es nötig, das thermische Rauschen außerhalb der Pendelresonanzfrequenz zu messen. Speziell für zukünftige Gravitationswellendetektoren, wo höhere Empfindlichkeiten bei niedrigeren Frequenzen angestrebt werden, sind diese Messungen von großem Interesse, denn die thermische Pendelbewegung dominiert die anderen Formen des thermischen Rauschens bei kleinen Frequenzen.

Diese Arbeit beschreibt den Aufbau eines Experiments, um das thermische Rauschen der Pendelbewegung außerhalb der Resonanzfrequenz direkt zu messen. Dazu wurde ein Aufbau aus zwei unabhängig voneinander aufgehängten Spiegeln verwendet. Diese Spiegel bilden einen Fabry-Perot Resonator dessen differenzielle Spiegelbewegung interferometrisch ausgelesen wird. Hierbei wird das Feedbacksignal einer Pound-Drever-Hall Regelung detektiert, welche die Resonatorlänge auf die Frequenz eines eingestrahnten Lasers stabilisiert. Lange Messzeiten und stabile Messbedingungen werden durch ein automatisches Alignmentssystem garantiert, welches den Laserstrahl mit der Resonatormode in vier Freiheitsgraden überlappt. Um die Empfindlichkeit zu verbessern, wird die Laserfrequenz mit einer weiteren Regelung auf einen Referenzresonator stabilisiert.

Ein Haupthindernis beim Erreichen des thermischen Rauschens ist die seismische Bewegung des Bodens. Um die Spiegel davon zu isolieren, wurde eine mehrstufige Aufhängung entworfen. Zur Stabilisierung der unabhängig voneinander aufgehängten Spiegel auf die Laserfrequenz ist es notwendig, die Resonanzfrequenzen der einzelnen Freiheitsgrade aktiv durch verschiedene Regelkreise zu dämpfen. Eine Simulation für die Pendelbewegungen in allen Freiheitsgraden wurden entwickelt und die Aufhängung wurde mit Hilfe der Simulation weiter verbessert. Zur Isolation der Spiegel von Einflüssen durch die umgebende Luft befindet sich das gesamte seismische Isolationssystem in einem Vakuumtank. Andere Störeinflüsse der Umgebung, sowie die Rauscheigenschaften des Lasers und der verwendeten Elektronik wurden untersucht und verringert, um eine hohe Empfindlichkeit zu erreichen.

Stichworte: Gravitationswellendetektion, Thermisches Rauschen, Seismische Isolation

Summary

For current and future gravitational wave detectors, thermal noise will set a limit to the achievable sensitivity. It is therefore of great interest to build experiments that can measure the different forms of thermal noise, in order to verify the existing models and to find ways to lower the sensitivity limits set by these noises. Several groups around the world are currently contributing to this important field of research.

Some forms of thermal noise lead to a motion of only the surface of the mirrors that are used in gravitational wave detectors, other noises excite the pendulum mode of the mirror suspension. For this pendulum thermal noise, different models predict a different noise slope at frequencies far from the pendulum resonance. To make a conclusive distinction between these models, it is necessary to build an experiment that is able to measure the off-resonant noise floor of the thermal pendulum motion of a suspended mirror. Especially in future detectors where higher sensitivities at lower frequencies are targeted, this research could be of great interest, because the thermal noise of the pendulum dominates the different forms of internal thermal noise at low frequencies.

This work describes an effort to build an experiment to directly measure the off-resonant thermal noise of a pendulum mirror. For this purpose a set-up of two independently suspended mirrors was chosen. These mirrors form a Fabry-Perot resonator. The differential movement of the two mirrors is detected interferometrically by monitoring the feedback signal of a Pound-Drever-Hall stabilization of the resonator length to the laser frequency. Long locking times and stable measurement conditions are ensured by an automatic alignment system that overlaps the laser beam with the mode of the optical resonator in four degrees of freedom. In order to increase the sensitivity of the experiment, the laser frequency is stabilized to a reference resonator by an additional control system.

A major obstacle in reaching the thermal noise level is the seismic motion of the ground. A multiple stage suspension system was designed to isolate the mirrors from this seismic motion. In order to lock the independently suspended mirrors to the laser frequency, the pendulum movement at the resonance frequencies of the different degrees of freedom is actively damped by several feedback loops. The influence of all degrees of freedom of the pendulum motion was simulated and the seismic isolation system was improved according to the simulation. The whole seismic isolation system is located inside a vacuum tank to isolate the suspended mirrors from air fluctuations. Several other noise sources that are related to the laser, the environment and the electronic have also been investigated and reduced to reach a high sensitivity.

Keywords: Gravitational wave detection, thermal noise, seismic isolation

Contents

Zusammenfassung	i
Summary	iii
Contents	v
1. Gravitational wave detection	1
1.1. Introduction	1
1.2. Gravitational wave research	2
1.3. The GEO 600 gravitational wave detector	3
2. Thermal noise	7
2.1. Introduction	7
2.2. Velocity damping	7
2.3. Brownian noise	9
2.3.1. The loss function of a pendulum	11
2.4. The violin modes	13
2.5. Linear and nonlinear thermoelastic noise	15
2.6. Thermal noise of the mirror	16
2.6.1. Coating noise	17
2.6.2. Thermorefractive noise	17
2.6.3. Photothermal noise	18
2.6.4. Additional noise in real suspensions	18
2.6.5. Prediction of the thermal noise	18
2.7. Previous measurements of the loss function	19

3. Optical set-up	23
3.1. Introduction	23
3.2. The Pound-Drever-Hall frequency stabilization	24
3.3. Detecting mirror movement	29
3.3.1. The longitudinal feedback loop	29
3.3.2. Actuators for the longitudinal lock	33
3.3.3. Calibration of the detected signals	37
3.4. The laser system	39
3.4.1. The frequency stabilization	40
3.5. The automatic alignment system	44
3.5.1. Misaligned optical beams	45
3.5.2. Detection of misalignment	47
3.5.3. Actuators for the alignment	51
3.5.4. Performance of the system	54
4. The seismic isolation	57
4.1. Introduction	57
4.2. Seismic noise	58
4.3. The basic idea of seismic isolation	59
4.3.1. Coupling of the different degrees of freedom into longitudinal	61
4.4. Building blocks of the seismic isolation system	64
4.4.1. The pendulum chain	67
4.5. Damping of the pendulum resonances	72
4.5.1. Prealignment of the interferometer	74
5. Sensitivity of the experiment	77
5.1. Introduction	77
5.2. Frequency noise	78
5.3. Intensity noise	81
5.4. Additional noise sources	86
5.4.1. Residual gas	86
5.4.2. Electronic noise	87
5.5. Seismic noise	89
Conclusion	99

A. Material parameters	101
B. The linear spectral density	103
Bibliography	105
Acknowledgements	111
Curriculum vitae	113
Publications	115

List of figures

1.1. Optical layout of GEO 600	4
1.2. Sensitivity of GEO 600	5
2.1. Structural and viscous damping	10
2.2. Violin modes of a pendulum	13
2.3. Thermal noise prediction	19
2.4. Internal thermal noise	20
3.1. Optical set-up of the experiment	23
3.2. Electromagnetic fields in an optical resonator	24
3.3. Amplitude and phase of light reflected from a resonator	25
3.4. Measured Pound-Drever-Hall signal	28
3.5. Generalized feedback loop	30
3.6. Controller transfer function	32
3.7. Transfer function for the notch filters	34
3.8. Suppression of noise at the error point	35
3.9. Actuators for longitudinal feedback	36
3.10. Frequency disturbance at the feedback point	38
3.11. Schematic view of the laser interior	39
3.12. Geometry of the laser crystal	39
3.13. Frequency stabilization scheme	41
3.14. Actuators for changing the laser frequency	43
3.15. Frequency noise of the laser	44

3.16. Misalignment of optical beams	45
3.17. Guoy phase of a propagating beam	49
3.18. Frequency response of the quadrant diode	50
3.19. Measurement of galvanometer scanner resonance frequencies	51
3.20. Transfer function of a controller for the automatic alignment	52
3.21. Set-up for the automatic alignment system	53
3.22. Performance of the alignment channels	54
4.1. Schematic view of the seismic isolation system	57
4.2. Seismic motion	59
4.3. Idealised pendulum	60
4.4. Pendulum transfer functions	62
4.5. Degrees of freedom for a Pendulum	63
4.6. Stack with active isolation	65
4.7. Transfer function of the active seismic isolation	66
4.8. The first two pendulum stages	67
4.9. Frame structure	68
4.10. The two pendulum mirrors	69
4.11. The complete pendulum chain inside the tank	71
4.12. Shadow sensor	72
4.13. Transfer function of the damping control electronic	73
4.14. Coil positions	74
4.15. Damping of the pendulum movement	75
5.1. Sensitivity with suspended and unsuspended frame	78
5.2. Frequency noise of the unstabilized laser	79
5.3. Coherence between acoustic noise and the feedback signal	80
5.4. Frequency noise of the stabilized laser	81
5.5. Shot noise and radiation pressure noise	84
5.6. Noise contributions from amplitude fluctuations	85

5.7. Stabilization to high order modes	87
5.8. Residual gas noise	88
5.9. Noise at the feedback point and at the error point	89
5.10. Sensitivity improvement with higher reflectivities	90
5.11. Coherence between seismic motion and the spectrum	91
5.12. Sensitivity of a fixed cavity	93
5.13. Simulation of the seismic	94
5.14. Improvement from increased moment of inertia	95
5.15. Pendulum stages with high moment of inertia	96
5.16. Sensitivity with big arms	97
5.17. Improvement from active isolation	98

List of figures

Chapter 1

Gravitational wave detection

1.1. Introduction

For a long time all of our knowledge about the universe beyond the boundaries of the solar system was derived from the detection of some high energy particles and from the observations of the electromagnetic spectrum. Telescopes have been build on earth and in space to probe all interesting frequency regions of the electromagnetic spectrum and to observe a wide variety of astronomical phenomena. However, the emitted light often originates in the outer regions of these phenomena and provides only limited information of the inner dynamics of many high energy cosmic events. In addition, many interesting objects like black holes and dark matter do not emit any light at all. The detection of gravitational waves that are emitted by accelerated massive objects is complementary to the electromagnetic observations and would provide us interesting new insights in the dynamics of these objects.

Gravitational waves were first predicted by Albert Einstein, but for a long time it seemed unlikely that they would ever be detected. Although these waves that travel with the speed of light carry a lot of energy, their interaction with the rest of the universe is usually too weak to cause any observable effects. Most likely no man-made gravitational wave will ever be strong enough to cause a signal in a gravitational wave detector. Only waves that are produced when huge masses are strongly accelerated in cosmic events are strong enough to be detected. Because of their weak interaction with the rest of the universe, the emitted gravitational waves reach earth almost undisturbed. Here they cause a length l perpendicular to their direction of propagation to be expanded by a small fraction Δl , while a length perpendicular to this is contracted by the same fraction. After half a wavelength, the other directions are expanded and contracted.

Different groups around the world are trying to measure this effect with Michelson interferometers. These are especially sensitive to differential length changes of the interferometer arms:

- TAMA [65] in Japan with an interferometer arm length of 300 m. This detector is in operation for some time now and a next generation detector is already planned.
- The two LIGO detectors [63] in the USA with an arm length of 4 km each and an additional 2 km detector. Operations have just begun and the next generation is also already in development.

-The VIRGO detector [71] in Italy with 3 km arm length. Commissioning of the detector is well under way and operation will start soon.

-The GEO 600 detector [76] in Germany with an arm length of 600 m. This detector and the problems of interferometric gravitational wave detection are explained in more detail in section 1.3.

The numerous detectors are needed to gain confidence in a possible detection by coincidence measurements. Only simultaneous detection can distinguish conclusively between a gravitational wave signal and other noises. All detectors reach a high sensitivity in the range from above 50 Hz up into the low kHz frequencies and thermal noise is one of the major noise sources at these frequencies. A lot of effort is invested to improve these detectors, but the field of gravitational wave research is much broader than this and includes also other detection schemes.

1.2. Gravitational wave research

The ground-based Michelson detectors are not the first gravitational wave detectors. The oldest detection scheme is that of a bar detector, pioneered by Joe Weber. These detectors consist of a massive metal bar that is suspended to seismically isolate it from the environment. A gravitational wave excites the internal resonance frequency of this bar and the vibrations can be detected by the excitation of a resonant system attached to the bar detector. These bar detectors are sensitive only in a narrow region around their resonance frequencies. These are usually located at ~ 1 kHz. This is in contrast to the broader sensitivity of the Michelson interferometers. A whole network of bar detectors has formed around the world [56] to be able to perform coincidence measurements, and additional bar detectors with broader sensitivities are already under construction. The sources that emit gravitational waves of detectable strength in the Hz and kHz region are merging black holes, black hole - neutron star mergers, neutron star - neutron star mergers, spinning neutron stars with surface deformations and supernova explosions. An additional interesting source is the gravitational wave background radiation from the big bang. It forms a noise floor at all frequencies of the gravitational wave spectrum. The current detectors are starting to set upper limits for all these sources, but a detection has not yet been achieved.

The spectrum of gravitational waves, similar to the electromagnetic spectrum, stretches over many decades of frequencies and ground-based detectors are only able to probe the highest of these frequencies. Every binary star system emits gravitational waves at two times its orbital frequency, but these frequencies are far below the detection band of ground-based gravitational wave detectors. The astronomers Russel Hulse and Joseph Taylor were awarded the Nobel price for discovering and observing the first binary pulsar system [36]. It is called PSR 1913+16 and emits gravitational waves at 7.17×10^{-5} Hz. For this system an energy loss that results in a slow increase of the orbiting frequency of the binary system was detected and the measurements are fully consistent with the predicted energy loss by the emission of gravitational waves [66].

Besides binary neutron stars, also binary black holes and even binary white dwarfs are sources of detectable gravitational waves in the mHz region and below. Other sources at these frequencies are the background radiation, the mergers of supermassive black holes that can be found in the center of every galaxy and also the merger of a black hole, a neutron star or a white dwarf with such

a supermassive black hole. Upper limits for these sources are currently being set by the CASSINI mission on its way to Saturn. A Doppler tracking system is used to measure disturbances in the relative velocity between the earth and the spacecraft that might be caused by gravitational waves [67].

A much more sensitive instrument in this frequency region will be the LISA space mission [18]. It consists of three separate spacecrafts that form three Michelson interferometers. In contrast to ground-based detectors where the vacuum system sets a limit to the achievable arm length, the LISA spacecrafts will be separated by 5×10^6 km. Another advantage of this mission is the absence of seismic noise that makes low frequency measurements on earth impossible. Follow on missions to LISA are already under review.

At even lower frequencies (10^{-7} to 10^{-9} Hz) the observation of fluctuations in the time of arrival of the signals coming from pulsars, believed to be extremely stable natural clocks, has set an upper limit to gravitational waves [39]. The only known source in this frequency region is the background radiation, but still unknown phenomena might produce additional signals.

Also the frequency region from 10^{-15} to 10^{-18} Hz is of interest for gravitational wave research. The PLANCK mission that will study the anisotropies in the cosmic microwave background will also search for polarization patterns that were imprinted in the microwave background by gravitational waves in the early universe [14].

1.3. The GEO 600 gravitational wave detector

The GEO 600 detector has started taking data in the search for gravitational waves, and first upper limits have been set in a coincidence run with the LIGO detectors. The detector was build by a German-British collaboration in Ruthe near Hannover. The most sensitive choice for the arm length of an interferometer would be one quarter of the wavelength of the gravitational wave, because then the light travelling back and forth in one arm is subject to the maximum phase shift possible. The problem with this is that for frequencies close to 1 kHz where detectable gravitational waves are predicted, the vacuum systems housing these interferometer arms of optimum length would get too long and by this too expensive. The GEO 600 vacuum systems consists of two arms with a length of 600 m, short of the 75 km that would be the optimum choice for detecting a gravitational wave at 1 kHz. However, very sensitive measurements are still possible if optical techniques are included in the detector design to increase the effect of the gravitational wave on the output signal.

The optical set-up of the GEO 600 detector (see figure 1.1) starts with a master laser that is similar to the laser used in our experiment (see section 3.4). It has an output power of 0.8 W at a wavelength of 1064 nm. To reduce the limit set by the shot noise of the laser light, the laser power is increased up to 14.4 W after leaving the optical resonator of a slave laser. Master laser and slave laser are located on an optical table. The amplitude and frequency noise of this laser system is reduced by feedback loops. After entering the vacuum system, the laser beam is transmitted through two triangular resonators that consist of independently suspended mirrors. The purpose

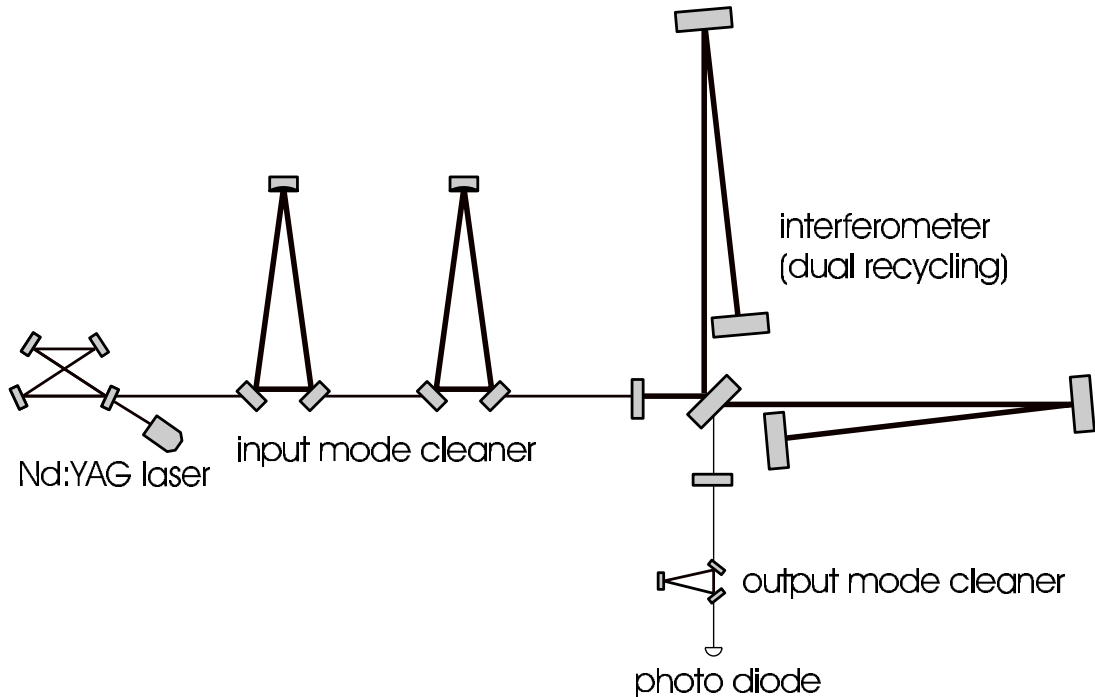


Figure 1.1.: *Optical layout of GEO 600, consisting of a master-slave laser system, two mode cleaner ring cavities, a dual recycled Michelson interferometer with folded arms and an output mode cleaner.*

of these mode cleaner cavities is a filtering of the transverse fluctuations of the laser beam. These fluctuations can be expressed by higher order modes (see section 3.5.1) that are reflected by these resonators. The optical round-trip length of each of the mode cleaners is 8 m. The mirrors are suspended as two stage pendulums for seismic isolation.

To increase the travel time of the light in the two arms of the Michelson interferometer, these arms are folded back onto two additional mirrors near the beam splitter. This doubles the effective arm length, but it also adds an additional mirror to each arm, which is subject to position fluctuations. The detection sensitivity of GEO 600 is limited by shot noise at high frequencies. The sensitivity can be improved by increasing the light power inside the resonator, but a laser that is orders of magnitude more powerful is not available for this purpose. A technique that is called power recycling is used instead. The Michelson interferometer is operated at the dark fringe, meaning that the arm length difference is such, that the output remains dark and all of the light is reflected back to the input. A power recycling mirror is placed at the input and reflects the light back into the Michelson interferometer. The designed power enhancement by this technique is a factor of 2000 for GEO 600.

Another technique to increase the sensitivity that is used exclusively in the GEO 600 detector is signal recycling. If a gravitational wave passes the detector, it produces signal sidebands to the light inside the interferometer arms. These sidebands leave the interferometer at the dark output

and can be detected there. It is also possible to reflect these sidebands back into the detector where they are further enhanced by the gravitational wave. This is done by an additional signal recycling mirror at the output. This technique can be optimised only in a narrow range and decreases the sensitivity at other frequencies. The value of the optimum frequency can be changed by moving the position of the signal recycling mirror, and the strength of the signal recycling changes with the mirror reflectivity. Behind the signal recycling mirror the light passes an additional output mode cleaner before it is detected by a photo diode. This mode cleaner filters out scattered light and higher order modes.

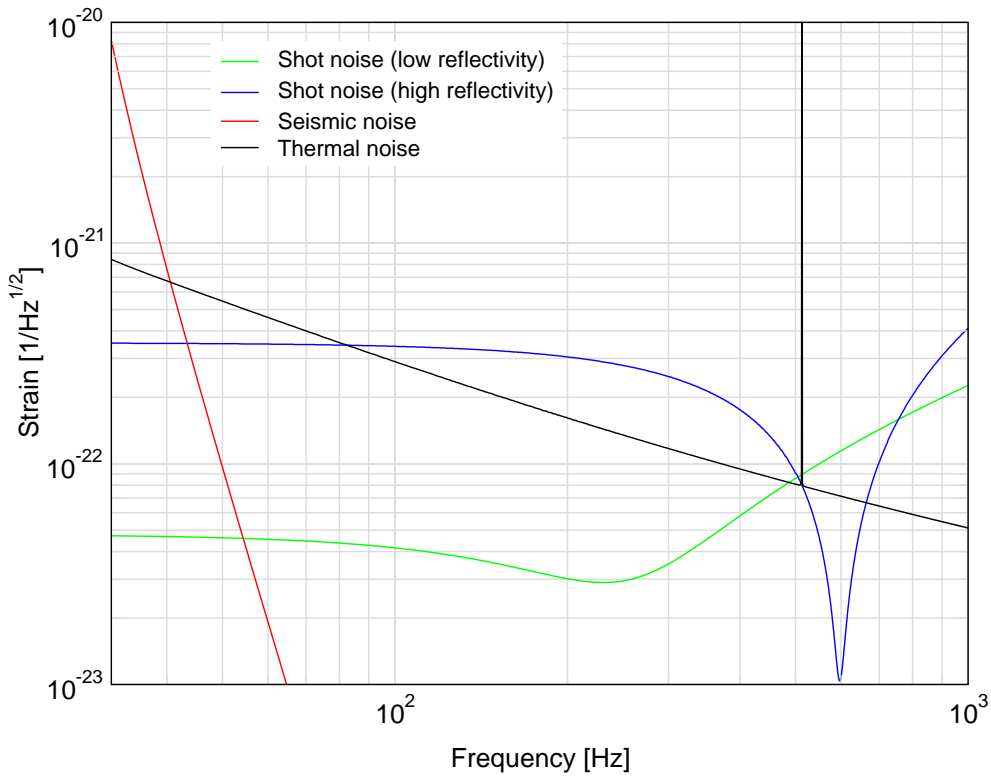


Figure 1.2.: *Expected noise limits for the sensitivity of the GEO 600 gravitational wave detector. The shot noise depends strongly on the reflectivity of the signal recycling mirror.*

The mirrors of the main interferometer are suspended to three pendulum stages to keep them isolated from the seismic motion of the environment. Although this suspension system reduces the seismic influence at high frequencies a lot, ground motion still remains the limiting noise source below 50 Hz. The shot noise is dominant at high frequencies, but in between there is a frequency decade where thermal noises set a limit to the performance (see figure 1.2).

The sensitivity of a detector is usually described by the strain h that a gravitational wave has to cause to produce a signal bigger than the noise of the detector. If a gravitational wave causes the length l to change by Δl , h is given by

$$h = 2 \frac{\Delta l}{l}. \tag{1.1}$$

To keep the thermal noise as low as possible, the mirrors of the GEO 600 detector are suspended as monolithic pendulums. The mirror and the fibers to which it is suspended form one monolithic structure and sliding friction of the fibers is eliminated. The mirrors in the other detectors are still suspended by steel wires, but the technique of monolithic suspensions will be adopted in all next generation detectors.

Several technical noises from electronic noise to scattered light influence the sensitivity of the detector and make the thermal noises hard to reach, but after optimising the performance of the detector, thermal noises will set the fundamental limit at the intermediate frequencies. It is therefore of great interest to detect and to characterize these noises in separate laboratory experiments and to find ways to reduce them even further. In our experiment we tried to measure the pendulum thermal noise that moves the whole pendulum, in contrast to internal thermal noises that act only on the mirror itself.

Chapter 2

Thermal noise

2.1. Introduction

Thermal noise is the excitation of a mechanical system due to the thermal energy that is associated with each mode of oscillation. A first indication of this effect was detected by Robert Brown in 1828 when he observed the fluctuating movement of dust in water. A mathematical description of this motion was given by Albert Einstein in 1905 [21][22]. In a gravitational wave detector thermal noise was first measured as a noise source in 1966 by Joe Weber [72]. This noise excited the mechanical resonance of a bar detector and thereby limited the achievable sensitivity. To reduce the effect of this noise, today's bar detectors are cooled down to ~ 1 K.

Today's interferometric gravitational wave detectors are not designed to have their maximum sensitivities at the mechanical resonance frequencies of their test masses and suspensions, but rather in the regions in between. Off-resonant thermal noise sets a limit to the sensitivity for these detectors. There are many contributions to this, because there are many different ways in which thermal noise can excite the suspended mirrors which form the Michelson interferometer. One of them is the thermal excitation of the pendulum mode. It is important to measure this pendulum thermal noise above the resonance frequency, because different models predict a different frequency dependence. Depending on its slope, pendulum thermal noise can limit the achievable sensitivity for interferometric gravitational wave detectors at the lower end of the detection band. There are other forms of thermal noise that can excite the mirror itself. These will be dominant at higher frequencies.

2.2. Velocity damping

The energy dissipation of an oscillating system due to external damping mechanisms and internal friction is related to the thermal noise of the system. This was first described in 1951 with the fluctuation-dissipation theorem (FDT) [16][15]. Every dissipation mechanism causes a fluctuating force on the system. According to the FDT, the spectral density of this force is given by

2. Thermal noise

$$S_F(\omega) = 4k_B T \Re(Z(\omega)) \quad (2.1)$$

Here k_B is the Boltzmann constant and T is the temperature. $\Re(Z(\omega))$ is the real part of the impedance of the system. If an external force $F_{\text{ext}}(\omega)$ is applied to the system, it will cause the sinusoidal velocity of $v(\omega) = i\omega x(\omega)$ with $x(\omega) = x_0 e^{i\omega t}$. The impedance is simply the ratio between the two.

$$Z(\omega) \equiv \frac{F_{\text{ext}}(\omega)}{i\omega x(\omega)} \quad (2.2)$$

We can rewrite the FDT into a more useful form that gives us the spectral density of the displacement directly

$$S_x(\omega) = \frac{4k_B T}{\omega^2} \Re\left(\frac{1}{Z(\omega)}\right) \quad (2.3)$$

If the system is a suspended mirror, the most obvious damping mechanism will originate from the molecules of the surrounding gas. If the mirror moves with the velocity $v(\omega)$, it will receive more momentum from the molecules hitting the mirror from the forward direction than from those at the other side. The frictional force F_{fric} that slows down the pendulum movement is given by [62]

$$F_{\text{fric}} = -\frac{1}{4} \frac{p}{k_B T} A m_g \bar{v}_p v(\omega) \equiv -\gamma i\omega x(\omega) \quad (2.4)$$

Here we have introduced the damping constant γ . A is the mirror surface area, p is the pressure of the surrounding gas, m_g is the mass of one molecule of this gas and \bar{v}_p is the average velocity of these molecules. With this damping force proportional to the velocity of the mirror, the equation of motion is

$$-m\omega^2 x(\omega) = -kx(\omega) - i\omega\gamma x(\omega) + F_{\text{ext}}(\omega) \quad (2.5)$$

where m is the mass of the mirror and k is the restoring spring constant of the pendulum movement. The impedance of this system is

$$Z(\omega) = \gamma + i\omega m - i\frac{k}{\omega} \quad (2.6)$$

Combining this with the resonance frequency of the system, $\omega_{\text{res}} = \sqrt{k/m}$, gives us the thermal noise spectrum of a velocity damped pendulum.

$$S_{\text{vel}}(\omega) = \frac{4k_{\text{B}} T \gamma}{m^2 (\omega^2 - \omega_{\text{res}}^2)^2 + (\gamma\omega)^2} \quad (2.7)$$

The thermal noise spectrum is constant below the resonance frequency and drops with ω^{-2} above the resonance. In both regions it is proportional to the level of the damping as described by γ . To reduce the thermal motion of the system at frequencies far from the resonance, the amount of damping on the system has to be reduced. The integral over the spectral density of the thermal noise does not depend on the damping, so a reduced noise away from the resonance leads to an enhanced motion at the resonance frequency itself.

Gas damping is not the dominant damping mechanism in interferometric gravitational wave detectors, because the pendulums are suspended inside vacuum systems. In our experiment we have a pressure of 10^{-7} mbar, reducing the gas damping below internal damping mechanisms of the pendulum. Internal damping is in most cases not proportional to the velocity of the system and requires a more general description.

2.3. Brownian noise

Damping by internal friction in the material of a mechanical oscillator leads to a heat storage in the material that causes fluctuations in the system. We will call this Brownian noise, to distinguish it from other forms of thermal noise described in the next sections. Internal damping mechanisms are best described by a generalisation of Hooke's law with a complex spring constant

$$F(\omega) = -k(1 + i\phi(\omega))x(\omega) \quad (2.8)$$

For $\phi(\omega) \ll 1$, we can approximate $\phi(\omega)$ as a phase by which $x(\omega)$ lags behind an external force $F(\omega)$. The impedance for this system is

$$Z(\omega) = \frac{k\phi(\omega)}{\omega} + i\omega m - i\frac{k}{\omega} \quad (2.9)$$

By applying the fluctuation-dissipation theorem, we can calculate the spectral density of the thermal noise

2. Thermal noise

$$S(\omega) = \frac{4k_B T \omega_{\text{res}}^2 \phi(\omega)}{m\omega[(\omega^2 - \omega_{\text{res}}^2)^2 + \omega_{\text{res}}^4 \phi^2(\omega)]} \quad (2.10)$$

Decreasing ϕ increases the thermal fluctuations near the resonance frequency, but decreases them at all other frequencies. In gravitational wave detectors it is therefore desirable to make ϕ as small as possible to increase the achievable sensitivity away from the resonances.

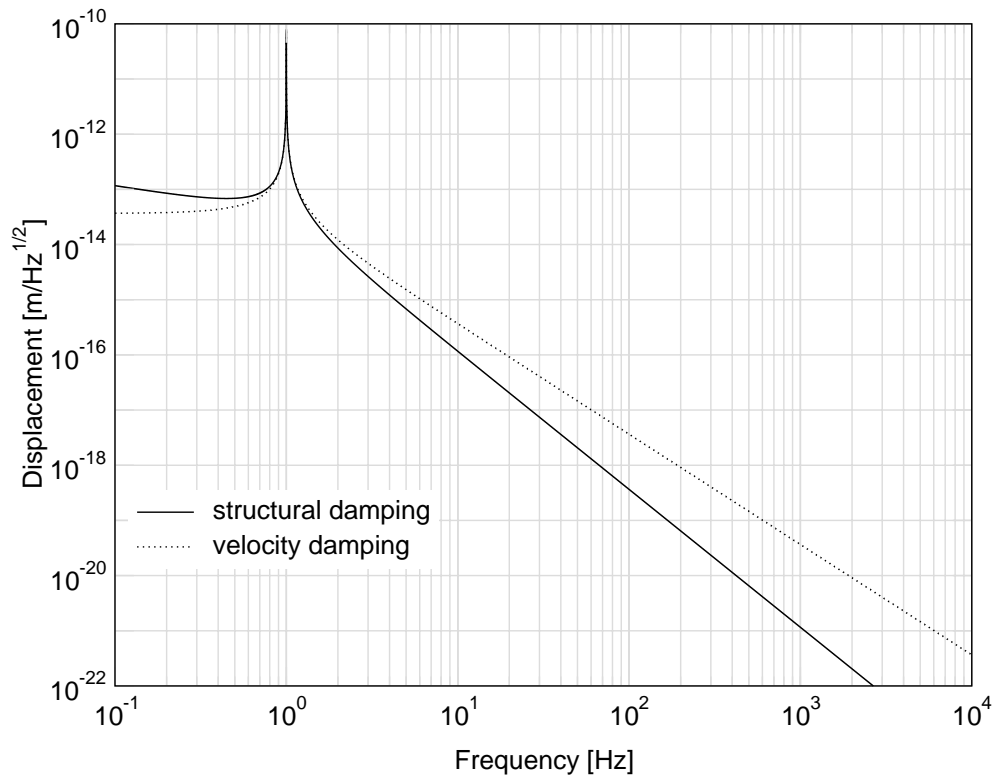


Figure 2.1.: *The thermal noise of a pendulum mode with the assumption of structural damping and velocity damping ($\phi(\omega_{\text{res}}) = 10^{-6}$).*

With $\phi(\omega) = \gamma\omega/k$, equation 2.10 is identical to equation 2.7 and we have a velocity damped pendulum. For internal damping it is widely believed that this model is not the correct description of the pendulum behaviour. It is often assumed that ϕ is independent of frequency. Such a case is called structural damping, causing the thermal noise to drop with $\omega^{1/2}$ below the resonance frequency and with $\omega^{5/2}$ above the resonance (see figure 2.1). This is very different from velocity damping and it is therefore important to know which of the two models for $\phi(\omega)$ is more applicable to the suspended mirrors in gravitational wave detectors, because the achievable sensitivity due to thermal noise depends on it.

Because the spectral density of thermal noise is proportional to the temperature, thermal noise can be reduced by cooling the suspensions to cryogenic temperatures. However, it is not easy to

cool a pendulum suspended from thin wires. To avoid heating by radiation, the whole environment would have to be cooled too, and the absorbed power from the laser would have to be very low. Also ϕ itself is temperature dependent and might even increase with lower temperatures. Currently only the next generation detector in Japan is planning a cooling scheme for the mirrors, and the construction of a cryogenic 100 m prototype interferometer is under way [51].

2.3.1. The loss function of a pendulum

An oscillating system where a distortion $x_0(\omega)$ creates the displacement $x_1(\omega)$ can be described by the transfer function $T_f(\omega) \equiv x_1(\omega)/x_0(\omega)$. Such a system is often characterized by the quality factor Q , which is defined by [62]

$$Q \equiv \frac{\omega_{\text{res}}}{\Delta\omega} \quad (2.11)$$

where $\Delta\omega$ is the full width of the resonance peak at $1/\sqrt{2}$ of the maximum amplitude (That is equal to the width at 1/2 of the maximum power). For velocity damping Q is given by $Q = \omega_{\text{res}} m/\gamma$. It is often more useful to rewrite equation 2.11 into a different form.

$$Q = \frac{|T_f(\omega_{\text{res}})|}{|T(0)|} \quad (2.12)$$

For a system with a complex spring constant, this transfer function is

$$T_f(\omega) = \frac{k + ik\phi(\omega)}{-m\omega^2 + k + i\phi k} \quad (2.13)$$

From the above and with $\phi(\omega) \ll 1$, we get the useful relation

$$Q = \frac{1}{\phi(\omega_{\text{res}})} \quad (2.14)$$

A measurement of the quality factor of an oscillator makes it possible to determine the size of ϕ at the resonance frequency. For a precise measurement of the Q of a system, often the impulse response of the system to an external disturbance is observed. The quality factor is given by

$$Q = \frac{1}{2} \omega_{\text{res}} \tau \quad (2.15)$$

2. Thermal noise

Here τ is the time it takes for the amplitude of a sinusoidal oscillation ($A \sin(\omega t)$ where $A = A_0 e^{-t/\tau}$) to decay by $1/e$ of its original value. The decay of the energy can be described by

$$E(t) = E_{\text{kin}} + E_{\text{pot}} = E_0 e^{-2\frac{t}{\tau}} \sin^2(\omega_{\text{rest}} t) + E_0 e^{-2\frac{t}{\tau}} \cos^2(\omega_{\text{rest}} t) \quad (2.16)$$

The energy the system loses per cycle is given by

$$\Delta E = 2\pi E \phi(\omega_{\text{res}}) \quad (2.17)$$

with the assumption $\phi(\omega) \ll 1$. Now we have a much more instructive picture of ϕ . It describes the fraction of energy that is dissipated per cycle. That is why ϕ is often simply referred to as the loss function of the system. In the case of a single free wire, $2\pi\phi_{\text{wire}}$ is equal to the energy loss E_{loss} in the wire divided by the energy stored in the bending of the wire E_{wire} . A pendulum behaves very differently. If the mass moves away from its rest position, most of its energy is transformed into potential energy in the gravitational field E_{grav} , and this process is lossless. Only a very small fraction of the energy is stored in the bending of the wires and thereby subject to internal friction. The loss function of a pendulum is given by

$$\phi_{\text{pend}} = \frac{E_{\text{loss}}}{2\pi(E_{\text{grav}} + E_{\text{wire}})} \approx \phi_{\text{wire}} \frac{E_{\text{wire}}}{E_{\text{grav}}} \equiv \frac{\phi_{\text{wire}}}{D} \quad (2.18)$$

The factor D that connects the loss in a pendulum wire with the loss of the whole pendulum is called dilution factor. It is given by [44]

$$\frac{1}{D} = \frac{E_{\text{wire}}}{E_{\text{grav}}} \approx \frac{N\sqrt{T_w Y I}}{2mgl} \quad (2.19)$$

were N is the number of wires with the length of l , g is the acceleration of gravity, $T_w = mg/N$ is the tension in each of the wires, $I = \pi r^4/2$ is the moment of inertia of the wire cross section (r is the radius of the wire) and Y is the Young modulus which describes the elasticity of the wire material. For a suspension similar to those of GEO 600, the dilution factor can be as big as $\sim 10^3$. Because of this factor, it is possible to achieve a much lower loss functions for the pendulum than that of the wire material itself.

In equation 2.19 it was assumed that the pendulum is able to tilt when the pendulum mode is excited. In such a case, the bending that occurs is almost entirely confined to the material close

to the upper suspension point. The rest of the fiber is unbent and therefore not subject to losses from internal friction. If the separation of the wires in the direction of the pendulum movement is not small compared to the dimension of the mass, tilt motion is no longer possible and bending occurs at both ends of the wires. This doubles the losses and the loss function has to be multiplied by two.

2.4. The violin modes

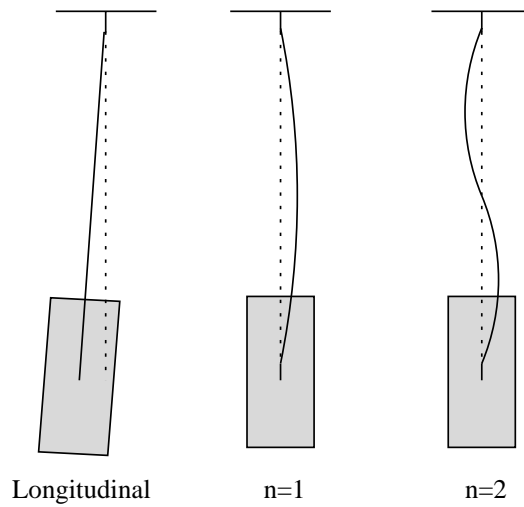


Figure 2.2.: *The longitudinal mode and the first two violin modes of a pendulum a mass. Bending occurs mainly at the upper suspension point for the pendulum mode and at both suspension points for the violin modes.*

The violin modes of a pendulum are the different transversal modes of oscillation of the suspension wires (see figure 2.2). Their shape is comparable to the modes of a violin string. The frequency of the n -th mode is given by [74]

$$\omega_n \approx \frac{n\pi}{l} \sqrt{\frac{T_w}{\rho_1}} \quad (2.20)$$

ρ_1 is the linear density of the wire material ($\rho_1 l = \rho \pi r^2 l$ is the mass of a wire with the density ρ). Similar to the pendulum mode, most of the energy of the violin modes is stored losslessly in the gravitational field. This leads to very low loss functions for the violin modes. The gravitational energy of the violin modes for each wire can be approximated with

$$E_{\text{vgrav}} \approx \frac{1}{4} T_w l \theta^2 \quad (2.21)$$

2. Thermal noise

θ is the angle of the wire at the suspension point. This formula does not depend on which violin mode is chosen. If we compare the energy of all wires to the energy stored in the gravitational field by the pendulum mode, we get

$$E_{\text{grav}} = \frac{1}{2}kx^2 = 2E_{\text{vgrav}} \quad (2.22)$$

The violin modes bend the wires at both suspension points. This doubles the losses in the wire. With equation 2.19 we can calculate the loss function of the violin modes

$$\phi_{\text{v}} = \phi_{\text{wire}} \frac{2E_{\text{wire}}}{E_{\text{vgrav}}} = 2\sqrt{\frac{YI}{T_{\text{w}}l^2}} = 4\phi_{\text{pend}} \quad (2.23)$$

The different violin modes are independent of each other, so we can calculate them separately and add their contributions to the displacement of the pendulum in the end [24]. Using equation 2.10, we get

$$S_{\text{v}}(\omega) = \sum_{n=1}^{\infty} \frac{4k_{\text{B}}T\omega_{\text{n}}^2\phi_{\text{v}}(\omega)}{m_{\text{v}}\omega[(\omega^2 - \omega_{\text{n}}^2)^2 + \omega_{\text{n}}^4\phi_{\text{v}}^2(\omega)]} \quad (2.24)$$

m_{v} is not the mass of the pendulum, but the effective mass for each of the violin modes. It is given by

$$m_{\text{v}} = \frac{1}{2}m \left(\frac{\omega_{\text{n}}}{\omega_{\text{res}}} \right)^2 = \frac{(\pi mn)^2}{2\rho_1 l} \quad (2.25)$$

The effective mass gets very big for higher order modes, resulting in smaller noise contributions from these modes. Even for the first mode, the movement of the pendulum mass due to the wire oscillation is scaled with the mass ratio between the wire and the pendulum mass. This is because the small mass of the wire is barely able to pull the massive mirror sideways. The violin mode contribution is significant only at the violin mode resonance frequency. This is especially true for very low loss suspensions. For GEO 600, the high Q resonances of the fused silica fiber violin modes even have to be damped, because otherwise they would cause instabilities in the interferometer length control feedback servos [27].

It should be noted that the summation of supposedly orthogonal modes, the so called multi-mode expansion, as done in equation 2.24, does no longer give the correct result if the loss of the system is distributed inhomogeneously. It was recently pointed out [45] and experimentally confirmed [77], that localized losses couple the modes to each other and make it necessary to measure the losses of all modes combined and to apply the fluctuation-dissipation theorem to the overall loss, instead of treating the modes independently.

2.5. Linear and nonlinear thermoelastic noise

Internal friction is not the only source of energy dissipation within the wire. The bending of the wire causes one side of the wire to be expanded and the other to be compressed. Because of the nonzero thermal expansion coefficient of the wire material, one side of the wire is heated and the other is cooled down. This causes an irreversible heat flow from one side to the other, which dissipates energy out of the pendulum movement. The loss function of such a system is given by [78]

$$\phi_{te} = \frac{TY\alpha^2}{C_V} \frac{2\pi f_c \omega}{(2\pi f_c)^2 + \omega^2} \quad (2.26)$$

C_V is the specific heat per unit volume. It is related to the usual heat capacity C by $C_V = \rho C$. α is the linear thermal expansion coefficient ($\alpha = (1/l)dl/dT$) and f_c is the characteristic frequency of the system where the loss has its maximum. It is given by

$$f_c = 0.539 \frac{D}{r^2} \quad (2.27)$$

r is the radius of the wire and D is the thermal diffusion constant with $D = \kappa/C_V$. κ is the thermal conductivity. The characteristic frequency typically ranges from ~ 100 Hz to a few kHz, depending on the wire material [11][59]. At lower frequencies we can approximate the loss function of the thermoelastic damping to be proportional the ω , resulting in a frequency dependence of the thermal noise as described by velocity damping.

The above is often referred to as linear thermoelastic noise as opposed to the nonlinear noise associated with a temperature dependent Young's modulus. A temperature fluctuation causing a temperature gradient from one side of the wire to the other will not only cause a compression and an expansion of the two sides of the wire due to the thermal expansion coefficient, but also due to the temperature dependence in the Young's modulus. Both effects will result in an enhanced displacement of the pendulum. The strength of the contribution of the Young's modulus depends on the tension in the wire. To include this effect, we expand equation 2.26 to [13]

$$\phi_{nl} = \frac{TY}{C_V} \left(\alpha - \frac{u_0}{Y(T)} \frac{dY(T)}{dT} \right)^2 \frac{2\pi f_c \omega}{(2\pi f_c)^2 + \omega^2} \quad (2.28)$$

u_0 is the static relative length change of the wire material that is caused by a pressure p

$$u_0 = \frac{p}{Y} = \frac{T_w}{\pi r^2 Y} \quad (2.29)$$

Depending on the choice of parameters, the thermoelastic damping can be dominated by the non-linear thermoelastic noise, but one could also imagine to choose the tension in the wire as such, that the two effects cancel each other out. If $u_0 = \alpha Y / (dY/dT)$, then a small bending of the wire will cause no temperature change and therefore no thermoelastic noise. Fused silica is one of the few materials where the derivation of the Young's modulus with the temperature is positive and such a cancellation of thermoelastic noise is possible, but this has yet to be confirmed experimentally.

2.6. Thermal noise of the mirror

All forms of thermal noise considered so far move the pendulum as a whole. There are additional mirror noises that result in a vibration of the mirror surface where the laser beam is reflected. A brief summary of these noises will be given here.

For the internal mirror motions, there is no dilution factor storing energy in the gravitational field. The size of the internal Brownian noise depends directly on the loss function ϕ_{subs} of the mirror material. That is the reason that materials with very low loss functions, like fused silica or sapphire, are used for the mirrors of interferometric gravitational wave detectors. The internal resonance frequencies are usually well above 10 kHz and thereby above the measurement band of interest. We will only consider the behaviour of the mirrors below the resonance frequencies. The Brownian noise can be calculated as [4]

$$S_m(\omega) = \frac{4k_B T}{\omega} \frac{1 - \sigma^2}{\sqrt{\pi} Y w_m} \phi_{\text{subs}} \quad (2.30)$$

σ is the Poisson coefficient and w_m is the radius of the laser beam at the mirror surface where the intensity has dropped to $1/e^2$ of its value at the center of the beam¹. The results given in this section are valid for a mirror shape of an infinite half space. A finite size mirror requires corrections of a few percent to the results given here.

There is also a thermoelastic noise contribution to the vibrations of the mirror. This noise introduces local fluctuations of the mirror surface, in contrast to the overall surface motion of the internal modes that are excited by the Brownian noise. This results in a much stronger dependence on the size of the laser beam for the thermoelastic noise. A large beam size is preferable, because surface fluctuations are averaged out more effectively. The thermoelastic noise is given by[6]

$$S_{\text{mte}}(\omega) = \frac{16k_B T^2}{\sqrt{\pi}} \alpha^2 (1 + \sigma)^2 \frac{\kappa}{C_V^2 w_m^3 \omega^2} \quad (2.31)$$

¹In some publications, a different beam radius r_0 is used, where the intensity has dropped to $1/e$ of its center value. It is related to w_m by $\sqrt{2}r_0 = w_m$

2.6.1. Coating noise

If the material properties of the coating are different from those of the mirror substrate, the fluctuations due to the coating have to be considered separately. Mirror coatings in gravitational wave detectors consist of alternating layers of two materials with different refractive index, most commonly made of SiO_2 (fused silica) and Ta_2O_5 (tantala). The coating usually has a much higher loss function than the mirror substrate, but on the other hand the thin coating does not excite the modes of the massive substrate very strongly. The contribution of the surface loss function ϕ_{coat} to the overall mirror loss function scales with the thickness d of the coating, divided by the beam size [31]. The effect of the Brownian noise of the coating is

$$S_{\text{coat}}(\omega) \approx \frac{4k_{\text{B}}T}{\omega} \frac{(1-\sigma^2)(1-2\sigma)d}{\pi Y(1-\sigma)w_{\text{m}}^2} \left(\frac{Y}{Y_{\text{coat}}} + \frac{Y_{\text{coat}}}{Y} \right) \phi_{\text{coat}} \quad (2.32)$$

Y_{coat} is the Young's modulus of the coating. For the thermoelastic noise, another property of the material is important. It scales with the square of the thermal expansion coefficient. If α_{coat} is identical to the expansion coefficient of the substrate, then equation 2.31 is already sufficient to describe the thermoelastic noise. Otherwise there is an additional thermoelastic noise from the coating that is given by [9]

$$S_{\text{cte}}(\omega) = \frac{16k_{\text{B}}T^2}{\sqrt{2\pi}} (\alpha_{\text{coat}} - \alpha)^2 (1+\sigma)^2 \frac{d^2}{w_{\text{m}}^2 \sqrt{\kappa C_{\text{V}} \omega}} \quad (2.33)$$

2.6.2. Thermorefractive noise

Thermal fluctuations in the mirror not only lead to an expansion of the surface due to the thermal expansion coefficient, but if the refraction index is temperature dependent, they also result in a change of the optical thickness of the layers in the mirror coating. This temperature dependence, expressed by $\beta_1 = dn_1/dT$ and $\beta_2 = dn_2/dT$ for the two layer materials, introduces a phase noise to the light reflected in the coating [7]. This can be translated into a corresponding mirror movement.

$$S_{\text{tr}}(\omega) = \frac{8\sqrt{2}\beta_{\text{eff}}^2 \lambda^2 k_{\text{B}}T^2}{\pi w_{\text{m}}^2 \sqrt{\omega C_{\text{V}} \kappa}} \quad (2.34)$$

λ is the wavelength of the incoming light and β_{eff} is given by

$$\beta_{\text{eff}} = \frac{n_2^2 \beta_1 + n_1^2 \beta_2}{4(n_1^2 - n_2^2)} \quad (2.35)$$

2.6.3. Photothermal noise

An additional noise source is linked to the incoming laser beam. A fraction of the light is absorbed in the coating layers and these randomly absorbed photons create local heating in the mirror. This leads to a displacement of the mirror surface of [6]

$$S_{\text{pt}}(\omega) = 2\alpha^2 (1 + \sigma)^2 \frac{\hbar \omega_L P_{\text{abs}}}{(\pi C_V w_m^2)^2} \frac{1}{\omega^2} \quad (2.36)$$

P_{abs} is the absorbed light power, ω_L is the laser frequency and \hbar is the Planck constant divided by 2π . Photothermal noise was experimentally confirmed when the effect was increased by modulating the amplitude of the incoming laser beam [19].

2.6.4. Additional noise in real suspensions

A noise that depends strongly on the inner structure of the wire material was detected in steel wires under strong tension. The stationary creep leads to spontaneous relaxation of tension in the wire material, creating small bursts in the mirror movement [12][1].

If steel wires are used to suspend the mirrors, these wires have to be clamped to the mirror, and at the clamping point sliding friction will cause additional losses [35]. The presence of strong localized losses at the suspension points not only increase the losses in the pendulum mode, but also those of the internal mirror modes, resulting in an increased Brownian noise of the mirror. This can be reduced by a harder clamping material and stronger tension on the wire.

Sliding friction can be avoided completely by using monolithic pendulums. For the GEO 600 detector, the suspension fibers are welded to attachment structures that are silicate bonded to the sides of the mirrors. All components are made of the same material (fused silica) and form one monolithic block. There is no longer a necessity for clamps. The contribution of the increased loss function in the bonding area should be considered, but it is usually small [64].

Thin fibers made of fused silica are hard to handle, but compared to steel they have the additional advantage of a lower internal loss function. Of the current detectors only GEO 600 is using monolithic suspensions, but the next generation detectors are expected to adopt this scheme in the future.

2.6.5. Prediction of the thermal noise

With the exception of the loss function, the noises described above depend only on well-known parameters. Some are experimental parameters that depend on the individual set-up, others are material parameters that have already been measured in previous experiments. A list of the necessary material parameters for calculating the different forms of thermal noise is given in appendix A.

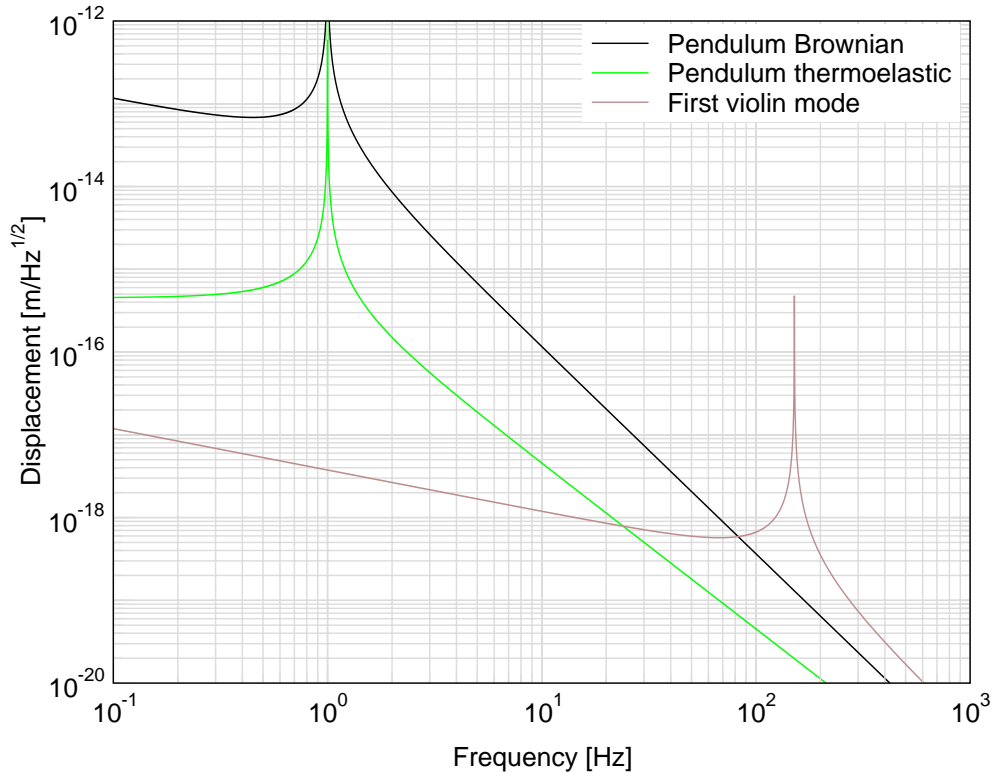


Figure 2.3.: *Theoretical predictions for the different forms of thermal noise for the smaller of the two mirrors in our set-up.*

For the smaller one of our two pendulums, the thermal noise predictions can be seen in figure 2.3 and figure 2.4. We have assumed the model of structural damping. Reducing the mass and lowering the pendulum Q would enhance the predicted pendulum noise level. Also the assumption of viscous damping would result in a higher prediction above the resonance (see figure 2.1). Our mirrors are made of BK7, which has an internal Q of only ~ 4000 . The use of fused silica mirrors would reduce the Brownian noise of the mirror a lot. Other parameters used: $P_{\text{abs}} = 4 \times 10^{-6}$ W, $w_0 = 230 \mu\text{m}$, $r = 45 \mu\text{m}$, $m = 50$ g (see chapter 4). It should be remembered here that the predictions made by the models above still require experimental verification, which is difficult to obtain and in most cases is not yet achieved.

2.7. Previous measurements of the loss function

The Brownian noises depend on the loss functions of the wire, of the mirror material and of the coating. The size and the frequency dependence of these loss functions is not so easy to determine, because the losses in a good suspension are designed to be very small. If we adopt the assumption that the loss function for the materials of interest (steel, fused silica, ...) are independent of

2. Thermal noise

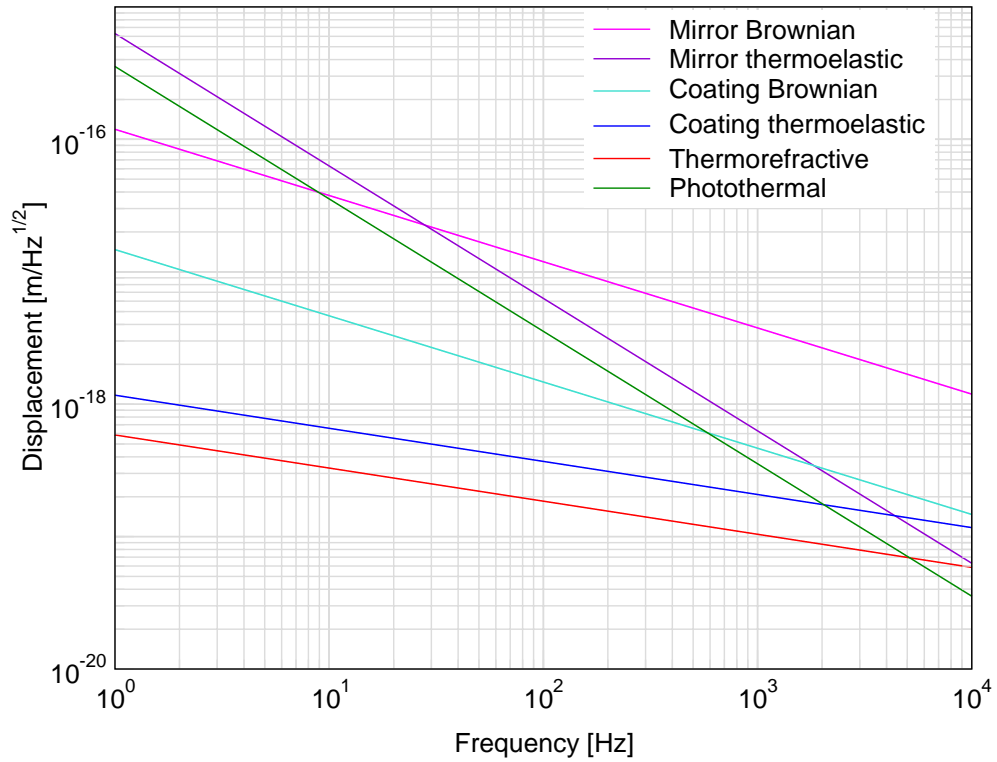


Figure 2.4.: Prediction for the different forms of internal thermal noise in our set-up

frequency, it would be sufficient to measure the loss function at one frequency to calculate the Brownian noise for all other frequencies, but also the assumption of frequency independent loss requires experimental confirmation.

The easiest way to determine the loss function at one frequency is to excite the pendulum at one of the resonance frequencies and to observe the decay time of the oscillation. With equation 2.15 the Q of the system can be calculated, and the inverse is the value of the loss function at the resonance frequency.

This scheme is problematic for the pendulum resonance. For high Q pendulums the decay time can be of the order of years [8] and the measured loss function ϕ can easily be dominated by losses in the support structure. If the pendulum mode is coupled to a mode of the support structure, a fraction of the energy of the pendulum mode is stored in the support and dissipates there. This form of damping is called recoil damping and can be described by [61]

$$\phi = \phi_{\text{pend}} + \phi_{\text{supp}} \frac{m_2}{m_1} \frac{\omega_1 \omega_2^3}{(\omega_1^2 - \omega_2^2)^2} \quad (2.37)$$

ϕ_{supp} is the loss function of the support structure and $m_1, m_2, \omega_1, \omega_2$ are the mass of the support,

the mass of the pendulum, the resonance frequency of the support and the resonance frequency of the pendulum.

It is easier to measure the decay times of the violin modes. The fact that there is more than one violin mode allows some estimation of the frequency dependence of ϕ . Usually a frequency independent ϕ_{wire} , superimposed with the typical shape of the thermoelastic damping ϕ_{te} is observed. ϕ_{wire} is $\sim 10^{-4}$ for steel [25] and can be measured at 10^{-8} for thin fused silica fibers if all other losses are reduced below this level [53]. If a weight is attached to the fiber, the dilution factor has to be taken into account in these measurements, but ϕ_{wire} itself seems to be independent of the applied tension [73]. In the absence of thermoelastic damping, the losses in the fiber are completely dominated by surface defects [29]. This can be described by

$$\phi_{\text{wire}} = \phi_{\text{mat}} + 4 \frac{h \phi_{\text{surf}}}{r} \quad (2.38)$$

ϕ_{mat} is the loss function of the fiber material itself ($\phi_{\text{mat}} < 10^{-8}$), r is the radius of the wire, ϕ_{surf} is the loss function at the surface ($\sim 10^{-5}$ for a good fiber) and h is the penetration depth of surface damages ($\sim 1\mu\text{m}$). This formula might indicate that fibers with bigger radius lower the thermal noise, but it should be remembered that the dilution factor scales with r^2 , and the overall noise is still increased by bigger fibers.

Decay time measurements can also be done at the internal resonances of the mirror for coated and uncoated substrates. The loss function ϕ_{subs} of a fused silica substrate will be $\sim 10^{-8}$ (for sapphire even 3.3×10^{-9} [58]) and a ϕ_{coat} of $\sim 5 \times 10^{-5}$ is achievable for a good coating [17][54].

A measurement of the loss function has also been achieved at the anti-resonance of a coupled oscillator [52]. Without losses, the transfer function from a force on the mirror to mirror movement turns to zero at

$$\omega_{\text{anti}} \approx \sqrt{\frac{m_2}{m_1}} \omega_2 \quad (2.39)$$

m_1 and m_2 are the two masses and ω_2 is the higher of the two resonance frequencies. The magnitude of the transfer function at this frequency is completely determined by the loss of the system.

All of the described methods are applicable only at a few fixed resonance frequencies. Usually none of them is located below 100 Hz, but this frequency region is of great interest in future gravitational wave detectors. There are some uncertainties associated with extrapolating the frequency behaviour of the loss function from the mechanical resonances down to 10 Hz or even 1 Hz. It would be very useful to have direct measurement of the off-resonant thermal noise in this region where decay time measurements are almost impossible.

It is not easy to achieve a direct measurements of the off-resonant fluctuations induced by thermal noise in high Q systems, because this requires very high sensitivities. With a moderate

2. Thermal noise

Q , a good agreement with structural damping was found in a torsion pendulum [26], while the displacement noise of a cantilever blade showed a viscous and a structural damping contribution [38]. There was some indication of off-resonant internal thermal noise of a greased mass [2], and remarkable measurements of the internal thermal noise have been done from 100 Hz to 100 kHz for high Q mirrors [50]. Two different mirror materials were used and Brownian noise and thermoelastic noise of the mirror substrates have been detected.

No measurements of the off-resonant thermal noise of the pendulum mode have been achieved to this date, and the behaviour of the loss function in the region of 10 Hz for high Q systems has yet to be evaluated. This was the main motivation for us to design an experiment that would be sensitive enough to detect the slope of the loss function in this region. Obviously ϕ cannot remain constant indefinitely towards lower frequencies, because the Brownian noise for structural damping rises even below the resonance towards lower frequencies. This results in unrealistically high noise far below 1 Hz. Besides our own effort, one other group is dedicated to the task of detecting the slope of the off-resonant pendulum noise [5].

Chapter 3

Optical set-up

3.1. Introduction

In order to detect displacements as small as those caused by thermal noise in a suspended mirror, a very sensitive detection scheme is necessary. We measure these displacements interferometrically by using two suspended mirrors that form a Fabry-Perot resonator. The length of this interferometer is actively stabilized to the frequency of an incoming laser beam. A displacement of one of the two mirrors causes a signal in this feedback loop that can be detected.

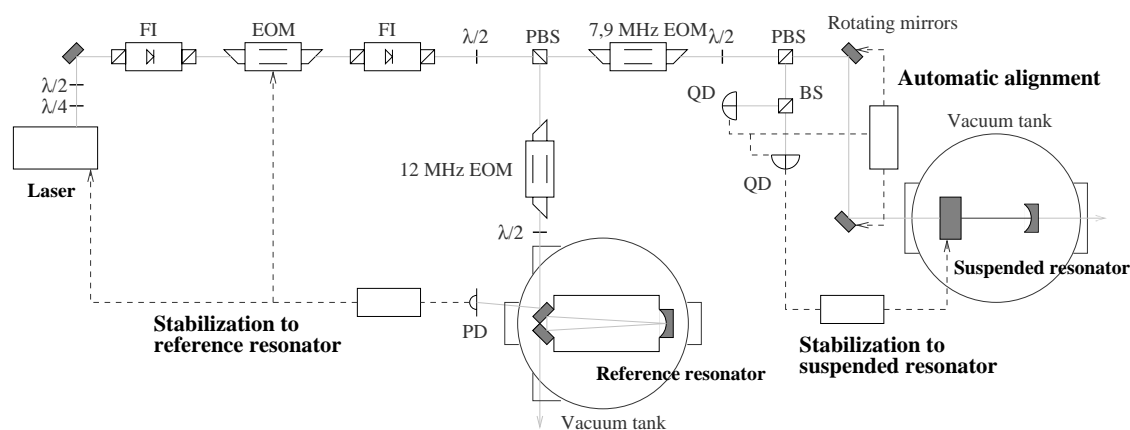


Figure 3.1.: *Optical set-up of the experiment. The laser frequency is stabilized to a reference resonator, the suspended resonator is locked to the laser and an automatic alignment system centers the laser on the resonator mode.*

In this scheme the requirements for the frequency stability of the laser are very high, because noise in the laser frequency cannot be distinguished from changes of the length of the suspended resonator. Therefore it is necessary to stabilize the frequency of the laser to a stable reference resonator, which is located in a separate vacuum tank (see figure 3.1). We also included an automatic

alignment system into the optical set-up that actively stabilizes the position of the laser beam to the eigenmode of the suspended resonator. This enables us to take measurements for longer times and under stable conditions.

Error signals that carry the information of the deviation of the parameter of interest have to be found for all these feedback loops, actuators are needed to change these parameters and stable feedback loops have to be designed to connect the two.

3.2. The Pound-Drever-Hall frequency stabilization

The Pound-Drever-Hall technique [20] to stabilize the frequency of a laser to an optical resonator was developed in 1983 and has become a standard tool ever since. Because this technique is essential for this experiment, its idea will be explained here.

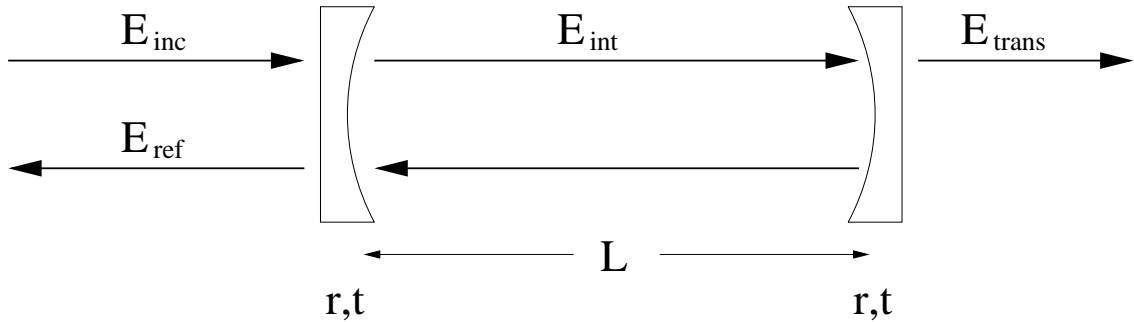


Figure 3.2.: Schematic view of the electromagnetic fields in an optical resonator.

The light reflected from a Fabry-Perot resonator (see figure 3.2) consists of two parts, the directly reflected component, which picks up a phase shift of π when reflected, and the light leaking out of the optical resonator. The strongest contribution to this made one round-trip after entering the resonator, picking up a phase shift of $-2L\omega_L/c$ in the process. L is the length of the Fabry-Perot cavity and $\omega_L = 2\pi f_L$ is the angular frequency of the laser measured in rad/sec, while f_L is the laser frequency in Hz. Additional lightfields that made more than one roundtrip and gathered additional phase shifts have to be added. Assuming a lossless optical resonator with equal amplitude reflectivity r and amplitude transmissivity $t = \sqrt{1 - r^2}$ for both mirrors and an incoming electromagnetic wave with the amplitude E_0 , the reflected light will be

$$E_{refl} = E_0 r e^{i(\omega_L t + \pi)} + E_0 t r t e^{i\omega_L(t - \frac{2L}{c})} + E_0 t r^3 t e^{i\omega_L(t - \frac{4L}{c})} + \dots \quad (3.1)$$

Usually almost all of the light is reflected. Only at the resonance where the cavity length L is a multiple of half of the laser wavelength, the directly reflected light interferes destructively with the light leaking out of the resonator, and almost all of the light is transmitted. After simplifying the

above equation, we get an expression for the reflected light divided by the incoming light, which we call $T_{\text{refl}}(\omega_L)$

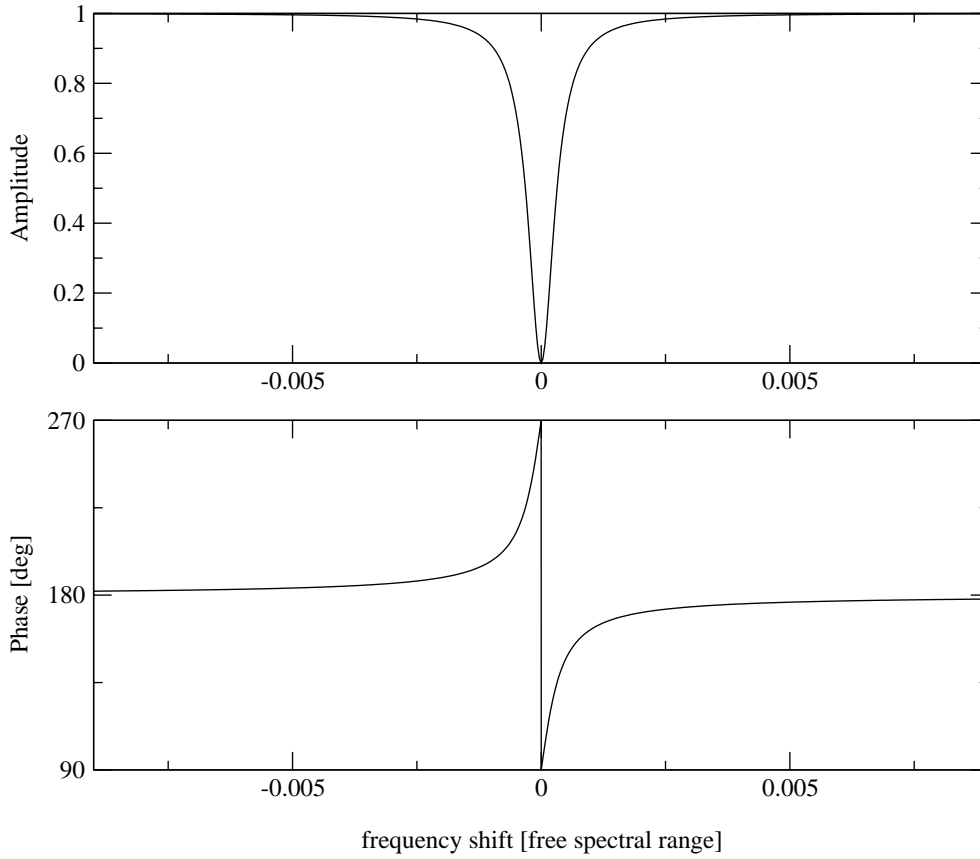


Figure 3.3.: Amplitude and phase of the light reflected from a Fabry-Perot interferometer, divided by the incoming light. This was calculated for a reflectivity of $r = 0.999$ for both mirrors.

$$T_{\text{refl}}(\omega_L) \equiv \frac{E_{\text{refl}}(\omega_L)}{E_{\text{inc}}(\omega_L)} = \frac{r(e^{i\frac{\omega_L}{\Delta_{\text{FSR}}}} - 1)}{1 - r^2 e^{i\frac{\omega_L}{\Delta_{\text{FSR}}}}} \quad (3.2)$$

$\Delta_{\text{FSR}} = c/(2L)$ is the free spectral range of the resonator. It is equal to the necessary frequency change of the incoming light to shift from one cavity resonance to the next. The above equation can be interpreted as a transfer function. If multiplied with the incoming light, it gives us the amplitude of the light that is reflected from the cavity. The amplitude of $T_{\text{refl}}(\omega_L)$ turns to zero at the resonance (see figure 3.3). The full width of the amplitude at half of the maximum (FWHM) is called the linewidth δ_{FWHM} of the optical resonator.

3. Optical set-up

Exactly at the resonance frequency, the amplitude signal cannot be used for a frequency stabilization. It is symmetric and therefore does not carry the information in which direction one has to change the frequency if it drifts off the resonance. One would have to choose an operation point away from the center of the resonance to use this signal for a stabilization. The phase signal, on the other hand, is strongly changing in different directions near the resonance. This would be a good signal for a frequency stabilization if it could be detected. Up to this day, it is not possible to measure the phase of a light beam with a THz frequency directly. Photo detectors are only able to measure the power $P = |E|^2$ of such a beam.

In order to detect the phase signal, we modulate the incoming light with an electro-optic modulator (EOM), which consists of a crystal that changes its refractive index when an external electric field is applied. If the polarization of the light, the electric field and the crystal axis are properly aligned, a pure phase modulation of the light without an amplitude modulation can be achieved. Usually the modulation frequency $f_m = \omega_m / (2\pi)$ is chosen to be in the MHz-region to avoid technical noise that disturbs measurements at lower frequencies. The modulated light can be described as

$$E_{\text{inc}} = E_0 e^{i(\omega_L t + m \sin(\omega_m t))} \quad (3.3)$$

where m is the modulation index, which we assume to be small ($m \ll 1$). This expression can be expanded using Bessel functions [3], but a first order Taylor expansion already leads to the correct result.

$$E_{\text{inc}} \approx E_0 (1 + i m \sin(\omega_m t)) e^{i\omega_L t} = E_0 (e^{i\omega_L t} + \frac{m}{2} e^{i(\omega_L + \omega_m)t} - \frac{m}{2} e^{i(\omega_L - \omega_m)t}) \quad (3.4)$$

The incoming light now possesses a component at the carrier frequency ω_L and two additional components at the frequencies $\omega_L \pm \omega_m$. These are called sidebands. Using equation 3.3, the reflected light can be calculated.

$$E_{\text{refl}} = E_0 (T_{\text{refl}}(\omega_L) e^{i\omega_L t} + \frac{m}{2} T_{\text{refl}}(\omega_L + \omega_m) e^{i(\omega_L + \omega_m)t} - \frac{m}{2} T_{\text{refl}}(\omega_L - \omega_m) e^{i(\omega_L - \omega_m)t}) \quad (3.5)$$

If the carrier frequency is at a cavity resonance or very near to it, the carrier gets almost completely transmitted, and we can assume that $T^2(\omega_L) \approx 0$. The sidebands are completely reflected if the modulation frequency is significantly larger than the cavity linewidth ($T(\omega_L \pm \omega_m) \approx -1$ if $\omega_m > 2\pi\delta_{\text{FWHM}}$, see also figure 3.3). If the reflected light power is detected with a photo diode, we get

$$P_{\text{refl}} = |E_{\text{refl}}|^2 = E_0^2 \frac{m}{2} ([T_{\text{refl}}^*(\omega_L) - T_{\text{refl}}(\omega_L)] e^{i\omega_m t} + ([T_{\text{refl}}(\omega_L) - T_{\text{refl}}^*(\omega_L)] e^{-i\omega_m t}) + \mathcal{O}(m^2) = iE_0^2 m \sin(\omega_m t) [T_{\text{refl}}^*(\omega_L) - T_{\text{refl}}(\omega_L)] \quad (3.6)$$

With the carrier frequency very near the resonance, we can assume that ω_L is an integer multiple of 2π times the free spectral range plus a very small deviation $2\pi\delta f_L$.

$$\frac{\omega_L}{\Delta_{\text{FSR}}} = 2\pi N + \frac{2\pi\delta f_L}{\Delta_{\text{FSR}}} \quad (3.7)$$

N is an integer. We also want to introduce a useful quantity for describing an optical resonator, called Finesse F .

$$F \equiv \frac{\Delta_{\text{FSR}}}{\delta_{\text{FWHM}}} \approx \frac{\pi r}{1 - r^2} \quad (3.8)$$

In the case of perfect modematching of the incoming light to the resonator mode, $1/\pi$ times the finesse is the factor by which the incoming light power is enhanced inside the cavity. We can now calculate that

$$T_{\text{refl}}^*(\omega_L) - T_{\text{refl}}(\omega_L) \approx \frac{2ir(1-r^2)}{1-2r^2+r^4} \frac{2\pi\delta f_L}{\Delta_{\text{FSR}}} = \frac{4i\delta f_L}{\delta_{\text{FWHM}}} \quad (3.9)$$

To read out the desired error signal, one needs to demodulate the reflected light that was measured by a photo detector with the modulation frequency. This is done by a mixer. The phase of the two signals with respect to each other has to be considered, because multiplying equation 3.6 with $\cos(\omega_m t)$ would produce a vanishing signal at the resonance while $\sin(\omega_m t)$ results in the desired signal. In a real experiment, the two signals will have a fixed, but arbitrary phase with respect to each other. This is due to signal travel times within cables, circuits and within other parts of the experiment. It is therefore necessary to include a phase shifter in the experiment to optimise this demodulation phase. After the multiplication with $\sin(\omega_m t)$, the error signal P_e will consist of a DC part and a component oscillating with two times the modulation frequency ω_m , which is removed by lowpass filters. The remaining signal takes the form

$$P_e = -\frac{E_0^2 2m}{\delta_{\text{FWHM}}} \delta f_L \quad (3.10)$$

3. Optical set-up

This is exactly the signal we were looking for. It does no longer contain any components that are oscillating with the modulation frequency, and it is directly proportional to the frequency difference δf_L of the carrier frequency with the cavity resonance. This signal is called Pound-Drever-Hall signal. If it is used in a feedback loop, the signal is usually kept at zero, corresponding to the situation that the laser frequency is exactly at a cavity resonance.

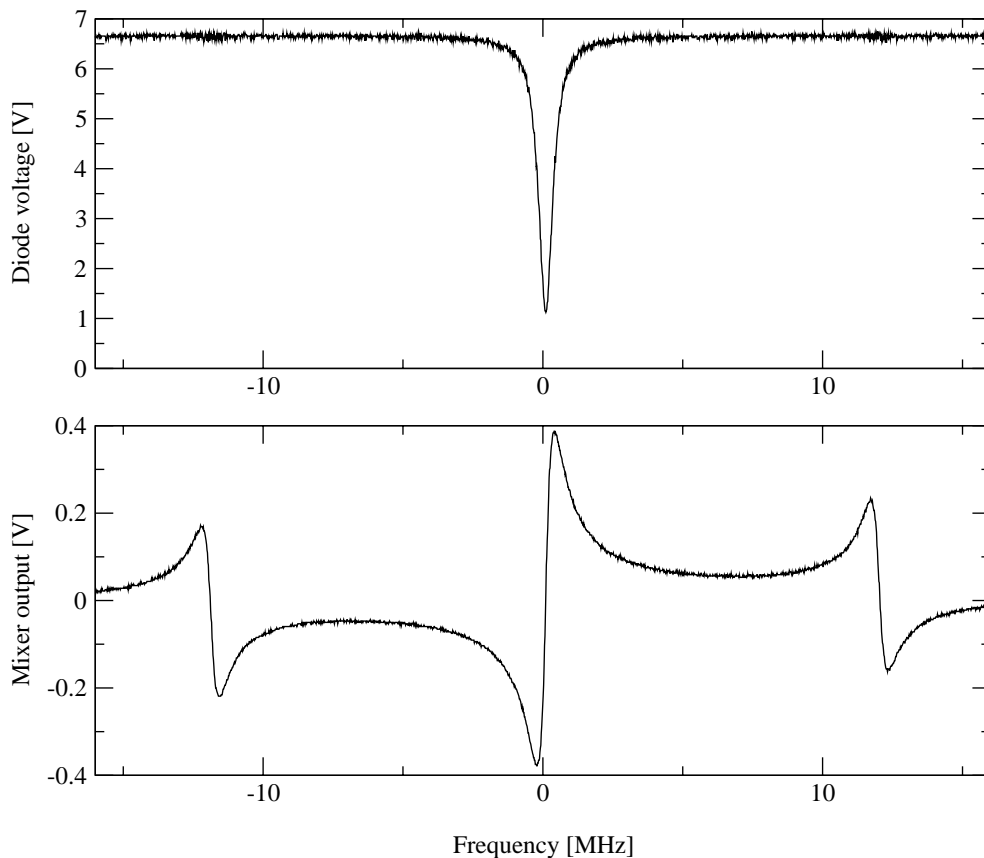


Figure 3.4.: *Photo diode signal in reflection (above) of the reference cavity and Pound-Drever-Hall signal at the mixer output (below), when the laser is swept through a resonance. The measurement was taken with the low cavity finesse (see section 3.4.1) and the modulation frequency was 12 MHz.*

An example of a Pound-Drever-Hall signal is shown in the lower diagram of figure 3.4. It possesses two additional zero crossings at a distance of the modulation frequency on both sides of the cavity resonance. A correctly designed feedback loop will not lock to these points, because these zero crossings have the opposite slope compared to the slope at the resonance.

3.3. Detecting mirror movement

The Pound-Drever-Hall technique is capable of detecting the frequency difference δf_L between the laser frequency and the resonance frequency of a cavity. If we consider the resonator to be stable, we could monitor this signal to detect laser frequency fluctuations. However, in the case of the suspended resonator, the cavity resonance is everything but stable, it changes with the length fluctuations of the resonator. This means that these length fluctuations appear in the Pound-Drever-Hall signal.

We assume that the suspended resonator has the length L and changes by ΔL . If the incoming laser beam stays at the resonance of this cavity, its wavelength λ has to undergo the same differential change than the total length L .

$$\frac{\Delta L}{L} = \frac{\Delta \lambda}{\lambda} \approx \frac{\Delta f_L}{f_L} \quad (3.11)$$

If we want to detect resonator length changes, the above equation describes how they appear in the Pound-Drever-Hall signal, which is proportional to Δf_L near the resonance. On the other hand, this equation points out the problem that changes of the laser frequency against the cavity resonance are indistinguishable from resonator length changes. To avoid that the Pound-Drever-Hall signal is dominated by laser frequency noise in a wide frequency region, one can either reduce the frequency noise (see section 3.4.1), or one can increase the effect of a mirror movement. As can be seen from the above equation, this is achieved by reducing the length L of the suspended resonator, which increases the differential length change.

In our experiment, we chose a resonator length between 2.5 cm and 3 cm. This is a compromise between reducing the influence of laser frequency noise and still retaining a resonator that we are able to align.

3.3.1. The longitudinal feedback loop

A drawback of the Pound-Drever-Hall technique is that it only provides valid signals as long as the laser frequency is near the cavity resonance. With the resonator length constantly changing due to pendulum movement, this will almost never be the case. That means that we need a feedback loop to keep the resonator length (and consequently its resonance frequency) fixed with respect to the laser frequency. If such a system is in place, mirror movements are suppressed by the feedback loop within the control bandwidth. That means that they no longer appear in the Pound-Drever-Hall signal, but they can still be detected by monitoring the feedback signal.

In a generalized feedback loop (see figure 3.5), there is usually a control electronic with a transfer function $C(f)$ and a system with a transfer function $S(f)$ that has to be controlled. The input to the system is called feedback point and the output error point. $S(f)$ can have a very strong

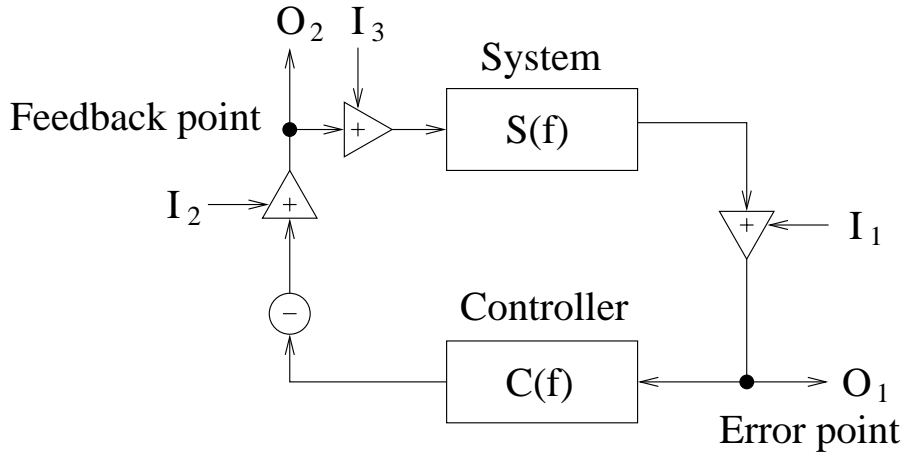


Figure 3.5.: Generalized feedback loop with disturbances added at the error point and at the feedback point.

frequency dependence. In many systems one can measure $S(f)$ by connecting a sine wave to the input of the system instead of the output of the control electronic. Then one monitors the output of the system divided by the input. This can be done with a network analyser.

In the case of a Pound-Drever-Hall stabilization, $S(f)$ cannot be measured when the feedback loop is open. Valid signals are produced only if the cavity is continuously kept near the resonance with the light, but that is not the case without the locked feedback loop. All transfer functions of the individual components of $S(f)$ in the closed loop state have to be evaluated separately. For the moment, we want to concentrate only on the frequency dependence and not the gain of the individual parts.

First there is an actuator transforming an applied voltage to a length change of the resonator. Its frequency response depends on the choice of the actuator (see section 3.3.2). Let us assume a coil-magnet actuator with a f^{-2} frequency dependence between 1 Hz and 1 kHz.

For frequencies much smaller than the average storage time of the light inside the resonator, the transfer function from the introduced length change to the information carried by the reflected light is flat. At high frequencies, the stored light, so far unaffected by the disturbance, averages out the effect of the length change. This can be approximated by a f^{-1} drop in the transfer function above a corner frequency. This corner frequency f_{cav} is given by

$$f_{\text{cav}} = \frac{1}{2} \delta_{\text{FWHM}} = \frac{\Delta_{\text{FSR}}}{2F} \quad (3.12)$$

In the case of a 2.5 cm short optical resonator and mirrors with a transmittivity of $t^2 = 1000$ ppm (parts per million), the corner frequency is 1 MHz, which is well above all frequencies of interest.

Finally the photo diode and the mixer have to be considered. These transform the optical signal back into an electronic one. Usually the overall transfer function of these is flat well up to the MHz region. For even higher frequencies the bandwidth of the individual electronic circuits has to be considered. In total, $S(f)$ is proportional to f^{-2} between 1 Hz and 1 kHz. With this knowledge it is possible to design the transfer function $C(f)$ for the control electronic, which should then keep the cavity at resonance. This means it should keep the Pound-Drever-Hall signal at the mixer output close to zero.

A factor of -1 will be needed, so that a disturbance entering the loop for example at the error point is fed back to this point with opposite sign and thereby reduced instead of enhanced. It is not possible to make a feedback loop infinitely fast because of signal travel times. There has to be a maximum feedback frequency where the total loop gain is one (unity gain frequency). Below this frequency, the gain of the complete system $S(f) \times C(f)$, the so-called open loop gain, is bigger than one, above it is smaller.

The phase of the open loop transfer function at the unity gain frequency is important for the stability of the feedback loop. If it is less than -180° , the system would oscillate and a stable lock would not be possible. A phase of -90° would be ideal and is usually achieved by crossing unity gain with f^{-1} . (For a more detailed analysis see [23]).

We want to achieve a unity gain frequency of a few hundred Hz. This means that $C(f)$ has to rise with f in that region to yield in the desired f^{-1} for the complete loop. At lower frequencies the gain should be very high to suppress the big pendulum movements. $C(f)$ of the controller can be seen in figure 3.6.

If the frequency dependence is designed correctly, a stable lock can be achieved after closing the feedback loop and after adjusting the overall gain until the unity gain frequency is in the desired region. To check the performance of the system in lock, it is helpful to measure noise suppression functions. If a disturbance of the strength I_1 is added at the error point, the signal at O_1 (see figure 3.5) can be described as

$$\begin{aligned} O_1 &= I_1 + (-1)C(f)S(f)O_1 \\ \Rightarrow \frac{O_1}{I_1} &= \frac{1}{1 + C(f)S(f)} \end{aligned} \quad (3.13)$$

O_1/I_1 can be measured with a network analyser. From this the unity gain frequency can be determined, which is where $|C(f) \times S(f)| = 1$. Below this frequency, the above is proportional to $(C(f) \times S(f))^{-1}$. $C(f)$ is known, so the transfer function $S(f)$ of the system could be calculated from this measurement.

Our goal is to detect a mirror movement caused by a noise source from outside the feedback loop. This movement can be described as a signal entering the loop at I_3 . This appears in the error point as

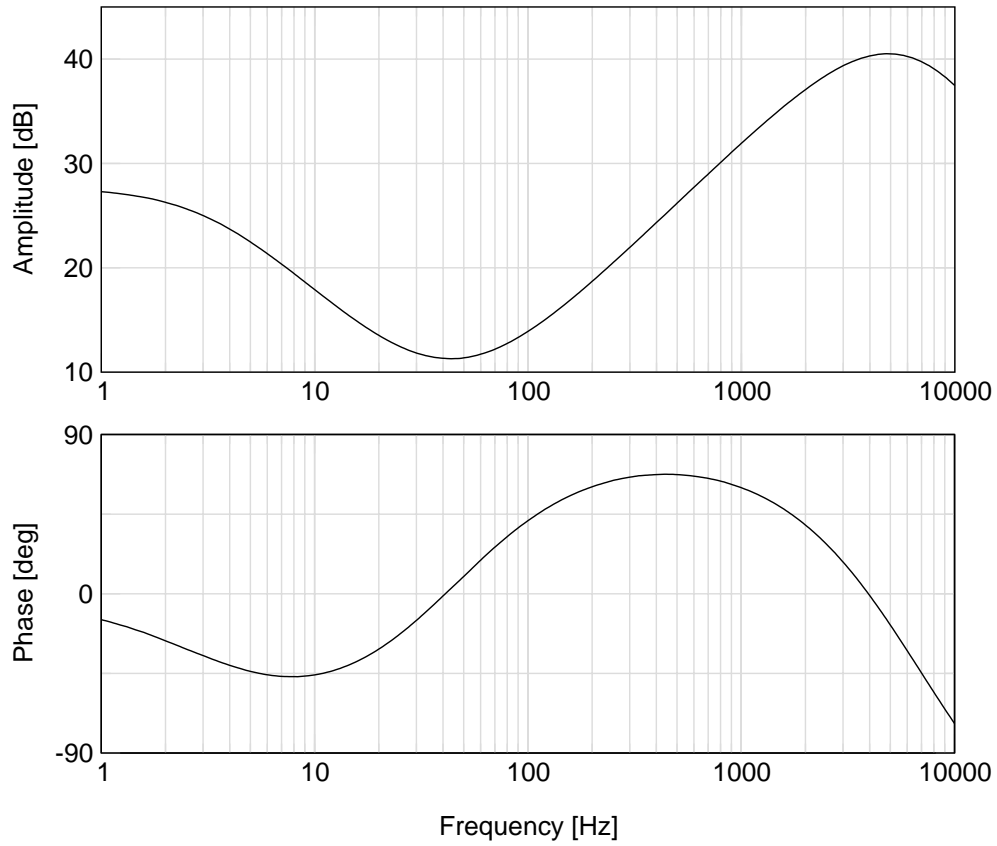


Figure 3.6.: Measurement of the transfer function of the controller for the longitudinal lock. The rising slope between 100Hz and 1kHz compensates for the pendulum transfer function.

$$O_1 = \frac{S(f)I_3}{1 + S(f)C(f)} \quad (3.14)$$

Above the unity gain frequency, the mirror movement can be detected in the error point, but below unity gain at the frequencies we are interested in, I_3 is suppressed by the gain of the controller. The feedback point is monitored instead. I_3 reaches this point as

$$O_2 = \frac{S(f)C(f)I_3}{1 + S(f)C(f)} \quad (3.15)$$

By monitoring O_2 , it is possible to measure the mirror movement below the unity gain frequency. Above unity gain, I_3 is suppressed by $S(f) \times C(f)$, which is smaller than one in that region.

Different noise sources that enter the loop at different points can significantly reduce the sensitivity. But not all noises enter the loop in the same way. A disturbance added to I_3 , which could be mirror movement caused by unwanted forces or noise of the actuator, enters directly into the signal we want to detect. Other noises entering at I_2 , like noises of the electronic at that point, are suppressed by the open loop gain and are therefore not equally critical. A noise analysis always has to consider where the noise enters the feedback loop and where the signal is measured.

3.3.2. Actuators for the longitudinal lock

In order to change the length of the optical resonator, three magnets are attached to the bigger of the two mirrors, and three coils are surrounding these magnets. The feedback signal is fed to the coils through current drivers. The resulting change in the gradient of the magnetic field of the coils generates a force that moves the mirror.

Three coils are necessary, because if only a single coil at the centre of the mirror would be used, this would not only block the laser beam, it would also introduce unwanted tilt and rotational movement if it does not act exactly on the center of mass. Even with three coils, placed as far away from the center as possible to avoid cutting the laser beam, there is still a small amount of tilt and rotational motion introduced when a longitudinal signal is applied. This comes from asymmetries in the pendulum suspension, as well as in the placement of the coils and the magnets.

To be able to reduce the introduced angular motion, it is necessary to have the possibility to change the gain of the three coils separately at the individual current drivers. To balance the gains with respect to each other, we monitor a laser beam that is reflected from the mirror onto a quadrant diode. A sinusoidal signal of a few Hertz is applied to all three current drivers and the gains are adjusted until the sine wave is no longer detectable with the quadrant diode. The resulting combination of coil gains will be different if the frequency of the applied signal is changed significantly, so a frequency close to those we want to measure should be chosen for this adjustment.

For the bigger of the two mirrors in the set-up, it was decided to use a design similar in mass and size to a GEO 600 mode cleaner mirror [28], but the frequencies of the internal mechanical resonances of our mirror are much lower and there are more of these resonances. This comes from the fact that we do not use an expensive solid mirror, but a small mirror attached to a big aluminium mass instead. The lowest internal resonance for a design like this usually lies somewhere between 2 kHz and 4 kHz, compared to more than 20 kHz for one solid mass. These resonances are easily excited if forces at their frequencies are applied to the magnets. The unity gain frequency of the feedback loop has to be well below these resonances, there are too many of them to place unity gain in between.

When the suspended resonator is locked to the laser, the limited unity gain causes stability problems. The mirror movements at the pendulum resonances of the different degrees of freedom near 1 Hz are very big, and a lot of gain is needed in this region to remain in lock. This requires a relatively high unity gain frequency, which would also be desirable for another reason:

If the pendulum swings through a resonance, there is a valid error signal only for a short time, and a slow feedback loop with a unity gain frequency of a few hundred Hz will not be fast enough

3. Optical set-up

to reduce the movement of one pendulum with respect to the other in the short time available. Because of that, we use a split feedback when we lock the system. The fast signals are given to the laser to change the laser frequency, which as we know from equation 3.11 is equivalent to a length change of the cavity.

The laser alone will also not be able to lock the system, because its dynamic range is not big enough to follow the pendulum movements. This comes from the fact that the suspended resonator is very short to be insensitive to frequency noise. Pendulum movements of a few μm already require bigger changes of the frequency than what the laser can provide. The locking near 1 Hz has to be done by the coils. Without this actuator for the pendulum resonance frequencies, no permanent lock can be achieved. This was the case in a previous attempt to build a similar experiment [69][37].

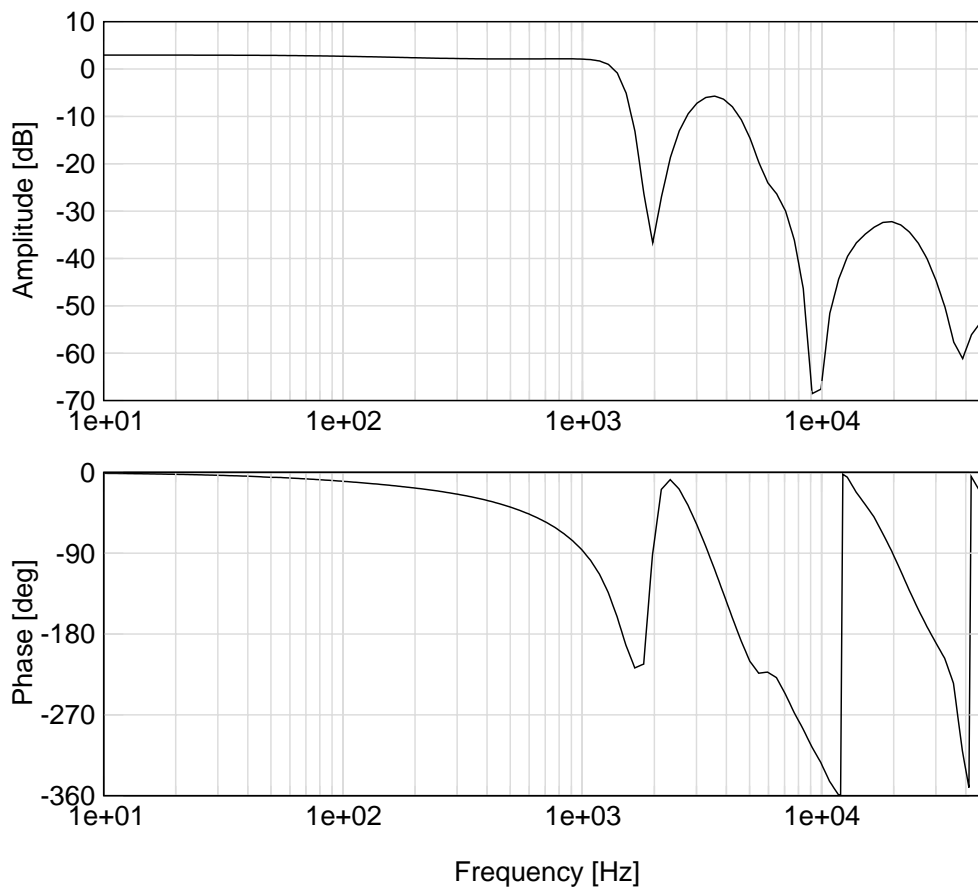


Figure 3.7.: *Measured transfer function of notch filters that are used to avoid excitation of the internal resonances of the suspended mass.*

In lock, the feedback to the laser has to be disconnected, because its frequency has to be locked to a stable reference and not to the suspended resonator. As soon as the coils alone are used for the lock, the first internal mechanical resonance of the mirror is strongly excited, making a stable

lock impossible. This resonance has to be notched out electronically in the feedback loop without changing the phase at unity gain too much. Also the next few resonances have to be notched out, even if the lock is already stable. If the mirror feedback loop oscillates around its operating point, this could produce a noise floor in the measurements due to the higher dynamical range that is required. The transfer function of the notch filters used in the experiment is shown in figure 3.7.

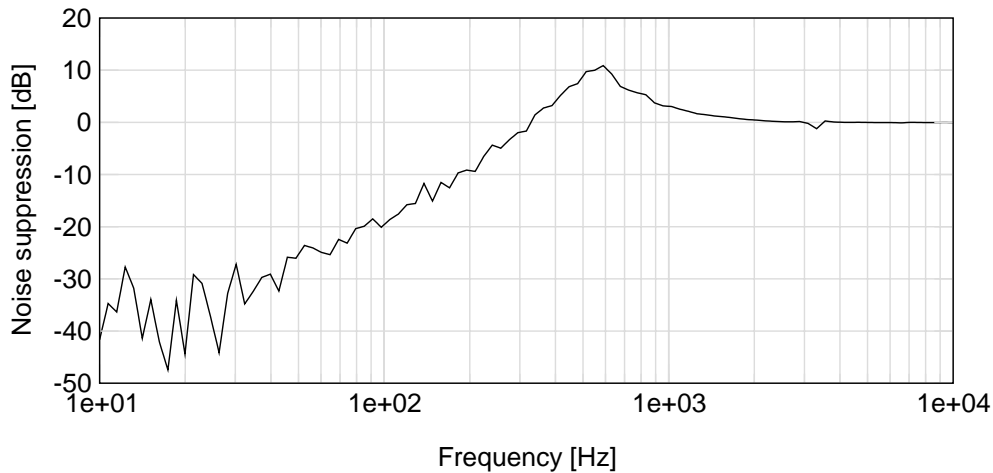


Figure 3.8.: *Suppression of noise by the feedback loop, measured at the error point. Unity gain is just above 300Hz.*

The suppression of noise injected at the error point can be seen in figure 3.8. The unity gain frequency that can be achieved ranges from 200 Hz to 400 Hz. If it drops below 100 Hz, the system does not lock any more, because the gain at low frequencies gets too small.

The actuator coils are attached to a frame structure that is seismically isolated, but at high frequencies it is not as quiet as the pendulum mirrors. Movements of the frame structure could couple to the mirror through the magnetic field. This is a second order effect, but could still limit the sensitivity. Another obvious noise source in this set-up is the electronic noise of the current driver. These noises are especially important, because unlike noise entering at the error point, they are not suppressed by the loop gain at the feedback point, and that is where the signal that is carrying the information about the mirror movement is extracted.

To check that these noises are not limiting, we temporarily switched to a totally different actuator, a piezoelectric crystal. This was glued to the suspended aluminium mass, and the mirror was glued to the piezo (see figure 3.9). We used the glue Vac-Seal, which does not contaminate the vacuum. The piezo has to have a hole in the middle, because the laser beam still has to reach the mirror. This set-up requires a much more careful alignment of the two suspended mirrors with respect to each other, because the outer parts of the mirror are covered by the piezo and it has to be avoided to cut the laser beam.

The piezo moves the mirror with respect to the one hundred times more massive aluminium mass. The internal resonances of the mass are therefore much less excited by the piezo than by the

3. Optical set-up

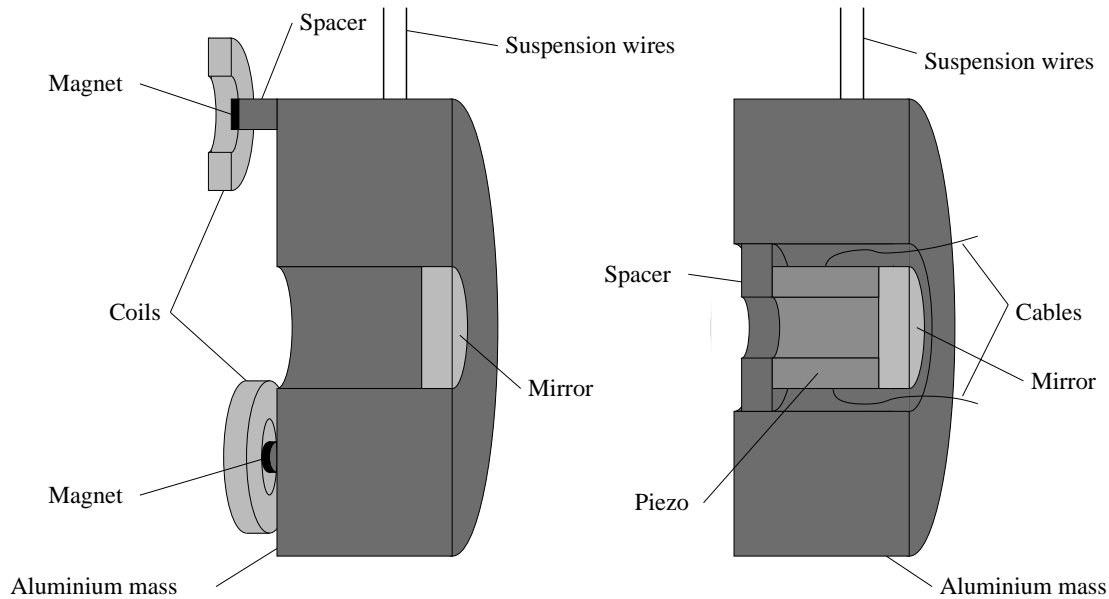


Figure 3.9.: *The two actuators we use for applying the longitudinal feedback. Most of the time we relied on a coil magnet system that moves the whole mass. Temporarily it was replaced by a piezo actuator that was attached to the mirror itself.*

coils that have to move the whole mass. On the other hand, additional resonances from the piezo appear, and those of the mirror glued to the piezo are always present. That means that notch filters are also necessary for the piezo, and we cannot achieve a higher unity gain frequency than with the coils.

Originally a piezo with an efficiency of $0.4 \mu\text{m}/100 \text{ V}$ was used, but its dynamical range turned out to be too small to follow the movements at the pendulum resonances, even if the applied voltage ranged from 0 to 400 V. With a second piezo with a displacement of $4 \mu\text{m}/100 \text{ V}$ we were able to lock the system. From this it can be concluded that the amplitudes of the resonant movement are $\sim 1 \mu\text{m}$ peak to peak. One problem of the second piezo is its bigger length, which makes it more difficult to include it in the mechanical set-up. The piezo has a cylindrical shape. Its length is 40 mm, it has a diameter of 25 mm, identical to the diameter of the mirror, and the diameter of the hole is 16 mm.

The piezo avoids seismic coupling through the coils, current driver noise and unwanted excitation of rotation or tilt motion of the pendulum, but it also brings disadvantages. The high voltage amplifier that is needed to achieve a big enough dynamical range is a source of additional electronic noise. Also two wires have to be attached to the pendulum to get the voltage to the piezo, and this is a potential seismic short-circuit. Nevertheless none of the mentioned noise sources seems to be a limiting factor for the achieved sensitivity, it remained exactly the same when we switched to the piezo and back to the coil magnet actuator.

Both actuators have a different frequency dependence. This has to be considered in the design

of the feedback loop. The piezo has a capacity of $C = 517.5$ nF. Together with the resistance of the cable, it forms a low pass with the corner frequency $(2\pi RC)^{-1}$. This frequency can be decreased if an additional resistor R is placed behind the high voltage amplifier that is driving the piezo.

The current drivers for the coils are designed to have a flat transfer function at the frequencies of interest. This holds from the input voltage at the current driver to the current through the coils to the force acting on the mirror, but the resulting movement of the mirror is not independent of frequency. The mirror is suspended as a pendulum, and above its resonance frequency f_{pend} , the resulting movement caused by an external force drops with f^{-2} . This effect has to be considered when calibrating the feedback signal.

3.3.3. Calibration of the detected signals

The same method is used to calibrate the signals at the feedback point and at the error point. A sinusoidal signal is fed to the laser piezo that causes a frequency disturbance of 2 MHz/V. The frequency of this signal has to be well below unity gain if we want to calibrate the feedback point, and well above for the error point. In the feedback loop, the frequency disturbance is indistinguishable from a length change of the optical resonator. With equation 3.11 it can be calculated to which length change it corresponds. The sinewave appears as a peak in the signal we want to calibrate. If the introduced length change is divided by the detected voltage, the calibration factor at the frequency of the sinewave in m/V is found.

At the error point above unity gain, the calibration factor is the same for all frequencies. At the feedback point, the situation is different. Because of the pendulum transfer function from an external force to a displacement of the mirror, the movement due to a signal at the coils falls off with f^{-2} above the pendulum resonance. If the feedback loop counteracts at different frequencies an identical length change of the optical resonator, just like the ones introduced by the calibration, than the feedback response will have to rise with f^2 to higher frequencies. The calibration has to include that.

Only well below the pendulum resonance, the calibration factor does not change from one frequency to the other. The easiest method would be to calibrate the system below f_{pend} and to multiply the resulting calibration factor with a transfer function $T_{\text{pend}}(f)$ with

$$T_{\text{pend}}(f) = \frac{1}{1 + \left(\frac{f}{f_{\text{pend}}}\right)^2} \quad (3.16)$$

to include the behaviour of the pendulum and to get a valid calibration for all frequencies away from the pendulum resonance (We are interested in absolut values and ignore the phase shift above the resonance, as well as the behaviour of the pendulum at the resonance itself). Locking times are often too short to allow calibration measurements below f_{pend} . It is also possible to calibrate above the resonance at f_{cal} and to multiply the detected voltage with $T(f_{\text{cal}})$ to evaluate the desired calibration factor below the pendulum resonance.

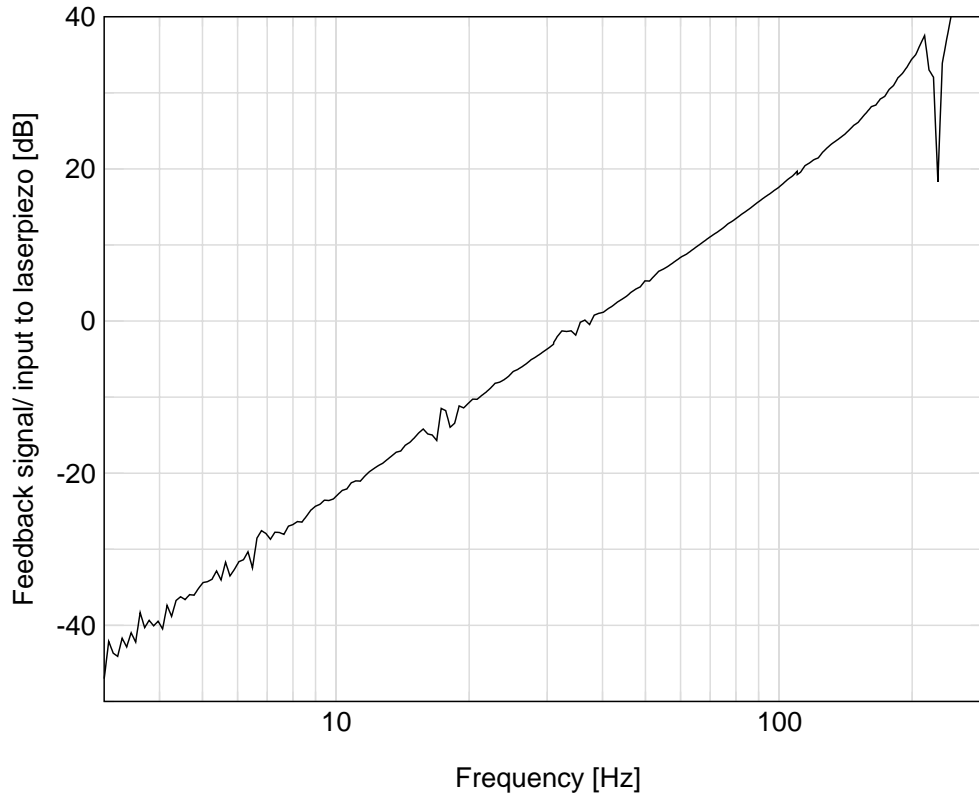


Figure 3.10.: *Implication of a frequency disturbance at the feedback point, measured by giving a signal to the laser piezo and dividing the feedback signal with the signal at the piezo. The f^2 rise in the signal is due to the pendulum transfer function.*

To make sure that the response at the feedback point to a frequency disturbance rises with the expected f^2 and no other overlooked frequency dependence is included in the system, the disturbance was swept through all frequencies of interest (see figure 3.10). A clear f^2 up to the unity gain frequency was found.

A calibration near the pendulum resonance itself would produce false results, because an active system is in place to damp the resonance movement of the pendulum. This reduces the effect of the feedback at these frequencies. Also the pendulum consists of multiple stages and has a complicated structure of more than one resonance near f_{pend} , and none of the resonances is included in the simple pendulum model given by $T_{\text{pend}}(f)$.

A disadvantage of this scheme is that it is problematic to calibrate during the measurement. To take good data, the laser has to be stabilized to a reference resonator. This makes adding a disturbance to the laser impossible, because this disturbance would be suppressed by the laser stabilization loop. The disturbance would have to be added to the error point of the frequency stabilization. It is easier to calibrate before or after the measurement. This is not a problem for the feedback signals. The transfer function from voltage at the current driver to movement of

the pendulum remains constant from one measurement to the next. At the error point this is not always the case, because the signal strength at this point depends on the laser output power and on the alignment of the laser beam to the resonator. One has to make sure that conditions during measurement and calibration are similar.

If we use the piezo actuator to lock the system instead of the coil magnet combination, the calibration scheme is similar. Instead of the f^{-2} from the pendulum transfer function, the low pass formed by the piezo capacity and the output impedance of the electronic driver has to be included. If there are other frequency dependences in the high voltage amplifier that is driving the piezo, these also have to be considered. The result of the calibration for the piezo can be compared to the calibration from the manufacturer of $4 \mu\text{m}/100 \text{ V}$, and the two are in agreement.

3.4. The laser system

The laser for the experiment was built by the Laser Zentrum Hannover. It consists of two pump diodes emitting light at a wavelength of 808 nm. The output power of these diodes is approximately 1 Watt each. This is strongly dependent on the temperature of the pump diodes. In order to be independent from temperature fluctuations of the environment and to prevent the pump diodes from overheating, their temperature is actively stabilized to a constant value by feedback loops. The light emitted by the diodes is linearly polarized and, by choosing different polarizations for the two, the light can be added at a polarizing beam splitter (see figure 3.11).

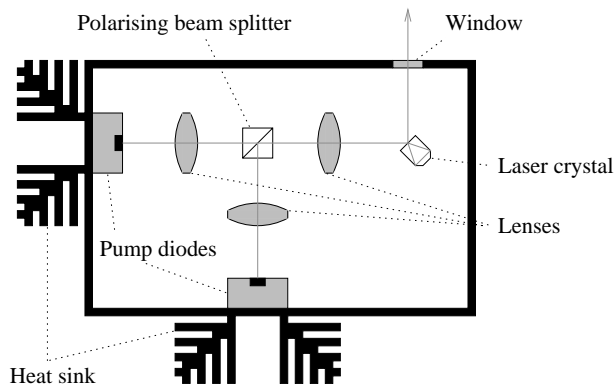


Figure 3.11.: Schematic view of the laser interior.

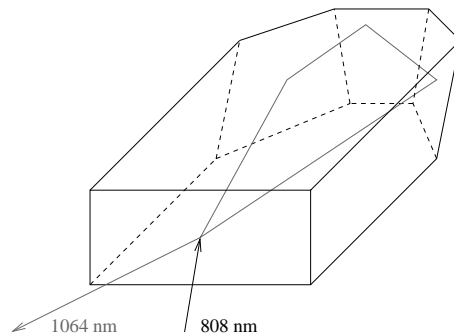


Figure 3.12.: Geometry of the laser crystal.

The light passes through two lenses and is thereby focussed into the laser resonator, which is a monolithic Nd:YAG crystal of $3 \times 8 \times 12 \text{ mm}^3$ (see figure 3.12). The surface of this crystal has a anti-reflective coating for the pump wavelength. The pump light is absorbed inside the crystal and leads to the emission of the laser light at a wavelength of 1064 nm. The output power of this laser can be 1 Watt at maximum, but this value degrades with time because of a reduction of the output power of the pump diodes. It is not necessary to run our experiment with the maximum

laser power. That allows us so to compensate a reduction of the power by increasing the current to the pump diodes.

The temperature of the laser crystal is also controlled as changes in the crystal temperature would lead to changes in the laser frequency. At certain temperatures the laser is running at two frequencies at the same time (multimode operation). If this unwanted effect should occur, a temperature change is necessary to return to normal operation. By adding a signal to the error point of the temperature control loop, the crystal temperature can be used as an actuator to deliberately change the laser frequency. Thermal effects are usually slow and the transfer function of this actuator decreases rapidly from 1 Hz on, so it cannot be used for high frequency actuation.

A piezo crystal is attached to the laser crystal. It applies mechanical stress and thereby also changes the laser frequency. The transfer function of this actuator is flat up to its internal resonances in the high kHz region. The efficiency of this actuator is 2 MHz/V.

3.4.1. The frequency stabilization

The laser already has a low frequency noise, because it consists of one compact monolithic crystal and not of a combination of mirrors and a separate active medium. Still the frequency noise is not yet good enough for the sensitivity we need to achieve. According to equation 3.11, this noise directly enters the measurement and it can lead to bigger signals than those caused by the pendulum movement (see section 5.2). A frequency stabilization that locks the laser to a reference resonator is needed.

Measurements of the frequency noise of the unstabilized laser have shown that it can be described by the simple formula

$$\Delta f_L(f) \approx 10^4 \frac{\text{Hz}}{\sqrt{\text{Hz}}} \times \frac{1 \text{ Hz}}{f} \quad (3.17)$$

This formula holds for all frequencies in the Hz and kHz region and is not limited to our individual laser, but also describes many similar lasers (see for example [47]). The frequency noise is caused by pump light fluctuations, leading to thermally induced fluctuations of the crystal length. A possible actuator for a frequency stabilization would therefore be the current to the pump diodes. This has been demonstrated in [75]. Such a stabilization has the potential not only to reduce frequency fluctuations, but also to minimize amplitude fluctuations in the process. Nevertheless we have decided not to use this rather complicated actuator.

Similar to the stabilization of the suspended resonator, the Pound-Drever-Hall technique is used for the frequency stabilization. A fraction of the light travelling to the suspended resonator is separated from the main beam and directed towards a reference resonator in a separate vacuum tank (see figure 3.13).

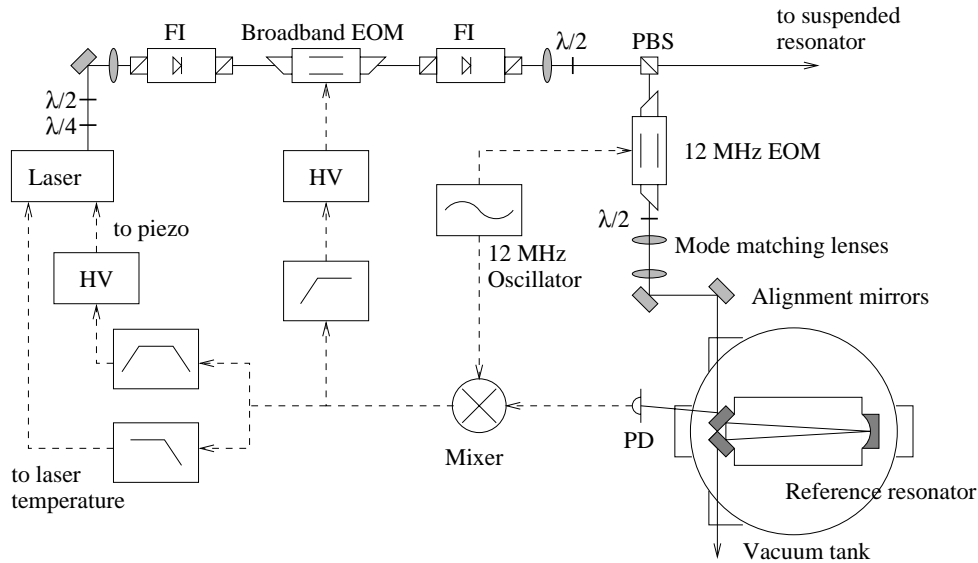


Figure 3.13.: Schematic view of the laser frequency stabilization to the reference cavity. Three actuators for different frequency regions are used in this feedback loop.

The light in the separate path passes an electro optic modulator to which a sinusoidal signal at the modulation frequency of 12 MHz is applied. We use different modulation frequencies for the frequency stabilization and for the suspended resonator to avoid crosstalk between the two systems. The capacitance of the EOM is part of a resonant circuit that is tuned to the modulation frequency in order to increase the modulation index. It is important not to pass the EOM with a fraction of the wrong polarization. This would produce an amplitude modulation that results in an offset at the error point (see section 5.3).

The light passes two lenses that are used to match it to the eigenmode of the reference resonator. If either the position of the focus of the light or its size do not match the resonator focus, a fraction of the light is always reflected, even if the light is in resonance with the reference cavity. This could lead to an increase in the noise, because this light contributes to the shot noise, but not to the signal. To achieve a good overlap, it is necessary to determine the parameters of the laser beam with a beam analyser and to calculate the size of the resonator eigenmode. To determine the focal lengths of the lenses and their position, we use the program Beam Profile Simulator¹ that describes a beam propagating through lenses.

It is as important to match the position of the laser beam to the resonator mode as it is to match the size. Two mirrors are being used to align the lateral position and the angle of the beam to the resonator mode. A camera can be placed behind the resonator to detect which mode is resonant in the cavity at a given time, but usually the camera will detect nothing as the laser frequency has to match one of the mode frequencies to get light into the resonator. A good alignment can be achieved if the laser frequency is swept permanently and the two mirrors are adjusted until

¹developed by M. Ando

3. Optical set-up

nearly all the light is in the lowest order mode. If one is unable to see any of the modes, it can be helpful to overlap the invisible laser with a visible one and to align the reflections from the different mirrors.

The reference cavity is a ring resonator that consists of an ULE spacer and three mirrors glued to it. The material ULE expands very little due to temperature changes. A ring resonator was chosen instead of a linear resonator, because the light reflected by the first mirror does not travel back towards the laser. It is reflected to the side and can be detected without using a quarter wave plate and a polarizing beam splitter. Two of the mirrors are flat, the third has a radius of curvature of 1 m. The length of the optical path for the light inside the resonator is 427 mm, and it has a finesse of 58000 for one polarization of the light and a finesse of 1150 for the other.

The resonator is located in a vacuum tank for several reasons. This avoids refractive index changes inside the resonator that are caused by air fluctuations, the reference cavity is less sensitive to temperature fluctuations of the environment that would otherwise change the length of the spacer, and finally the resonator is isolated from acoustic disturbances which would excite the internal resonances of the spacer. The vacuum tank is located on a seismically isolated table and the spacer resonances are excited only very little by seismic motion. Because of that, it is not necessary to suspend the reference resonator for further seismic isolation.

A photo diode detects the reflected light, and the resulting signal is given to a mixer where it is multiplied with the modulation frequency. The resulting error point signal is given to three different actuators via different electronic paths in a split feedback arrangement. The different electronic paths will have to compensate for the f^{-1} drop in the transfer function of the optical resonator at high frequencies and for the different actuator transfer functions. They also have to be designed in a way that at the crossover frequencies between the actuators the phase difference is close to 90° , so that the different actuators do not work against each other at these frequencies.

The first two of the actuators for changing the laser frequency are inside the laser housing and have been mentioned above already: For very low frequencies signals are given to the laser crystal temperature. The second actuator is the piezo attached to the laser crystal. Its internal mechanical resonances start at 150 kHz, which allows a control bandwidth of up to ~ 100 kHz.

To increase the loop bandwidth, we use a broadband EOM as a third actuator outside the laser crystal [48]. An EOM does not provide the possibility of a DC frequency change, but it is efficient in the high frequency region. The reason for that is that an EOM modulates the phase of the light, and the equivalent frequency change for an applied voltage rises proportional with frequency. The frequency change per Volt for the piezo and for two different EOM's, the PM 25 from Gsänger and the 4004 M from New Focus, can be seen in figure 3.14. The PM 25 showed many mechanical resonances above 20 kHz and has a smaller modulation efficiency, so the 4004 M was used. To increase the achievable frequency change introduced by the EOM and by the laser piezo, both of them are driven by a high voltage amplifier.

During many measurements it was not necessary to use the temperature path. The absence of the frequency stabilization via the laser crystal temperature does not affect the performance in the Hz region, and locking times even without this actuator can be up to an hour before the laser frequency drifts off the cavity resonance due to temperature changes in the environment.

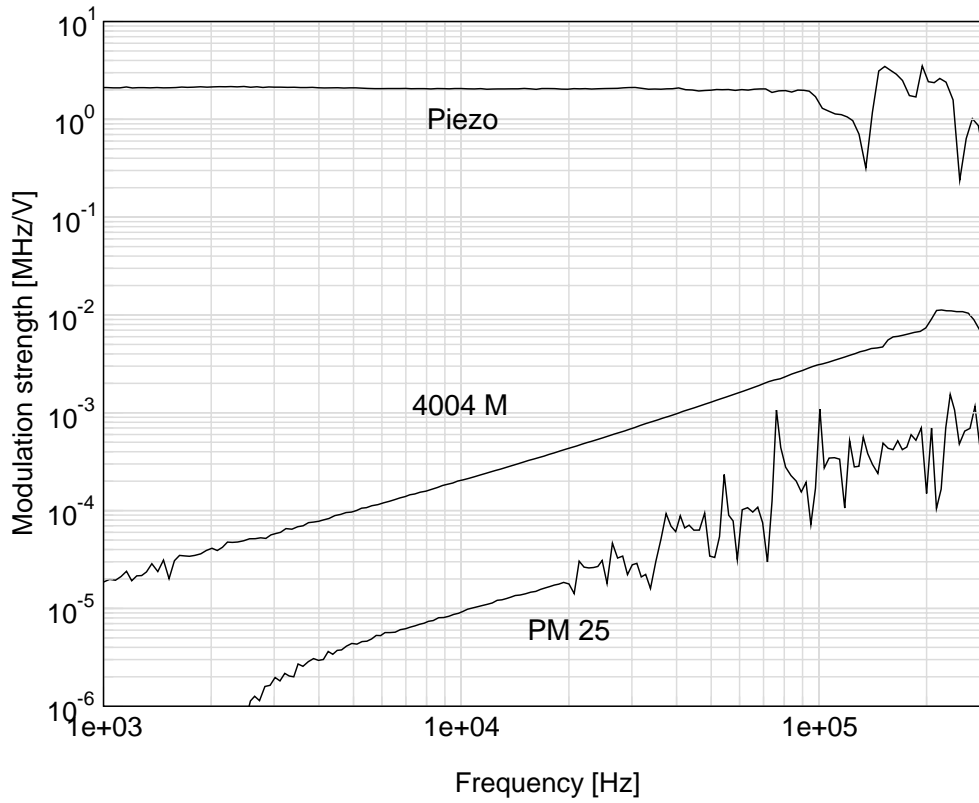


Figure 3.14.: *Transfer functions from applied voltage to frequency change for different frequency actuators: The piezo attached to the laser crystal and of two different external EOM's.*

The complete feedback loop achieves a unity gain frequency well above 200 kHz. The frequency noise of the unstabilized laser and that of the stabilized one, measured in loop at the error point, are shown in figure 3.15. The effect of the stabilization is very big, but an in loop measurement like this does not show the true noise of the system. Frequency fluctuations from seismic and acoustic vibrations of the optical components, refractive index fluctuations in the beam path and changes of the length of the reference resonator are suppressed at the error point, but they are still fed back to the laser frequency.

To make a measurement of the true frequency noise, a second independent identically stabilized laser system would be needed for a beat measurement. Another alternative would be to give a fraction of the light to a second reference resonator. The frequency of this light would have to be tuned by an acousto optic modulator to the resonance of the second cavity to measure the frequency noise. We did not check the out of loop frequency noise, but beat measurements on two laser systems with exactly identical frequency stabilizations showed that we can expect the frequency noise to be well below $1 \text{ Hz}/\sqrt{\text{Hz}}$ at all interesting frequencies [10].

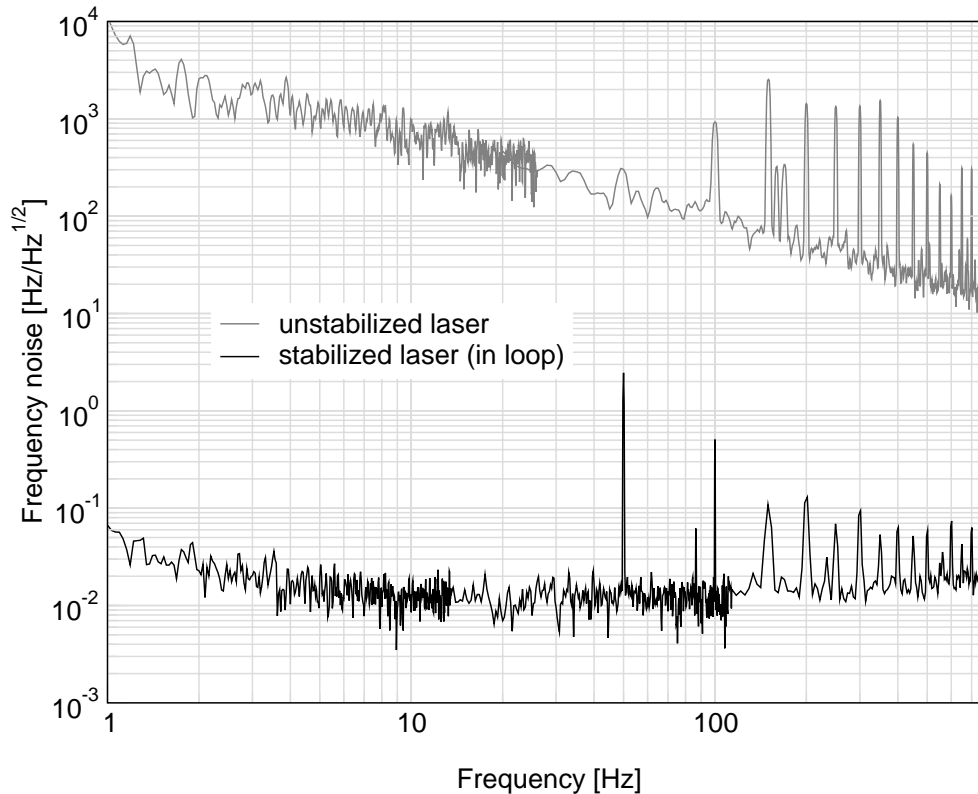


Figure 3.15.: *Frequency noise of the unstabilized and of the stabilized laser. The latter is an in loop measurement, taken at the error point.*

3.5. The automatic alignment system

Due to the seismic isolation system, the mirrors in the main interferometer move very little at high frequencies. On the other hand, at the resonance frequencies in the Hz region they move quite significantly. This movement leads to a shift and a rotation of the mode in the optical resonator with respect to the incoming laser beam.

The laser and all the other optical components are mounted on an optical table, which is seismically isolated to minimize excitations of these components. This optical table slowly drifts and on a timescale of about one minute, a laser beam that was in perfect alignment with the Fabry-Perot resonator that is not placed on the optical table would lose its alignment completely. Measurements over longer periods of time would be impossible, and even during short measurements the alignment to the optical resonator and with it the light power within the resonator would already change significantly.

To avoid these unwanted effects, an automatic alignment system was included in the experiment. This keeps the laser beam aligned to the resonator mode and therefore ensures long locking times and reproducible measurement conditions.

3.5.1. Misaligned optical beams

A laser beam can be misaligned with respect to the mode of an optical resonator in different ways. There can be a mismatch against the resonator mode in waist size and in the longitudinal waist position, as well as a mismatch in the lateral beam position and in the angle of the laser beam. The former two are usually matched by a lens system and do not change much by movement of the resonator mirrors or the optical table. The Pound-Drever-Hall stabilization for locking the resonator length to the laser frequency works satisfactorily, even if no active feedback is applied to optimise the alignment in these two degrees of freedom. Our automatic alignment system minimizes the lateral and angular mismatch of the laser beam in the horizontal and vertical direction.

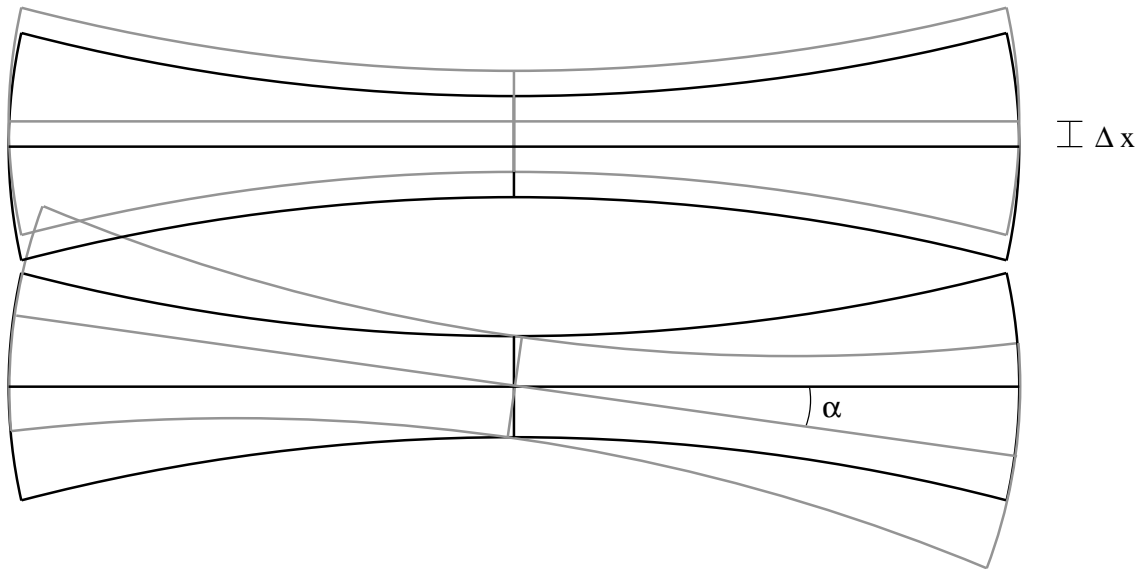


Figure 3.16.: *Misalignment of an optical beam with respect to a reference. The wave front of a beam shifted laterally by Δx is very different far away from the beam waist. The wave front of a beam rotated by α is very different at the beam waist itself.*

As we can see in figure 3.16, these two kinds of mismatches change the wave front of the laser beam with respect to the resonator mode in a different way. The wave front and therefore the local phase of a beam shifted laterally by Δx differs far away from the beam waist, while the wave front of a beam rotated by α is very different at the beam waist itself. The technique of differential wave front sensing [46] measures these phase shifts.

The simplified approach we used in section 3.2 to describe a light field with $E_0 e^{i\omega_L t}$ is not sufficient here, the full spatial distribution of the light has to be taken into account. A good description of the different spatial modes of a laser beam is given in [60]. With z as the direction of propagation, the mode of the order m, n in the x and y direction is given by its amplitude

3. Optical set-up

$$E_{mn}(x, y, z, t) = E_{mn} \frac{w_0}{w(z)} h_m(x, w(z)) h_n(y, w(z)) \times \exp\left(-i\left(kz - \omega_L t + (1+m+n)\Psi(z) + \frac{k(x^2+y^2)}{2R(z)}\right)\right) \quad (3.18)$$

with $w(z)$ being the radius of the beam at which the field is reduced to e^{-1} of its maximum value and w_0 is the radius at the beam waist. The mode functions h_m and h_n are given by

$$h_m(x, w(z)) = C H_m\left(\frac{\sqrt{2}x}{w(z)}\right) e^{-\frac{x^2}{w^2(z)}} \quad (3.19)$$

H_m is the Hermite polynomial of the order m and C a normalizing factor. Out of different possible choices, we follow the approach used by [32] and [30] with

$$C = \sqrt[4]{\frac{2}{\pi w^2(z)}} \quad (3.20)$$

An important quantity in equation 3.18 is the Guoy phase $\Psi(z)$, which describes a phase shift of the different modes against each other that they pick up as they propagate. It is given by

$$\Psi(z) = \arctan\left(\frac{\lambda z}{\pi w_0^2}\right) \quad (3.21)$$

Finally $R(z)$ is the radius of curvature of the wave front. It is given by

$$R(z) = z \left(1 + \left(\frac{\pi w_0^2}{\lambda z}\right)^2\right) \quad (3.22)$$

For now we ignore the time dependence and consider only one lateral direction as the descriptions for the two are identical. At the beam waist ($z = 0$) we can describe a beam consisting only of the fundamental mode, but shifted in the lateral direction by Δx with

$$E(x + \Delta x, 0) = E_0 h_0(x + \Delta x, w_0) \approx E_0 h_0(x, 0) - E_0 \frac{\Delta x}{w_0} h_1(x, 0) \quad (3.23)$$

This means that a small lateral shift is equivalent to the addition of a small amount of the first order mode. We find a similar description for a beam rotated by a small angle α with

$$E(x, 0) e^{ik\alpha x} = E_0 h_0(x, 0) + E_0 i \frac{k w_0}{2} \alpha h_1(x, 0) \quad (3.24)$$

Here we also have the addition of the first order mode, but it is 90° out of phase with the fundamental mode. For a waist size and a waist position mismatch, a similar description could be found by the addition of a small amount of second order modes, in phase and 90° out of phase respectively. When these higher order modes propagate away from the beam waist, they pick up additional Guoy phase compared to the fundamental mode. For the first order mode, the additional phase is simply $\Psi(z)$.

3.5.2. Detection of misalignment

For the detection of misalignments as described above, we use two quadrant diodes that are placed in reflection of the optical resonator and a demodulation technique for each quadrant that is identical to the Pound-Drever-Hall method. Valid signals will only be produced when the longitudinal lock for the suspended resonator is already operating and the fundamental mode of the incoming light is resonant in the cavity.

We will assume the laser beam to be the stable reference and the eigenmode of the suspended resonator to be shifted or tilted against an incoming beam. The light leaving the optical resonator in reflection E_{res} can be described by the equations 3.23 and 3.24 if we include the factors for the propagation in the z direction. The light directly reflected from the resonator E_{refl} , which we assume to be phase modulated at the modulation frequency ω_m , can be described as

$$E_{\text{refl}} = E_0 (T_{\text{refl}}(\omega_L) - i m \sin(\omega_m t)) \frac{w_0}{w(z)} h_0(x, w(z)) h_0(y, w(z)) \times \exp \left(-i \left(k z - \omega_L t + \Psi(z) + \frac{k(x^2 + y^2)}{2R(z)} \right) \right) \quad (3.25)$$

Here we assumed $T_{\text{refl}}(\omega_L \pm \omega_m) = -1$. This is valid if the longitudinal lock keeps the laser at the cavity resonance (see section 3.2). If we detect the reflected light power $(E_{\text{refl}} + E_{\text{res}})^2$ with a photo diode and demodulate the signal, we get the Pound-Drever-Hall signal for the longitudinal stabilization. (We assume a photo diode far bigger than the laser beam, which justifies to integrate the intensity from $-\infty$ to ∞ . Then we get $\int_{-\infty}^{\infty} h_0^2 dx = 1$ and $\int_{-\infty}^{\infty} h_0 h_1 dx = 0$) If we detect the reflected light with a quadrant diode instead of a normal diode and subtract two quadrants on one side from the two on the other side, and if the cavity is shifted in the lateral direction, we get

3. Optical set-up

$$\begin{aligned}
& \int_{-\infty}^0 (E_{\text{res}} + E_{\text{dir}})^2 dx - \int_0^{\infty} (E_{\text{res}} + E_{\text{dir}})^2 dx \\
&= \left(E_0 \frac{w_0}{w(z)} \right)^2 im \sin(\omega_m t) (e^{i\Psi} - e^{-i\Psi}) \frac{\Delta x}{w_0} \left(\int_{-\infty}^0 h_0 h_1 dx - \int_0^{\infty} h_0 h_1 dx \right) \\
&= \left(E_0 \frac{w_0}{w(z)} \right)^2 m \sin(\omega_m t) 2 \sin(\Psi) \frac{\Delta x}{w_0} \sqrt{\frac{2}{\pi}}
\end{aligned} \tag{3.26}$$

This signal will also be demodulated, so only contributions at the modulation frequency have to be considered. The resulting signal is proportional to the lateral shift Δx . As this signal is also proportional to $\sin(\Psi)$, we will have to place the quadrant diode at a position where the Guoy shift of the first order mode against the fundamental mode is close to $\pm 90^\circ$. A rotated resonator results in a similar expression proportional to α and to $\cos(\Psi)$. To detect a rotation of the resonator eigenmode, we have to place the diode either close to the beam waist where $\Psi = 0$, or at a position where the Guoy phase has changed by additional 180° . Placing the diodes at random positions would lead to a mixing of the two signals. One could separate them again by building linear combinations, but this would make things unnecessary complicated.

To evaluate how the Guoy phase changes as the beam propagates, it has to be considered what happens at a lens (the propagation in free space is described in equation 3.21). The radius of curvature of the laser beam is changed by a lens of the focal length f_1 at a distance z_1 by

$$\frac{1}{R_{\text{new}}(z_1)} = \frac{1}{R_{\text{old}}(z_1)} - \frac{1}{f_1} \tag{3.27}$$

A good description of beam propagation can be found in [40]. The size of a freely propagating beam is described by

$$w^2(z) = w_0^2 \left(1 + \left(\frac{\lambda z}{\pi w_0^2} \right)^2 \right) \tag{3.28}$$

This does not change at a lens. In this equation, as well as in equation 3.22 for the radius of curvature of a freely propagating beam, the focus is assumed to be at $z = 0$. Keeping that in mind, we can calculate the position z_{new} of the new focus after the lens and the size w_{new} of the beam there. To evaluate the phase difference Ψ between the zero order mode and the first order mode at a distance z_2 where we might want to place the quadrant diode or simply another lens, we have to calculate the phase picked up on the way to the lens and add the phase from the lens to z_2

$$\Psi(d_2) = \arctan\left(\frac{\lambda z_1}{\pi w_0^2}\right) + \left(\arctan\left(\frac{\lambda(z_2 - z_{\text{new}})}{\pi w_{\text{new}}^2}\right) - \arctan\left(\frac{\lambda(z_1 - z_{\text{new}})}{\pi w_{\text{new}}^2}\right)\right) \quad (3.29)$$

From this we can calculate positions for the quadrant diodes where they are only sensitive to one kind of misalignment. However in the real experiment, one also has to make sure that the beam size at such a position remains within reasonable values. One will also run into problems if Ψ is strongly changing near the desired diode position and imperfect placing of the optical components would strongly change the Guoy phase at the diode.

Usually a system of at least two lenses is preferable to just one or even no lens at all, because then we have the possibility to design a desired value and slope of the Guoy phase and simultaneously a desired beam size at the position of the quadrant diode, while using standard lenses.

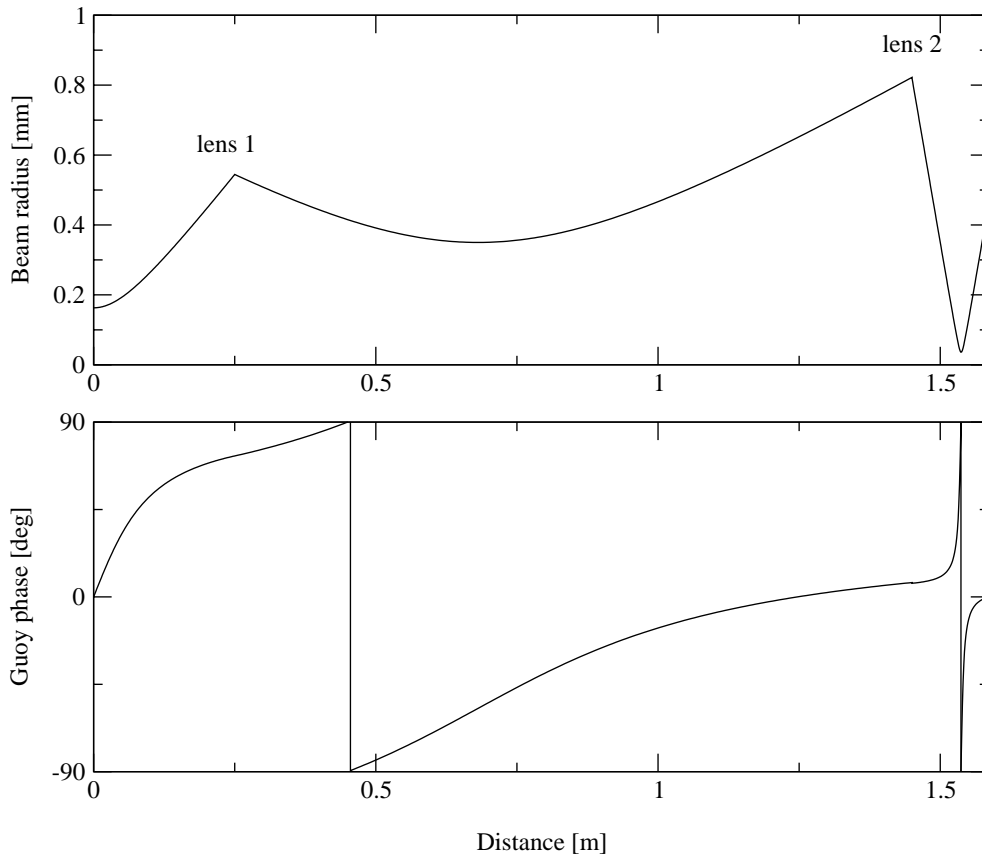


Figure 3.17.: Example of the beam waist and Guoy phase of a light beam propagating through a lens system of $f_1 = 0.2\text{m}$ at $z_1 = 0.25\text{m}$ and $f_2 = 0.08\text{m}$ at $z_2 = 0.981\text{m}$.

3. Optical set-up

In figure 3.17 we see an example of a two-lens system. The Guoy phase is zero at $z = 1.6$ m. This would be a possible place for a quadrant diode to detect angular displacement. On the other hand the beam size is relatively small and the slope of the Guoy phase is very steep, which would make the system susceptible to small misplacements of the diode or the lenses. For optimising all these parameters, we use a Mathematica program².

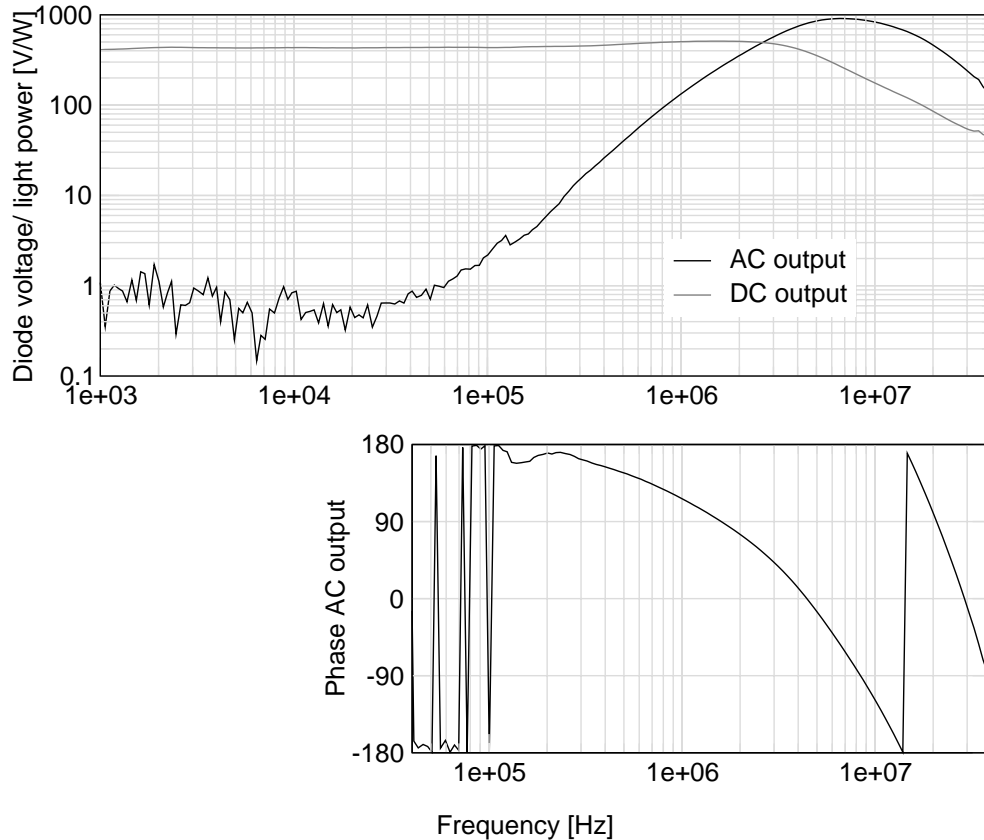


Figure 3.18.: *AC and DC response of a quadrant of the quadrant diode to an amplitude modulated light beam swept over all frequencies.*

The quadrant diodes used in the experiment are designed to be especially sensitive at the modulation frequency as we are only interested in detecting this single frequency. Other frequencies are suppressed to avoid adding unwanted noise contributions. The frequency response of one of the quadrants is shown in figure 3.18. It was measured by shining a laser beam that is modulated in amplitude onto one of the quadrants. The diode response was monitored while the modulation frequency was swept through the frequency range of interest.

²developed by G. Heinzl

3.5.3. Actuators for the alignment

After detecting the displacement signals, these can be used to overlap the laser with the resonator eigenmode. It would be possible to move the suspended resonator mirrors and thereby to shift the resonator mode, but we want to leave these mirrors as undisturbed as possible. The laser beam is shifted instead.

For that purpose C302 galvanometer scanners from General Scanning with a maximum range of 2° and a load free resonance frequency of 520 Hz are being used as actuators. The resonance frequency was expected to lower significantly after attaching a mirror. This could set a limit to what unity gain frequency can be achieved. The frequency of the second resonance would also be of interest, because if significantly far away from the first, one could place the unity gain frequency in between the resonances without exciting them too much.

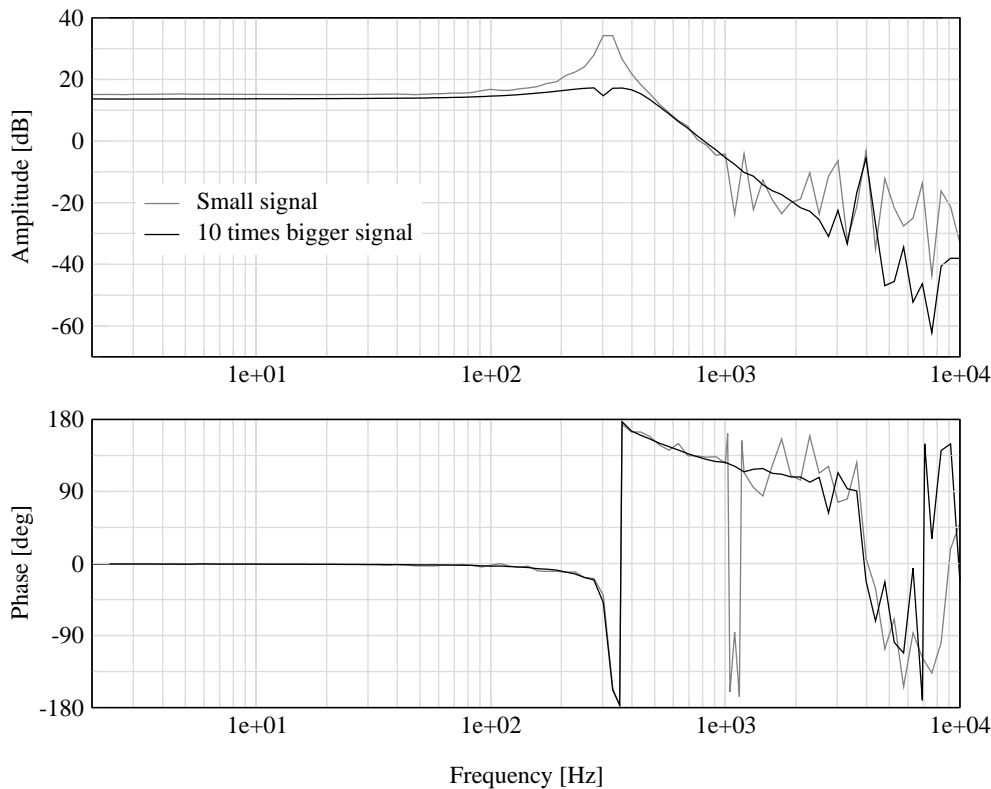


Figure 3.19.: Measurement to identify the galvanometer scanner resonance frequencies. It was done by reflecting a laser from the galvanometer mirror onto a quadrant diode. With too big signals at the scanner, the amplitudes at the first resonance frequency of 320 Hz exceeds the dynamic range of the quadrant diode. The second resonance frequency is at 4 kHz.

The resonance frequencies was measured by shining a laser on the mirror attached to the scanner and the light was reflected onto a quadrant diode. The signal at the quadrant diode divided

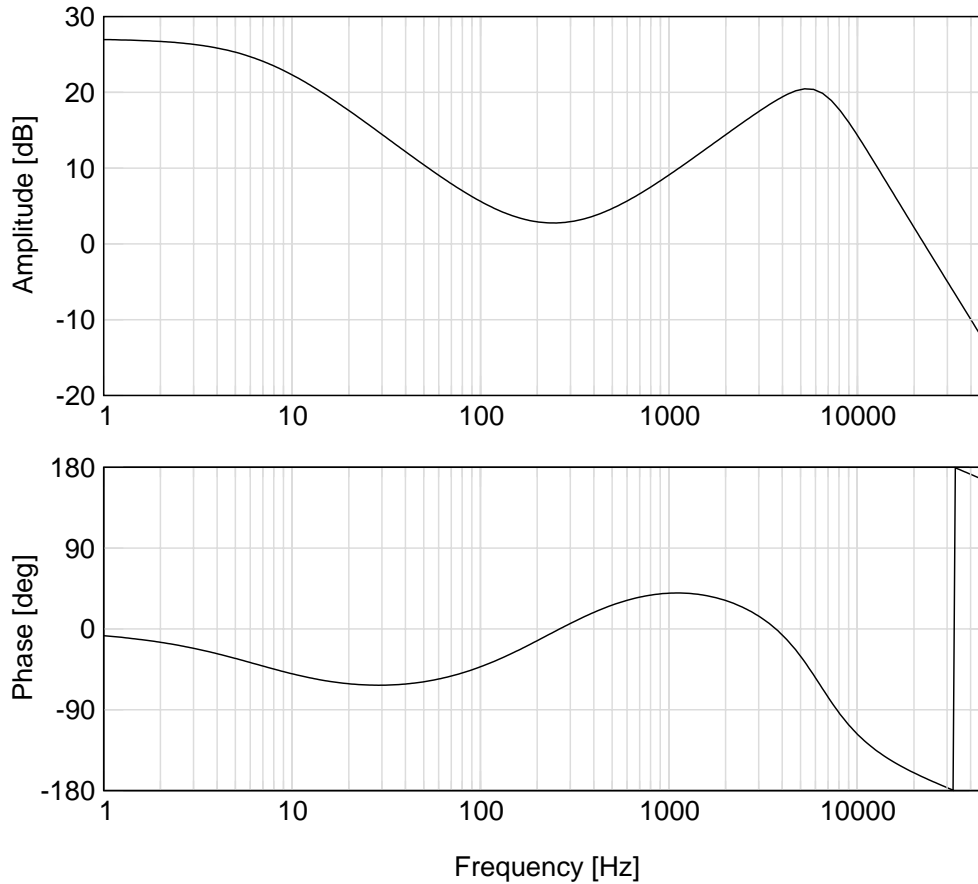


Figure 3.20.: *Measured transfer function of a controller for one automatic alignment channel. The rising slope around 1 kHz compensates for the galvanometer transfer function and allows a unity gain frequency in that region.*

by the signal at the scanner input is shown in figure 3.19. When the input signal was increased to make the second resonance more clearly visible, the movement at the first resonance exceeded the dynamic range of the quadrant diode. The first two resonance frequencies were measured to be at 320 Hz and 4 kHz, which is a big enough distance to build a feedback loop with a unity gain frequency in between. The slope which decreases by f^{-2} after the first resonance has to be compensated in this loop. The transfer function of a controller that is used for the automatic alignment system is shown in figure 3.20.

In total, four of these galvanometer scanners are needed to correct displacement and rotation of the laser beam in the x and y direction. As these actuators can only rotate around their axis, they produce only a rotation of the optical beam. During beam propagation, this introduced angle remains constant, while the distance to the old beam axis increases. Because of that, each actuator produces a linear combination of displacement and rotation of the optical beam away from the beam waist.

If the two actuators for the x direction are placed at two random points in front of the optical resonator, the detector signals for lateral shift and rotation could not simply be given to these actuators. None of them produces a pure rotation or shift at the resonator. That means that linear combinations of the detector signals are necessary before sending them to the galvanometer scanners.

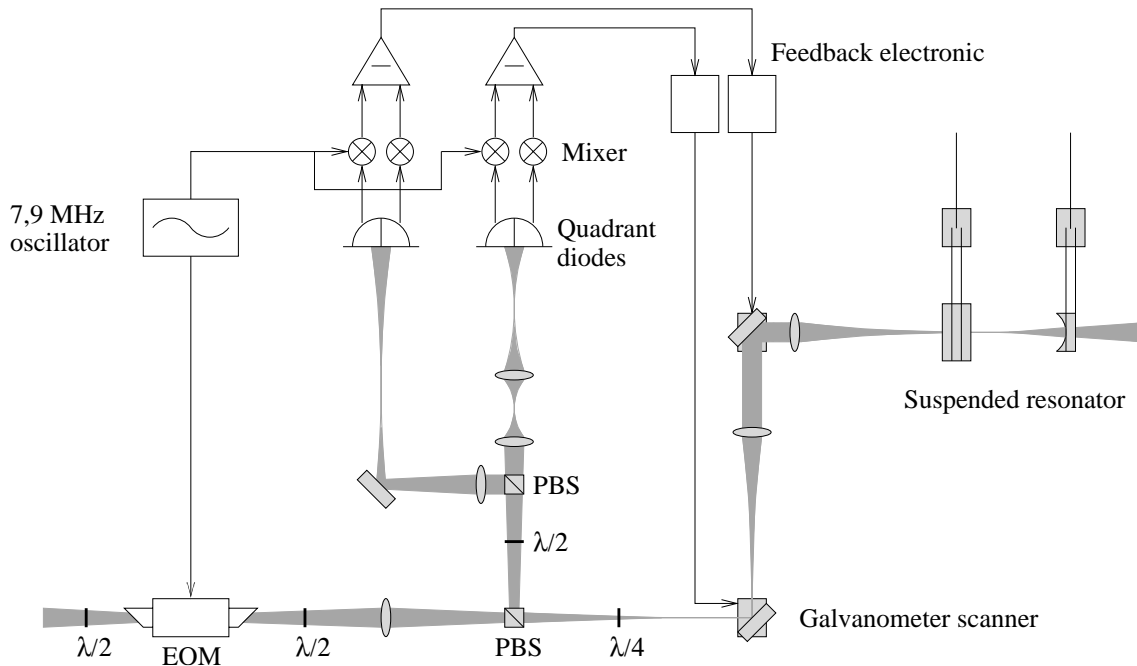


Figure 3.21.: *Set-up for the automatic alignment system. Several lenses are needed to match the laser beam to the optical resonator and to place the quadrant diodes at positions of correct Guoy phase and beam size. Two pairs of galvanometer scanners as actuators for beam rotation are placed in a focus, while the two actuators for lateral shift are placed far away from any focus.*

A proper placement of the actuators can avoid this problem (see figure 3.21). An actuator placed at the waist of the optical beam produces only a rotation and no lateral shift at the next beam waist. The optical resonator is also placed at a waist of the beam, which is carefully matched to the internal resonator waist by a lens system. Two actuators are needed for rotation, one in the x and one in the y direction. These two are separated from each other by a small distance (in this case 3 cm), but have to share one focus in the experiment. This means that both scanners will also produce a small shift of the beam at the resonator focus.

The actuators for lateral shift are placed far away from any beam waist (in this case 1.2 m). That will result in a strong beam shift at the resonator and only a small rotational contribution will be produced. Small unwanted actuations to the wrong degree of freedom can be tolerated, because they are strongly suppressed by the feedback loop for that degree of freedom.

Being able to completely separate the four alignment channels from each other has another

advantage. If only some or one of these channels is used, the other degrees of freedom remain nearly undisturbed.

3.5.4. Performance of the system

To close the alignment feedback loops, one has to keep in mind that the unity gain frequency is designed to be between two mechanical resonances. That means that we cannot slowly turn up the gain to the desired value, because the unity gain frequency would cross the first resonance where the phase is completely wrong and the lock would be lost. These kind of loop are known as conditionally stable and we have to close the loops with almost correct gains right from the beginning.

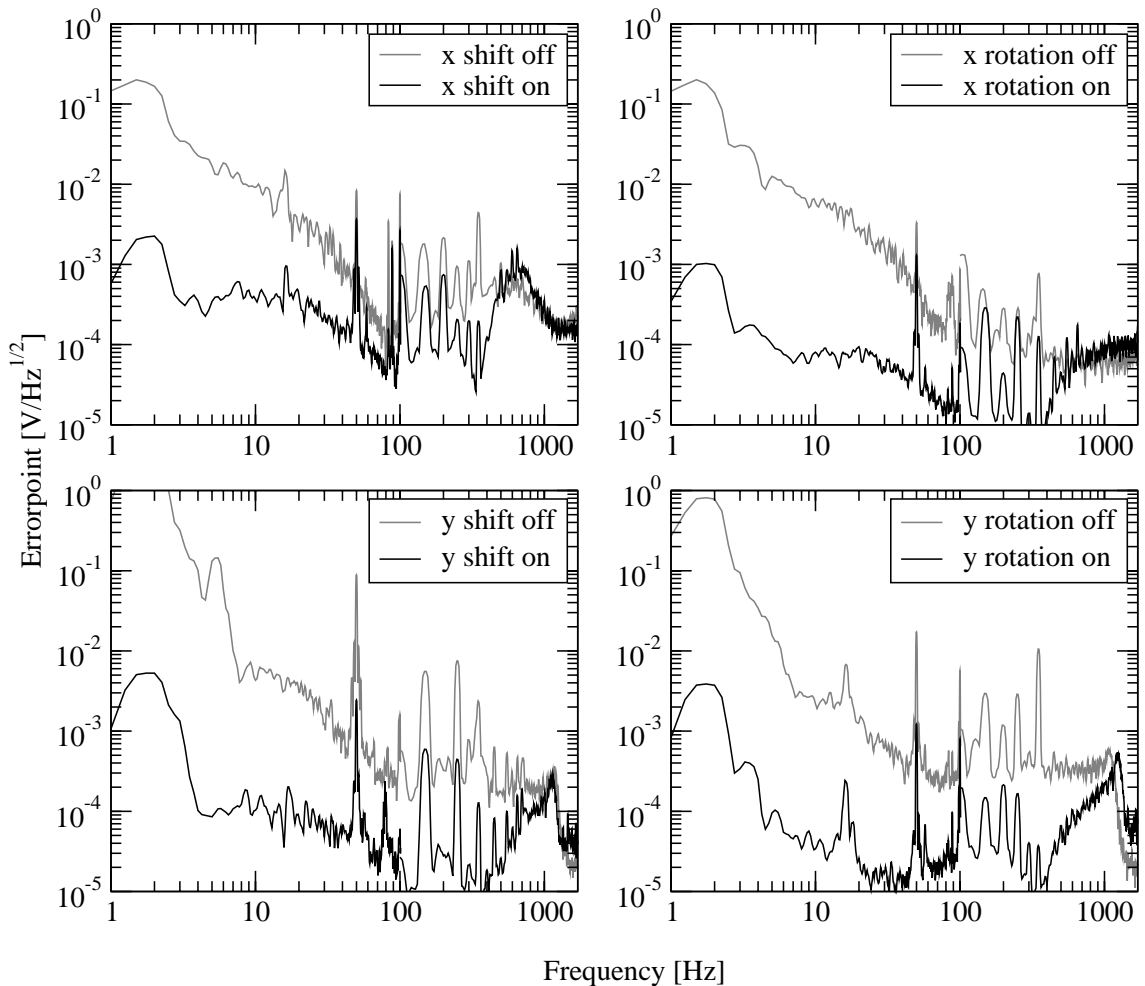


Figure 3.22.: Comparison of the error point signals of the different alignment channels when the feedback loop for each particular channel was operating and not operating.

From the error point signals of the different alignment channels (figure 3.22), the suppression of a disturbance in each channel can be seen when comparing these signals to those when the loop in that particular channel was not closed. The achieved unity gain frequencies are also visible. They range from 500 Hz to 1 kHz for the different degrees of freedom.

A disadvantage of the alignment system is the prolonged locking process. First the usual longitudinal feedback loop has to be switched on. Without it, the alignment system does not produce usable signals. After that the alignment channels are switched on one by one and each time it is possible that the longitudinal lock is lost again. The reason for that is that the better alignment leads to an increase of the light power in the cavity. This results in more gain in the longitudinal feedback loop, as well as in the alignment channels. Sometimes this produces strong oscillations due to the excitation of mechanical resonances and this could end the lock. The gain of the longitudinal channel and the alignment gains have to be reduced during the locking process. It is usually not possible to start with a low longitudinal gain right from the beginning, because the system would not be able to follow the big pendulum movements near 1 Hz. Reduced alignment gains are impossible, because unity gain would get too close to the 320 Hz galvanometer resonance.

The sensitivity of the experiment is neither increased nor decreased by introducing the automatic alignment system, which means that it is not limited by alignment noise. Before including the automatic alignment system into the experiment, the locking times were usually limited to one or two minutes due to the slow vertical drift of the isolated table and during the measurement the locking conditions were changing. Only with the optical table on the ground, long locking times have been achieved, but in that case the optical components were exposed to stronger seismic excitation. With the automatic alignment system locking times are of the order of one hour, sufficiently long for the measurements.

3. *Optical set-up*

Chapter 4

The seismic isolation

4.1. Introduction

Seismic noise is the biggest obstacle for an experiment where one tries to measure the thermal noise of the pendulum mode of a suspended mirror. A lot of effort was invested into building an effective seismic isolation system for this experiment. The main part of this isolation system is a multiple stage suspension system for the two mirrors (see figure 4.1). A computer program was developed to model the complex behaviour of these pendulums and to improve their performance.

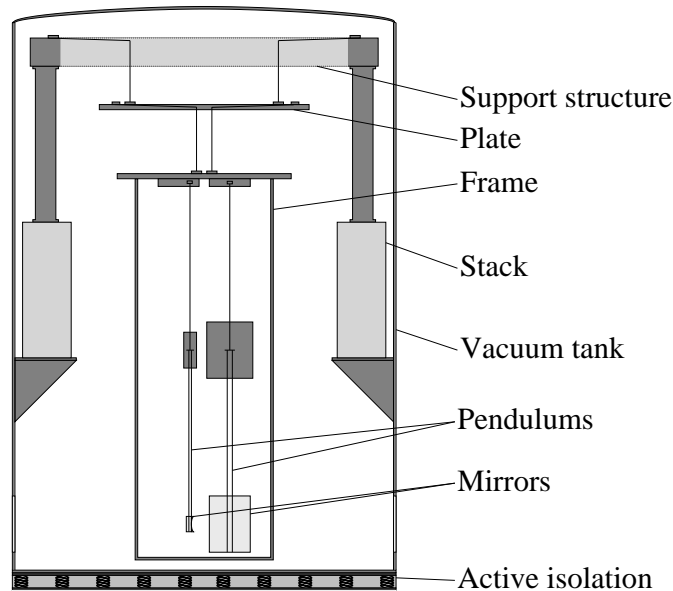


Figure 4.1.: *Schematic view of the seismic isolation system.*

A lot of attention has to be paid to the different degrees of freedom. Rotation and tilt motion, as well as the vertical motion, which does not get suppressed at all by a normal pendulum, couple

into longitudinal motion and cause a length change of the interferometer. This has to be considered when designing and building a seismic isolation system. During the suspension process, attention has to be paid to the alignment of the two mirrors with respect to each other, so that they form an optical resonator.

In a multiple stage pendulum, several pendulum resonances are present, and the seismic motion is significantly enhanced there. If the displacements at these frequencies are too big, locking could become altogether impossible. To reduce the resonant movement, an active damping system is applied to the pendulum chain, but one has to make sure that the performance of the seismic isolation is not degraded by this.

4.2. **Seismic noise**

Seismic noise has many different origins. They range from tectonic movements in the earth's crust, ocean waves hitting the land, wind shaking the building, cars passing by, people moving within the building to any other activity in which masses are being moved. Usually the seismic noise floor is slightly reduced at night because there is less human activity at these times. The location of the experiment can also play a role. For example at the site of the TAMA gravitational wave detector, located in the city of Tokyo, the seismic motion is significantly enhanced due to the higher tectonic and human activity there. In contrast to this, the GEO 600 detector is located away from the city with its human activity and it was build on a very solid basement. A good choice for any seismically sensitive experiment would be to locate it in former mine shafts within massive mountains where tectonic and human activity is reduced even further. This was the original plan for the GEO 600 detector and it is now planned for the next generation gravitational wave detector in Japan [42]. Our experiment is located within the city of Hannover at the ground floor of our institute. Compared to the GEO 600 detector we measure almost an order of magnitude more seismic motion.

The basic principle of an interferometric gravitational wave detector is to make very precise length measurements. If the mirrors used in these measurements move with unfiltered seismic against each other, the achievable sensitivity would be insufficient to detect gravitational waves. One possibility to overcome this problem would be to go to space where we have no seismic noise at all. This is one of the ideas behind the LISA mission.

Another alternative would be to try to isolate the mirrors from the motion of the environment. This can be done by springs or by suspending them as pendulums. The transfer function of a pendulum drops above its resonance frequency and isolation can be achieved, below the resonance frequency a pendulum does not provide isolation. If the suppression of one pendulum is not sufficient, one can cascade multiple pendulum stages to increase the achieved isolation. Exactly this feature is used in our experiment to achieve a rapid decrease of the seismic motion above the pendulum resonances.

Unfortunately, suspending the mirrors as pendulums also has its disadvantages. One of them is the appearance of pendulum thermal noise, which is what we want to investigate. Another one is

the enhanced motion of the pendulum chain at its different resonance frequencies. In gravitational wave detectors, pendulums with a very high Q are being used to reduce the pendulum thermal noise above the resonance, but this increases the seismic motion at the resonances even further. That is why an active damping system is needed at these frequencies.

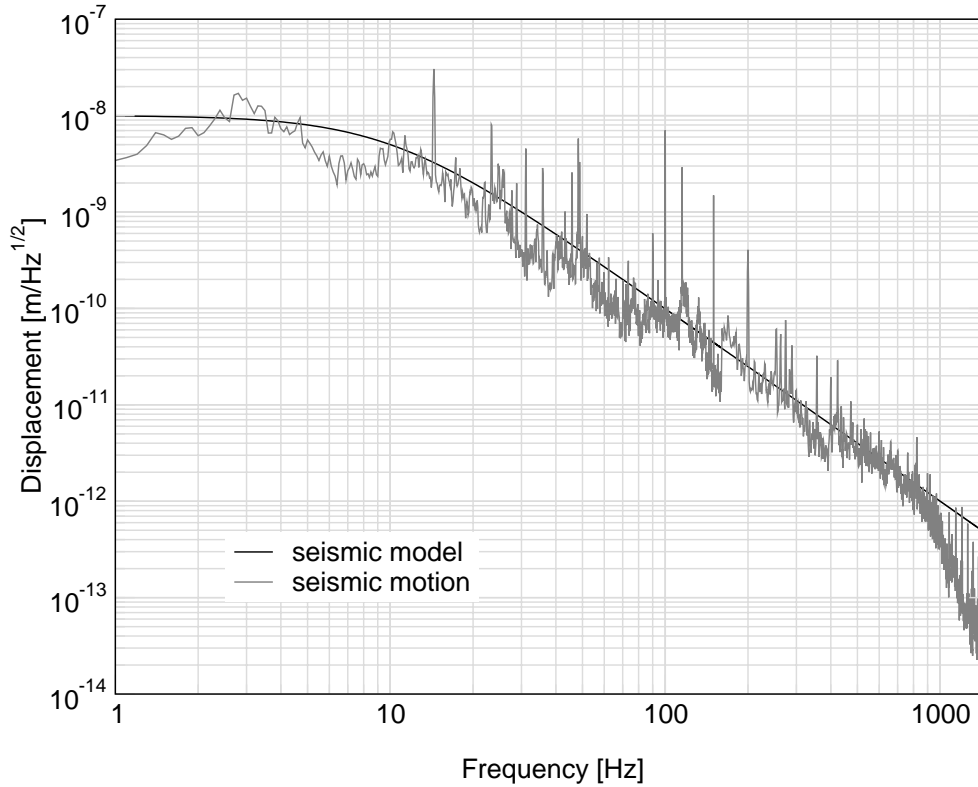


Figure 4.2.: *Seismic motion at the location of our experiment, measured in the vertical direction. Starting at 10 Hz, it drops with f^{-2} .*

A measurement of the seismic motion of the ground at the location of our experiment is shown in figure 4.2. The seismic noise is usually almost identical for the vertical and the two horizontal directions and can be approximated to be at a level of $10^{-8} \text{ m}/\sqrt{\text{Hz}}$ up to 10 Hz, after which it starts to fall with f^{-2} . The above measurement has a very typical shape for a seismic spectrum and this would not vary too much from location to location.

4.3. The basic idea of seismic isolation

To point out the general idea of seismic isolation, we will look at an idealised pendulum with a mass m and a length l , which is suspended at the center of mass (see figure 4.3). We will ignore all external forces to the pendulum except gravity, but we will allow the suspension point to move

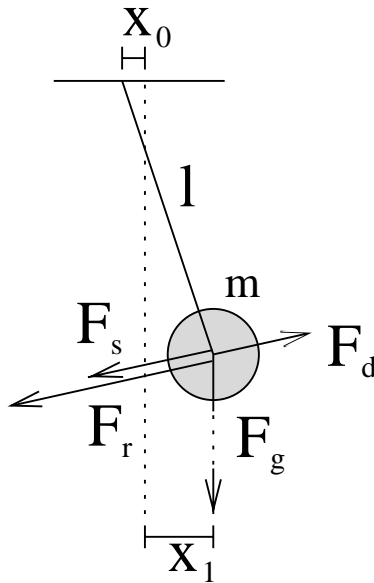


Figure 4.3.: *Idealised pendulum with the Forces acting on it.*

due to seismic. That means that we will not only get a restoring force $F_r = -kx_1$ if the pendulum has shifted away from its rest position by x_1 , we will also get a similar force F_s with opposite sign if the suspension point moves by x_0 . With this the equation of motion is

$$-m\omega^2 x_1(\omega) = -kx_1(\omega) + kx_0(\omega) + F_d \quad (4.1)$$

We ignored all damping forces F_d . The transfer function from a movement of the suspension point to a movement of the pendulum is

$$\frac{x_1}{x_0} = \frac{1}{1 - \frac{m\omega^2}{k}} = \frac{1}{1 - \left(\frac{\omega}{\omega_{\text{res}}}\right)^2} \quad (4.2)$$

This transfer function drops with ω^{-2} above the pendulum resonance frequency ω_{res} , which is given by

$$\omega_{\text{res}} = \sqrt{\frac{k}{m}} = \sqrt{\frac{g}{l}} \quad (4.3)$$

where g is the acceleration of the earth. For any reasonable pendulum length, the resonance

frequency will be near one Hertz. Below that, a pendulum does not provide any seismic isolation. It simply follows the movement of the suspension point. Near the resonance itself, the damping becomes important and equation 4.3 does not describe the true behaviour. Damping broadens the width of the resonance peak and it lowers its height, but for higher frequencies where ω^{-2} dominates, the description is valid again.

The ω^{-2} behaviour above the resonance provides a good seismic isolation for high frequencies, but in this experiment the suppression of seismic motion would not be sufficient at 10 Hz. To improve the isolation, one can suspend another pendulum stage from the first pendulum mass and additional pendulum stages after that. In such a chain, the mirror would be the mass of the last pendulum stage. The idea is that the suppressions of each individual stage add up to a big overall reduction of the seismic movement.

To calculate the effect of adding more than one pendulum stage together, one has to find a more elegant way than writing down the full analytical equations, because they get rather complex. That is why we describe the n th stage in a pendulum chain by a 2×2 matrix A_n . As an input to such a matrix we need the displacement of the previous pendulum stage x_{n-1} and the force F_n on the n -th stage due to this displacement. As an output, we get the displacement of the current stage x_n and the force F_{n+1} to the next. The multiplication of the matrices for the full chain will enable us to calculate the movement of the last stage due to a displacement of the suspension point of the first. It can be shown that the description for a single stage pendulum takes the form [70]

$$\begin{pmatrix} x_1 \\ F_2 \end{pmatrix} = \begin{pmatrix} 1 & -\frac{1}{k_1} \\ m_1 \omega^2 & 1 - \frac{m_1 \omega^2}{k_1} \end{pmatrix} \begin{pmatrix} x_0 \\ F_1 \end{pmatrix} = A_1 \begin{pmatrix} x_0 \\ F_1 \end{pmatrix} \quad (4.4)$$

For more stages, we have to multiply the result with A_2 and so on. Without a second stage, F_2 is zero and we get equation 4.3. The transfer functions for a single, double and a triple pendulum are shown in figure 4.4. The resonance frequencies of each individual stage in this simulation were 1 Hz, but when two or more stages are coupled together, the coupled resonances are shifted against the individual values. It can be seen that the overall suppression of a triple pendulum is already huge. It falls off with f^{-6} . Unfortunately, things are not that simple when we move from the idealized pendulums to real ones.

4.3.1. Coupling of the different degrees of freedom into longitudinal

In the case of an idealized suspension, an excitation of the other degrees of freedom in which the pendulum can move (see figure 4.5) does not affect the longitudinal motion. In a real suspension system, the situation is different. Each of these motions will result in a longitudinal movement of the mirror. The size of these contributions depends on the coupling between the different degrees of freedom into longitudinal and can be described by an effective coupling coefficient. These coefficients are usually very small, still we cannot neglect the influence of the other degrees of freedom. They are filtered in different ways by the pendulum chain, and if they are not suppressed

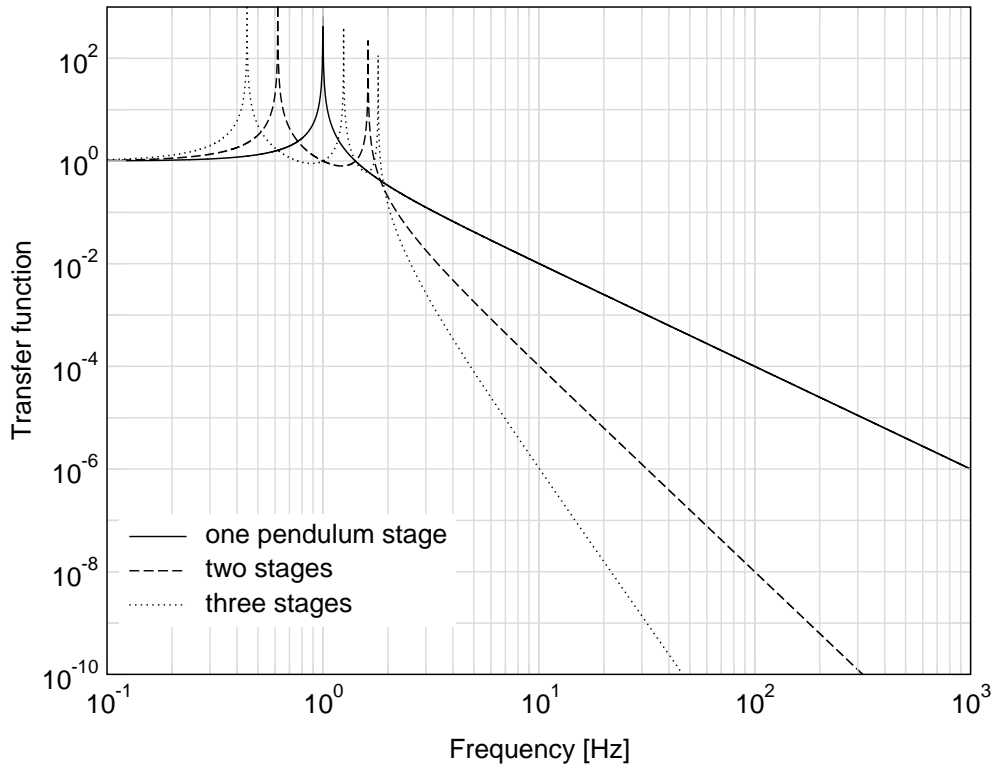


Figure 4.4.: *Transfer function from a movement of the suspension point to movement of the last stage of a single, double and a triple pendulum. The resonance frequency of each individual stage is 1 Hz.*

well enough, at some frequency one of these other degrees of freedom becomes the dominant noise source in the longitudinal direction.

In the case of rotation, the suppression of motion does not start with the longitudinal resonance frequencies, but with those for rotation. That means that during the design of the pendulum chain, one has to pay attention to the values of these resonances. They depend on many different parameters. It has to be remembered that the pendulum is not the previously assumed ideal one, suspended by only one wire in the center of mass. Such a construction would lead to an infinitely low rotational frequency. Four wires, attached at the outside of the mass, suspend the real pendulum. These are necessary in order to have well defined rest positions in tilt and roll. It also has to be remembered that the mass is not concentrated in the center, so the moment of inertia I plays a role. The full equation of motion for the rotation angle α in the case of a single stage pendulum is [68]

$$I\omega^2 \alpha(\omega) = \left[\frac{mg}{l \cos(\Omega)} (s^2 \cos^2(\Omega) + t_1 t_2) + \left(4k \frac{s^2 (t_2 - t_1)}{l^2} \right) \right] \alpha(\omega) \quad (4.5)$$

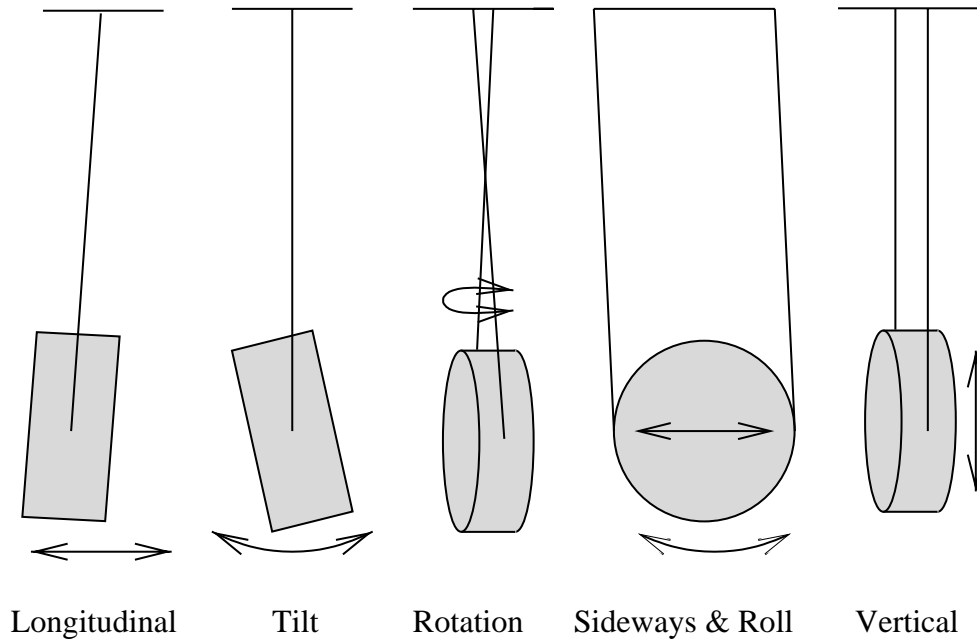


Figure 4.5.: *Degrees of freedom for a Pendulum. Longitudinal and tilt motion, as well as sideways and roll, are not independent of each other.*

s is half the separation of the wires on one side of the mirror from those on the other side. t_1 is half the separation of the wires on one side at the upper suspension point, and t_2 is half the separation at the lower suspension point. Ω is the angle in the wire caused by the difference between t_1 and t_2 and k is the spring constant of one wire. Damping is ignored here. The above equation has the same form than equation 4.1 without damping. That means that a 2×2 matrix can be found for rotation, similar to the one given by equation 4.4. With that matrix we can calculate the behaviour of the full chain in rotation.

So far we have only considered pendulum stages. A simple pendulum does not provide any filtering at all in the vertical direction. If the spring constant of the wire is included, we get some seismic isolation at high frequencies, but that is not sufficient. Over a wide range of frequencies, we would be limited by vertical noise coupling into the longitudinal. To avoid that, something similar to a pendulum is needed in the vertical direction. A spring would do the job, but it comes with too many internal resonances. Therefore we use cantilever blades at different stages. With this, a description similar to that in rotation can also be found for the vertical degree of freedom.

For tilt, and also for longitudinal, the situation is a lot more complicated. Tilt and longitudinal do not move independent of each other, and the two degrees of freedom have to be described with a combined 4×4 matrix for each stage. When we try to compute the complete transfer function for longitudinal or tilt from the overall 4×4 matrix, we have to pay attention to possible numerical instabilities [57]. Also, sideways and roll have to be described in a combined way.

We have developed a computer simulation for the behaviour of all the degrees of freedom of a multiple stage pendulum¹. After computing the seismic motion for all these degrees, we need the coupling coefficients to evaluate their effect on the longitudinal motion, which is the degree of freedom we are sensitive to (Note that some coefficients relate angular motion to longitudinal, in these cases they are not dimensionless). It is almost impossible to calculate the exact values of the coupling coefficients, because they strongly depend on unwanted imperfections in the suspension chain that are usually not included in theoretical models. Only a fit of the simulations to data of the longitudinal motion of a real pendulum gives us an estimate of the strength of the coupling.

It turns out that for frequencies below the pendulum resonances, the contribution of the different degrees of freedom is usually about a hundred times smaller than the longitudinal movement. For roll, it is even less than that. But at higher frequencies where the longitudinal drops rapidly, tilt or vertical can be the dominating noises, depending on the design of the pendulum chain. In such a case, the suppression of the seismic motion would be significantly less than what would be expected from the number of pendulum stages.

4.4. Building blocks of the seismic isolation system

To avoid excitation of the pendulum mirrors through the air by acoustic and by gas noise, and also to avoid refractive index fluctuations within the resonator, the mirrors are located within a vacuum tank with a pressure of $\sim 10^{-7}$ mbar. Because of that, the different elements of the seismic isolation have to be placed inside the vacuum chamber. To achieve a good vacuum, all components used within the tank have to be vacuum compatible. That means that no gas should evaporate from them. The main materials we used inside the vacuum system are steel and aluminium. Each part was cleaned in an ultrasonic bath before it was put inside the vacuum chamber, and after the cleaning process the materials were only touched with gloves to avoid contamination. We also used cleanroom cloths when working inside the vacuum tank.

The first element of the seismic isolation is a stack (see figure 4.6). It is identical to those included in the GEO 600 detector. The stack has a passive rubber stage and an active stage. The active stage consists of three geophones that are capable of measuring the motion of the stack in all three degrees of freedom. The geophones consist of a coil attached to a spring and a magnet, located within the coil. If the ground moves, the coil and the magnet move against each other and a Voltage proportional to the speed is produced. The measured signals are feedback to a piezo-electric actuator, capable of acting in all three spatial directions. In addition, there are two horizontal geophones on the ground and their signals are feedforward to the same piezo actuator. Because this is a feedforward loop, its signals do not interfere with the feedback signals when they are added to the same actuator. With the maximum voltage of 200 V, a dynamical range of $\pm 50 \mu\text{m}$ can be achieved for the piezo actuator.

Some of the components in the stack are not vacuum compatible. They have to be shielded from the rest of the vacuum chamber by a corrugated steel pipe. This has to be soft, not to

¹written by L. Ribichini

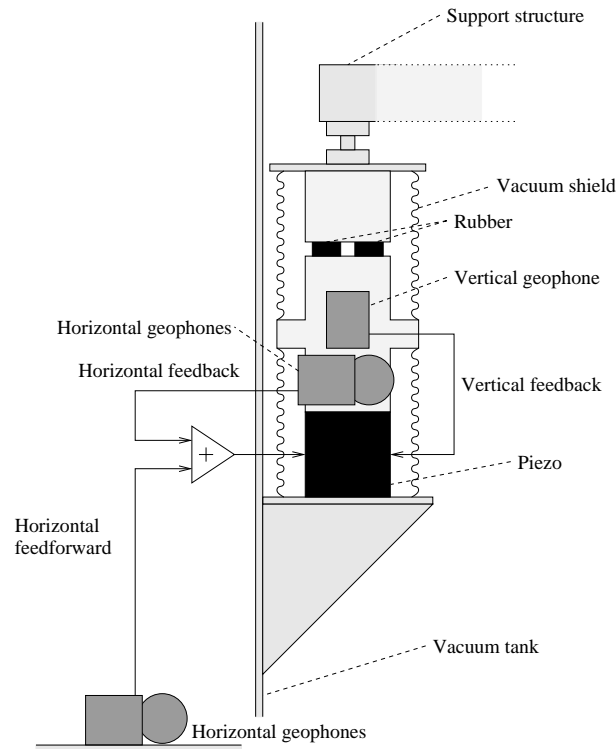


Figure 4.6.: Schematic view of a stack. The seismic isolation is achieved by a rubber stage and an active feedback system in the horizontal and vertical direction. In addition there is a feedforward system for the horizontal direction.

short-circuit the seismic isolation. The disadvantage of that pipe is, that the stack would expand significantly if the tank were evacuated. This would change the whole alignment of the pendulums in the tank. To avoid that, there is a separate vacuum system inside the pipe that has to be evacuated and vent simultaneously with the tank.

The suppression provided by the active isolation ranges in all directions from 2 Hz to 10 Hz and is usually less than a factor of three. The performance is limited by the sensitivity of the geophones at low frequencies and by internal mechanical resonances of the piezos at high frequencies [41]. This result is disappointing. There is no seismic isolation above 10 Hz, and around 1 Hz, where isolation would be important to have less excitation of the pendulum resonances, the stacks do not provide an improvement. In addition to that, the piezo in one of the three stacks used in this experiment is broken. The pendulums are suspended to a support structure that rests on all three of the stacks. This means that seismic motion reaches the suspension point almost unfiltered through the broken stack. Measurements usually showed no difference if the active isolation system was used or not.

Recently, a commercial active isolation system was purchased² and placed under the vacuum

²The MOD-SW 1050 from Halcyonics

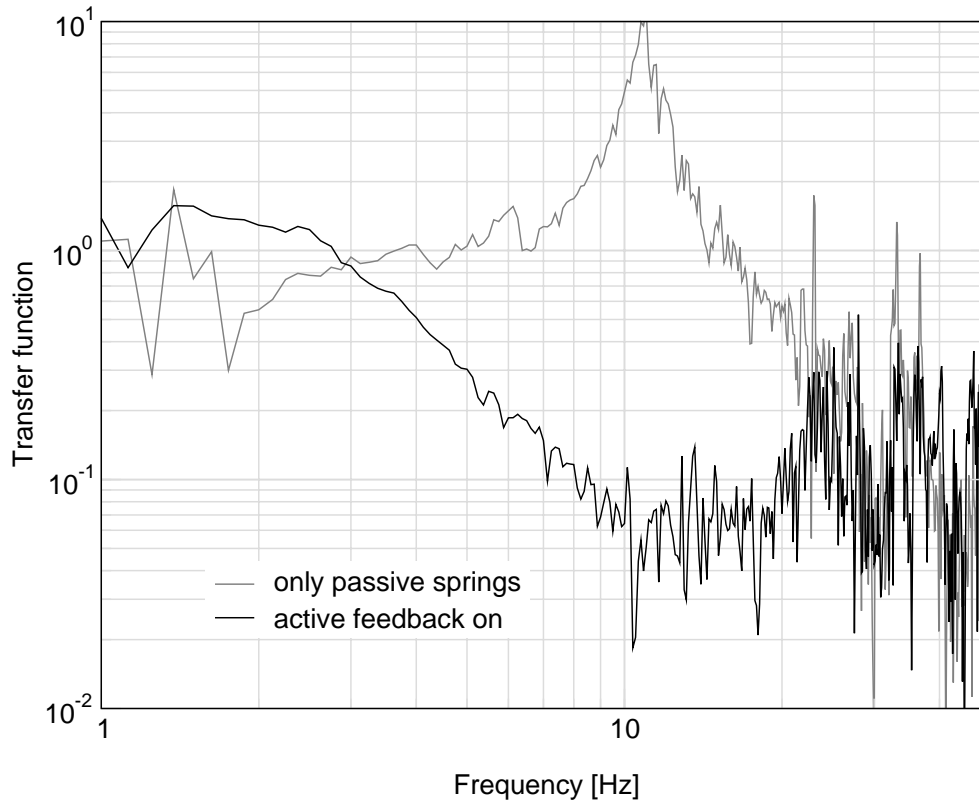


Figure 4.7.: *Transfer function of the commercial active seismic isolation with the feedback turned on and off. The measurement was taken in the horizontal direction with a geophone on the ground and a second one on top of the isolation system. The passive part of the isolation consists of springs with resonance frequencies at 10 Hz. With the active feedback, a suppression by a factor of 10 at 10 Hz is achieved.*

tank. The system is capable of supporting the weight of the tank, which is ~ 1000 kg. This system does also not provide any isolation at 1 Hz, but its transfer function drops to 10^{-1} at 10 Hz and remains at that level up to high frequencies without the addition of new internal resonances. A measurement of the performance of the system in the horizontal direction can be seen in figure 4.7.

The system relies on springs with 10 Hz resonance frequencies and an active feedback. Placing the tank on such a soft spring system has turned out to be a major problem, because it makes working inside the tank very complicated. The tank is easily shaken and that moves the pendulums a lot. Not only can this damage the pendulum stages, the alignment of the suspended mirrors with respect to each other is very complicated in the presence of big mirror movements. During measurements, movement in the laboratory could easily shake the tank and throw the system out of lock, but the sensitivity improved by adding this active stage.

4.4.1. The pendulum chain

The main part of the seismic isolation is done by the pendulum stages. The first two are identical for both mirrors (see figure 4.8). They both have a weight of 18 kg. The advantage of the identical weight for different stages is, that they have coupled resonances. These can be damped at either of the two stages, so it is not necessary to apply damping to each mass.

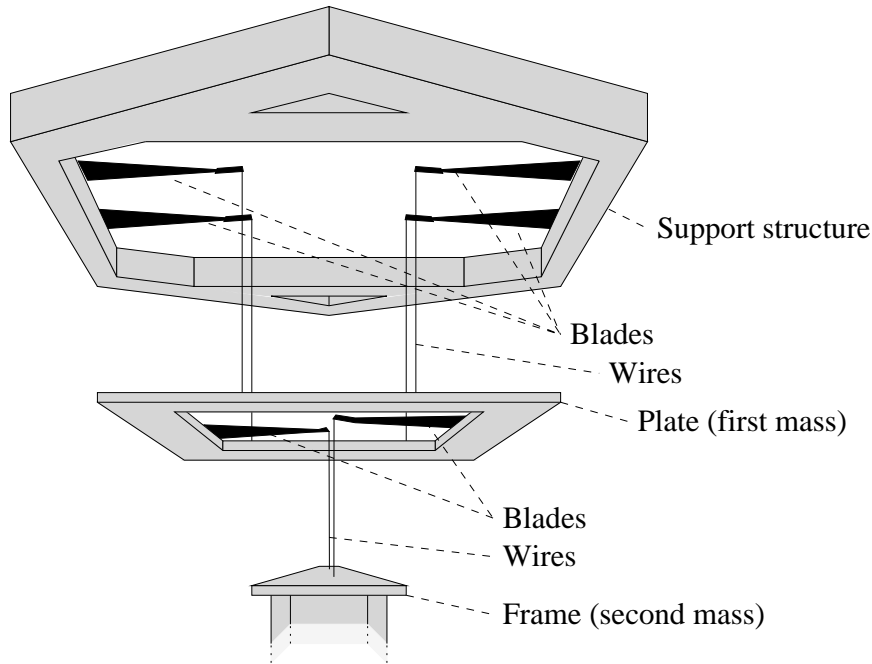


Figure 4.8.: *The first two pendulum stages. The plate with a mass of 18 kg is suspended to four cantilever blades for vertical isolation. The frame structure of the same weight is suspended to two blades that are identical to those above.*

The first mass, a simple steel plate, is suspended to four blade springs for vertical isolation. Each of these blades is bended upwards and is brought back into the vertical position by a specified load. For our blades, that load is 9 kg each. The vertical resonance frequency of the blades is 2.7 Hz and their length is 240 mm. They have a thickness of 2 mm. Identical blades are being used to isolate the GEO 600 mirrors that form the Michelson interferometer [55].

A second stage is suspended to the plate by two more of these blades. For the suspension of these first two stages, steel wires with a diameter of $550\ \mu\text{m}$ are being used. The length of the wires from upper to lower suspension point is 19 cm for the first two pendulum stages.

The second mass is a frame structure in which the main interferometer is suspended (see figure 4.9). The reason to use this rather complicated structure instead of a simple massive block lies in the fact that it has to house the three coils that are used for the longitudinal lock and the coils for the damping of the two pendulums. If these coils were simply attached to the ground, seismic

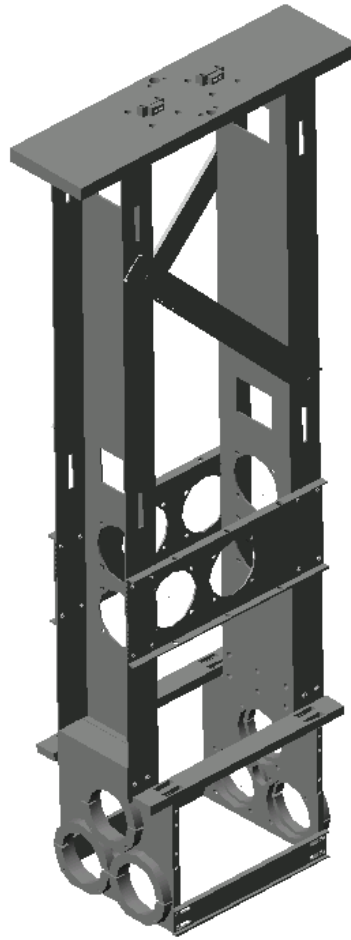


Figure 4.9.: *The second pendulum stage. It has a frame structure, because it houses the coils for locking and damping.*

motion might be coupled to the pendulum. This effect is reduced if the coils are attached to a pre-isolated structure.

The total height of the frame is 886 mm. The wires from the upper stage are attached at a steel plate at the top where most of the mass of the frame is concentrated. If the center of mass would be far below this suspension point, that would result in high tilt and roll frequencies for this stage.

If mechanical changes that include weight changes are applied to the pendulums within the frame, these changes have to be compensated for. To achieve that, the frame was designed to have a mass of less than 18 kg and removable weights are attached to it. If weight would be added to the pendulums without reducing the mass of the frame, this would overstretch the blades to which the frame is suspended. This could cause the operating point of the blades to leave the linear regime. In our set-up, there is also the possibility that the frame touches the ground if the blades bend

down too much. On the other hand, if the blades would be understretched by a weight reduction, their resonance frequencies would shift towards higher frequencies. A change of the vertical frame position could also cause the damping magnets to touch the glass cylinders that surround them (see section 4.5).

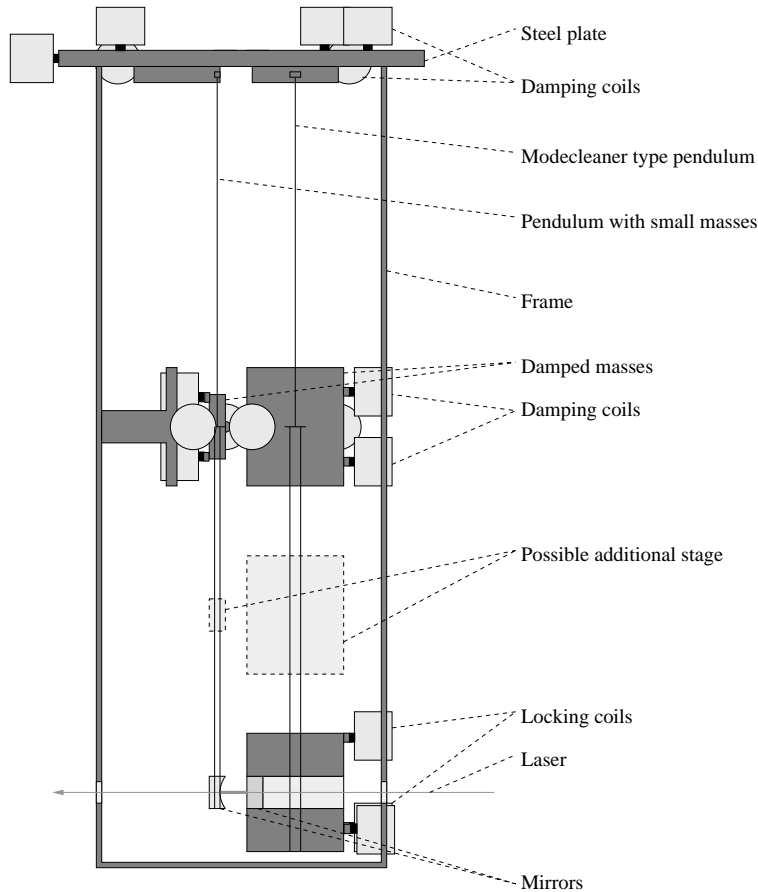


Figure 4.10.: *The mirrors are suspended within the frame as double pendulums. At some point, even a third stage was included, but it was removed later. The upper masses of the pendulums are damped against the frame. The coils for the longitudinal lock are also attached to the frame.*

Within the frame structure two mirrors are suspended as double or even triple pendulums (see figure 4.10). The more massive of the two pendulums is very similar to a GEO 600 modecleaner suspension. Its upper mass is a solid aluminium block of $50\text{ mm} \times 70\text{ mm} \times 85\text{ mm}$. The lower mass and the third mass that was used for some time are aluminium cylinders with a length of 50 mm and a diameter of 100 mm . In the middle of these is a hole with a diameter of 50 mm in which the mirror can be placed. All masses have the same weight of 800 g to ensure a good coupling between the resonances.

The damped mass is suspended by two steel wires with a diameter of $125\text{ }\mu\text{m}$. These are

4. The seismic isolation

attached at the height of the center of mass. From this stage, the mirror mass is suspended by two steel wire slings with a wire diameter of $100\ \mu\text{m}$. The upper suspension point of these wires is 12.5 mm below the center of mass of the damped stage, the lower suspension point is located 2.5 mm above the center of the mirror mass. The separation between the two wire slings is 4 mm. In principle, one would prefer to suspend each of these stages as close to the center of mass as possible to get very low tilt resonance frequencies, but the mass becomes impossible to handle if all wires are located very close to the center of mass, because the rest position will always be tilted. The length of the upper pendulum stage is 500 mm and that of the lower is 300 mm.

To increase the effect of pendulum thermal noise, a pendulum chain with very small masses would be desirable, because the effect of thermal noise increases with smaller masses (see equation 2.10). On the other hand, magnets have to be attached to the masses to damp the pendulums and to lock the interferometer. In addition, the size of the damping coils surrounding the magnets requires some spacing between neighbouring magnets, so that there is enough room for the coils. This puts constraints on how small we can make the masses. In the end we decided to build one small and one big pendulum. Including one big pendulum does not decrease the thermal noise, because we still have one small mass that can be moved by thermal effects. The locking magnets are attached only to the big pendulum because it provides enough space for them, and we want to leave the small pendulum that dominates the differential movement of the resonator as undisturbed as possible by other noises entering the system through the feedback.

The damped mass of the second pendulum has to include four magnets, and these magnets have to be placed within the damping coils. These are moved as close together as possible. The main part of the damped mass consists of four arms to connect the magnets and the wire suspension points with each other. The weight of this aluminium construction is 50 g and we chose the mirror mass to be of the same weight to achieve a good coupling. The mirror itself only weights 8 g, so it has to be surrounded by an aluminium mass to match the weight and to be able to attach the wires. The attachment points of the wires are 5 mm above and 5 mm below the center of mass at the damped stage and 2.5 mm above the center of mass at the mirror. The separation of the two wire slings is 2 mm.

The diameter of the upper two steel wires is $100\ \mu\text{m}$ and the diameter of the steel wires used to suspend the mirror is $90\ \mu\text{m}$. This was varied for some measurements. Thermal noise scales with the inverse of the square of the pendulum Q and this increases with smaller wires. We tried to enhance thermal effects by using 0.8 mm tin wires, and we reduced the mirror mass to 2 g. The pendulum Q of this set-up was determined by a ring down measurement. It was measured to be ~ 25 , with a resonance frequency of 7.5 Hz, but the construction did not behave like a normal pendulum any more. There was no longer a well-defined rest position and the sensitivity decreased a lot for this set-up. On the other extreme, we were able to suspend the mirror to tungsten wires with a diameter of no more than $26\ \mu\text{m}$. These are barely visible and very hard to handle. We even experimented with a $10\ \mu\text{m}$ wire.

Two pictures of the complete pendulum chain inside the vacuum tank can be seen in figure 4.11. The additional mass between the damped stage and the mirror was included at the time. The wires on both sides carry the necessary electronic signals to the coils that are attached to the frame.

4.4. Building blocks of the seismic isolation system

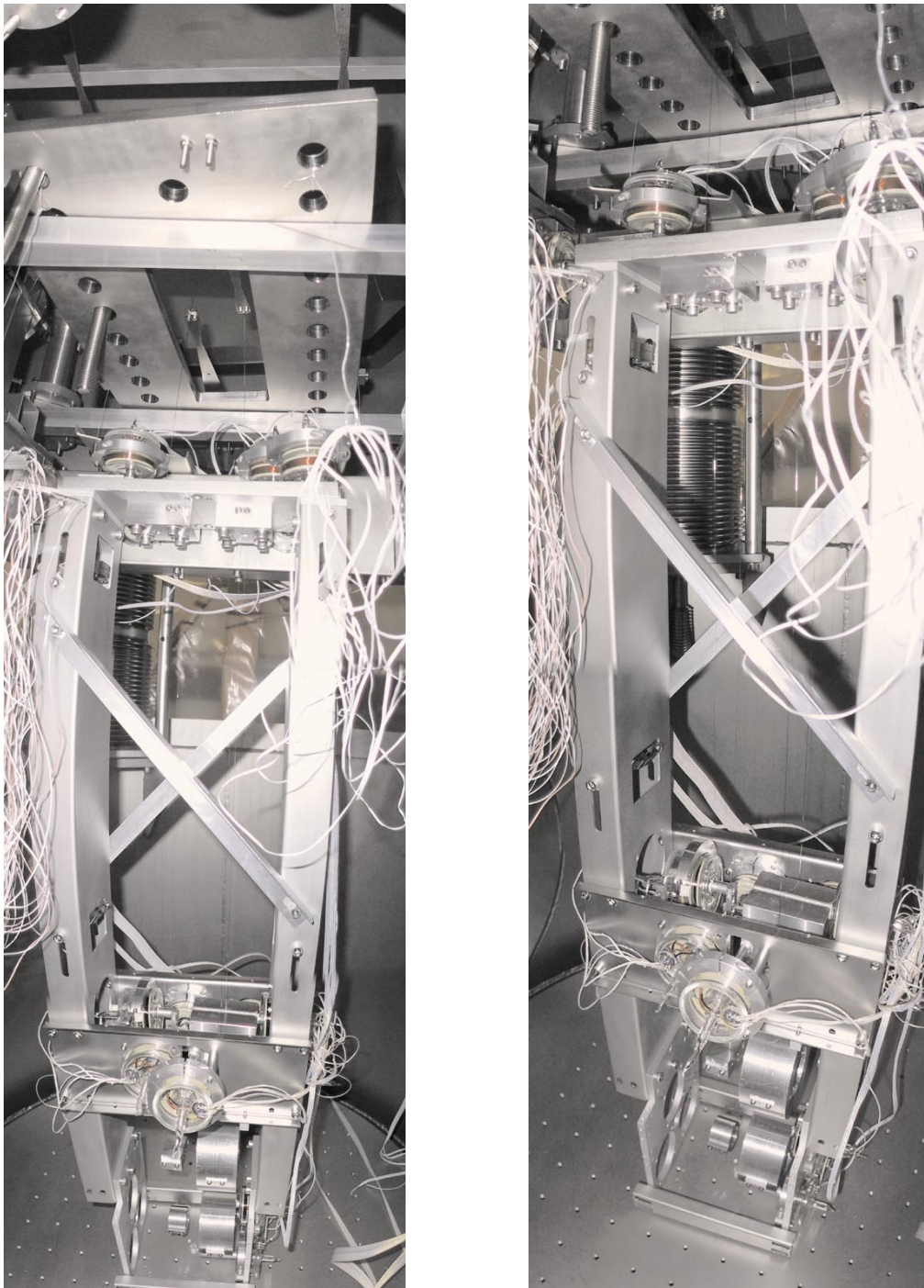


Figure 4.11.: *The complete pendulum chain inside the vacuum tank.*

These vacuum compatible wires are suspended from the steel plate and are unstretched, so that no movement from the ground is transmitted to the steel plate or from the plate to the frame.

4.5. Damping of the pendulum resonances

We use shadow sensors to detect the signals necessary to damp the resonant movement of the frame. Each of them consists of a LED that emits light onto a photo diode (see figure 4.12). A flag is attached to the pendulum stage and blocks part of this light, so that a movement of the pendulum changes the photocurrent. The photo diodes have an active surface of 3 mm^2 . This limits the dynamical range of the sensor to 3 mm. After suspending the pendulums, the positions of all the shadow sensors have to be adjusted to make sure that the flag is within the dynamical range.

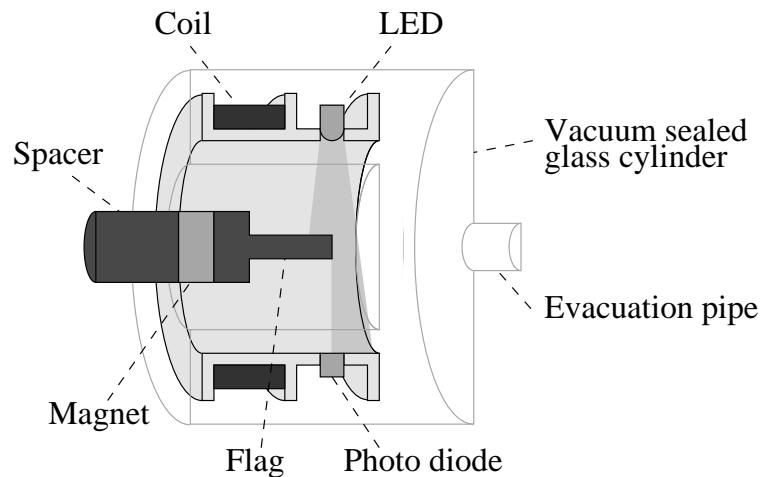


Figure 4.12.: *The vacuum sealed glass cylinder that houses the shadow sensor. It consists of a LED and a photo detector. A flag attached to the pendulum cuts a fraction of the light. The coil that acts on the magnet is also located in the cylinder.*

The shadow sensor signal is given to a control electronic and from there to a coil located in front of the shadow sensor. This produces a magnetic field gradient that acts on a magnet located behind the flag. The coil and the shadow sensor are not vacuum compatible, so they have to be placed within a vacuum sealed glass cylinder. The cylinder has to contain a feedthrough for the electronic signals. This is glued with Vac-Seal into a hole in the glass. The cylinders are leak checked, but to make sure that as little gas as possible leaks out of them, the inside of the glass cylinder is evacuated. To close the coils, the pipe through which the glass cylinder is evacuated has to be melted down while the cylinder is under vacuum.

The feedback loop for damping the pendulum resonances is designed to have two unity gain frequencies. The lower one is at $\sim 0.5 \text{ Hz}$, below the lowest pendulum resonance. Damping at even

lower frequencies would achieve nothing, because below the resonances the pendulum already follows the movement of the environment. The upper unity gain frequency is at ~ 4 Hz, just above the resonances. At even higher frequencies, damping must be avoided because it couples the pendulums to the environment and, by this, acts like a seismic short-circuit. It must also be avoided to couple noise from the damping electronic to the pendulum.

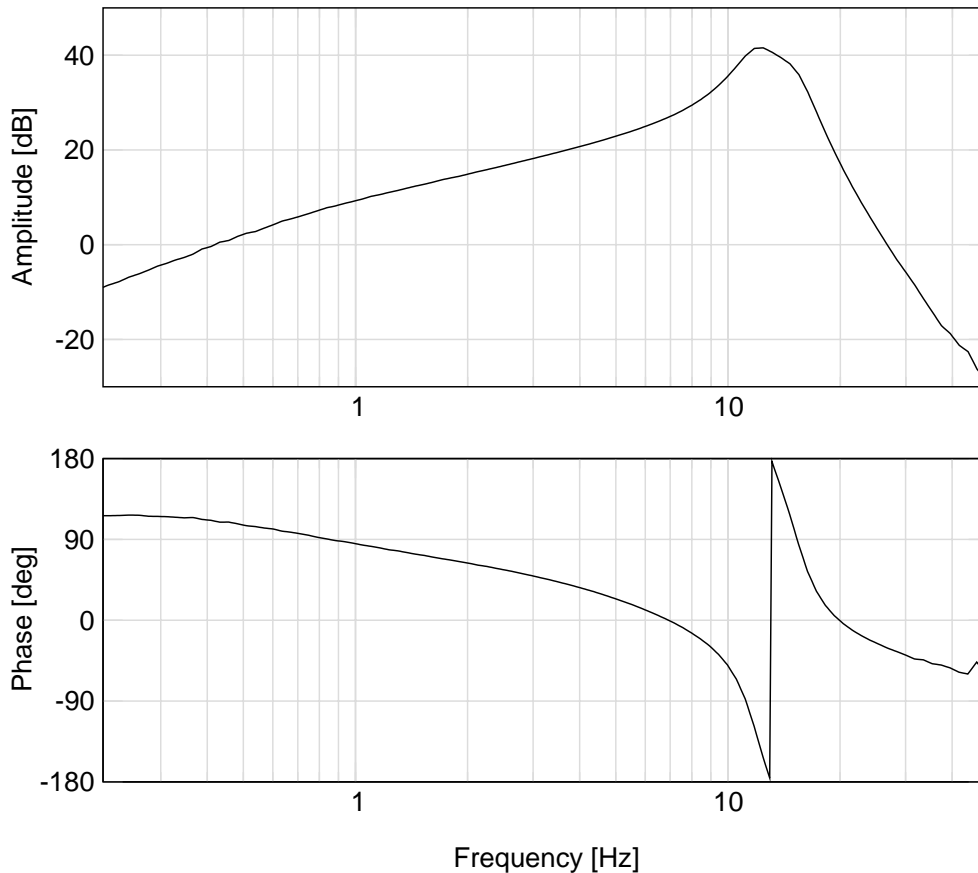


Figure 4.13.: *Transfer function of one channel of the damping control electronic. It rises at the upper unity gain frequency of ~ 4 Hz to compensate for the f^{-2} of the pendulum. After that it drops strongly to avoid excitation of high frequency resonances.*

The transfer function of the damping electronic rises at both unity gain frequencies with f (see figure 4.13). Together with the pendulum transfer function to an external force, which drops with f^{-2} above the resonances, the upper unity gain frequency is crossed with the usual f^{-1} . The strong drop in the electronic transfer function above 10 Hz avoids the excitation of higher frequency suspension resonances, the lowest of those is located at ~ 33 Hz. This is the first vertical resonance of the pendulums inside the frame. It is dominated by the stretching of the steel wires, because no blade stages are included here.

At the steel plate of the frame, all six degrees of freedom are damped (see figure 4.14). For the

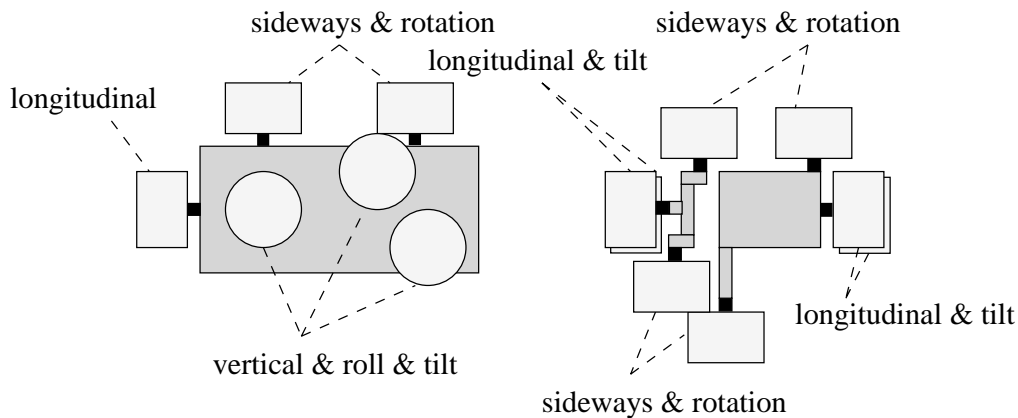


Figure 4.14.: Positions of the damping coils at the steel plate of the frame and at the damped masses, seen from above.

pendulums inside the frame, damping in vertical and roll is not necessary because the resonance frequencies for these degrees of freedom are very high. The seismic motion reaching the frame is already filtered at these frequencies and the resonances are not excited very much.

Most of the shadow sensors do not detect the movement of only one degree of freedom, but a mixture of two or three. It is not necessary to separate the different degrees of freedom by building linear combinations of the shadow sensor signals, because every coil acts back on the same combination of degrees of freedom that its shadow sensor detects. The advantage of locally reducing the movement of each flag with respect to its shadow sensor is that the electronic channels are independent of each other. Each of them can be changed or turned off almost without influencing the performance of the others.

An example for the damping of the resonant movement of the motion of the bigger pendulum is shown in figure 4.15. It was observed by detecting the shadow sensor signal of one of the coils. The damping clearly reduces the movement between 0.5 and 4 Hz. Without the damping of the pendulums against the common reference of the frame, the resonant movements of the individual pendulums are too big to allow a locking of the resonator. The damping of the frame is not equally critical. Long locking times can be achieved without it. The damping of the individual pendulums against the frame ensures that they follow the resonant movement of the frame and this common movement does not change the length of the resonator itself.

4.5.1. Prealignment of the interferometer

For the suspension of the pendulums we use a jig. That is a metal spacer on which the pendulum masses are fixed at the correct distance from each other. When the wires are attached to these masses, they are kept under tension by a weight that is equal to what they have to carry when the pendulum is suspended. This prevents a stretching of the suspended wires at a later point. The

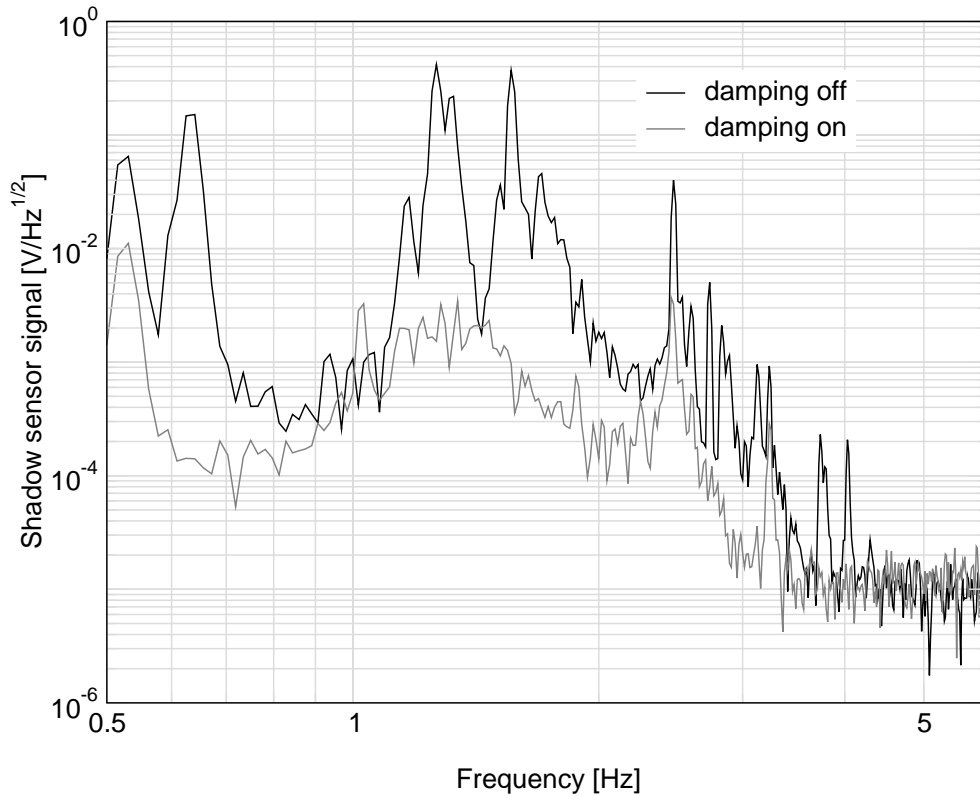


Figure 4.15.: Signal of the upper of the two shadow sensors for tilt and longitudinal at the big mirror. With the closed feedback loop the resonant movement between 0.5 and 4 Hz is significantly reduced.

separations of the wire slings from each other and their mean positions have to be as equal as possible on both sides of the mass to reduce a tilt or rotation of the rest position of the suspended masses. Still small imperfections in the suspension will always remain. With magnets from the two suspended pendulums close to each other, we can get an additional misalignment from the magnets acting on each other. Using weaker magnets could reduce this, but then stronger currents at the coils would be required.

Unwanted deviations of the rest positions of the pendulums from their designed values cause two problems. First, if the two mirrors are not parallel to each other, they do not form a cavity, and second, the damping magnets could touch the glass cylinders of the shadow sensors, which would lead to a seismic short-circuit of a pendulum stage. Each glass cylinder has to be checked for this, and its position has to be adjusted. To adjust the pendulums themselves, small weights can be added to the damped masses to level the tilt. In addition, the suspension points at the mirror masses are designed to be adjustable in the horizontal direction. Moving one of them causes a rotation and a tilt of the mirror mass at the same time. By moving the suspension points on both sides, the mirrors can be adjusted to parallel positions with respect to each other. It depends on

the curvature of the mirrors how parallel they have to be until there is a mode inside the suspended resonator. With two almost flat mirrors, the adjustment has to be more precise than with strongly curved ones, but strong curvatures also come with the disadvantage of a bigger beam away from the resonator.

The size of a propagating laser beam and of the resonator mode are described by equation 3.28. The beam size $w(z)$ is a hyperbola with asymptotes that have the angle θ with respect to the propagating axis.

$$\theta = \frac{\lambda}{\pi w_0} \quad (4.6)$$

The radius of curvature of the resonator mode at the mirror surface has to be equal to the curvature of the mirror. With equation 3.22 it is possible to calculate the beam waist inside the resonator. From this we get the angle θ , which gets bigger with stronger curved mirrors. If we propagate the resonator mode away from the beam waist, its size increases until it meets a lens. In this set-up where the last lens in the laser beam is outside the vacuum tank on the optical table and at least 1 m away from the resonator, the beam size might exceed the geometric dimensions of the optical components if it has to match a small resonator waist. Because of that, the choice of the radius of curvature for the resonator mirrors is a compromise between the laser beam size and the ability to align the resonator.

The bigger one of our mirrors is flat, and the smaller one has a radius of curvature of 1 m. With the resonator length of 2.5 cm, the beam waist is $230 \mu\text{m}$, located at the surface of the flat mirror. To check the alignment of these two mirrors, we overlap the incoming invisible laser with a visible one at a wavelength of 633 nm. A fraction of the light from the laser at this wavelength is reflected from the highly reflective sides of the mirrors, as well as from the non-reflective sides. If it is possible to overlap the reflection from the curved side of the small mirror with the superimposed reflections from the big mirror, there is a mode inside the resonator. If the reflection from the flat backside of the curved mirror is also overlapped with the others, the mode is in the center of that mirror.

The axis of rotation and tilt for the mirrors are supposed to be close to the center. If the resonator mode is nearby, it should be less sensitive to coupling from other degrees of freedom to the longitudinal. With only mechanical adjustment, it will almost never be possible to adjust the mode to this position, but it can be achieved with adjustable DC currents through the damping coils. If this is done, attention has to be paid to the noise in the electronic reference and to the position changes of the magnets inside the glass cylinder to avoid a seismic short-circuit there. Usually, the sensitivity of the experiment does not improve by moving the resonator mode exactly into the center of the mirror in the described way.

Chapter 5

Sensitivity of the experiment

5.1. Introduction

In order to read out the differential movement of the suspended mirrors, it is necessary to lock the length of the resonator to the laser frequency and to monitor the feedback signal. Below the unity gain frequency of a few hundred Hertz, this signal is proportional to the pendulum movement if the contributions of all other technical noises are sufficiently small. To achieve a lock, the frame had to be placed inside the vacuum system and the local damping of the resonant pendulum movement had to be used. When the pendulum movement was reduced sufficiently to allow the longitudinal actuator to lock the resonator length, the system was investigated to identify and to reduce the noise sources that limit the performance.

The first lock was achieved when the frame structure was still on the ground inside the vacuum tank and two 900 g mirrors were used. The sensitivity of this set-up was high enough to be limited by frequency noise of the unstabilized laser at high frequencies. The laser frequency stabilization had to be used to achieve a good performance. With the frame on the ground, the differential mirror movement at the pendulum resonance frequencies was smaller than with a suspended frame. This made it easier to lock the system, but the seismic motion contributed strongly to the pendulum movement at higher frequencies and limited the sensitivity.

With a frame suspended as a double pendulum and with blades for vertical isolation at both stages (see section 4.4.1), a much better sensitivity was achieved (see figure 5.1). The mass of the stages of one pendulum was reduced to 50 g without decreasing the performance of the system.

To achieve this sensitivity and to find ways to increase it even further, it was necessary to investigate all possible noise sources and to evaluate and possibly reduce their contribution to the spectrum. This includes:

- Optical noises that originate in the laser system or in the optical path of the laser beam. These can result in frequency noise, amplitude noise and a displacement of the laser beam.
- Electronic noises of the building blocks of the different feedback loops can limit the read-out sensitivity.

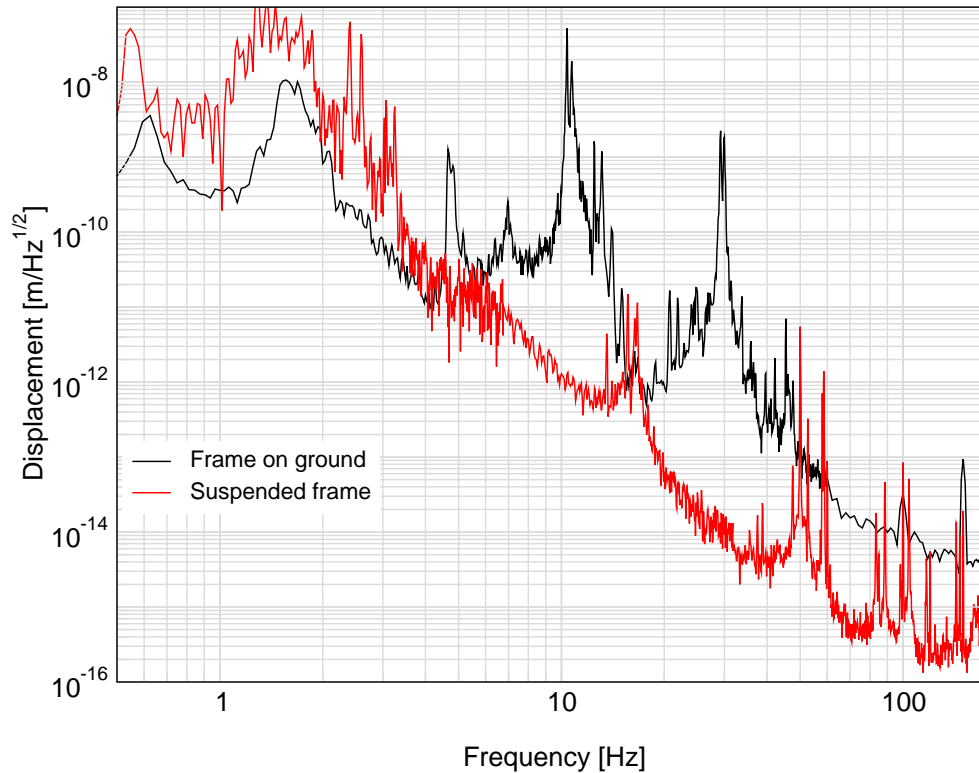


Figure 5.1.: Sensitivity for the frame on the ground inside the vacuum tank with two 900 g mirrors and for one 50 g mirror with the complete seismic isolation system in place.

-Noise forces that act on the pendulum directly. This not only includes seismic motion, but also other unwanted forces on the mirror from the seismic isolation system or from the environment.

5.2. Frequency noise

One noise source that has to be considered is laser frequency noise, because it is directly equivalent to a length noise of the cavity (see equation 3.11). If the laser frequency is not stabilized, this noise dominates the sensitivity from ~ 30 Hz up into the kHz region. (See figure 5.2). Unity gain for these measurements was at 200 Hz, at higher frequencies the error point signal has to be monitored instead of the feedback signal. The known magnitude of the laser frequency noise of the unstabilized laser provides a rough check of the calibration of the error point and the feedback point. From the length of the suspended resonator of 2.5 cm we can calculate that $10^{-16} \text{ m}/\sqrt{\text{Hz}}$ agrees with a frequency noise of $1 \text{ Hz}/\sqrt{\text{Hz}}$. The frequency noise reaches this level at 10 kHz, which is what we would expect from equation 3.17.

If the frequency stabilization is included (see section 3.4.1), the frequency noise of the laser system is reduced strongly and other noises limit the performance. Some of these could still be

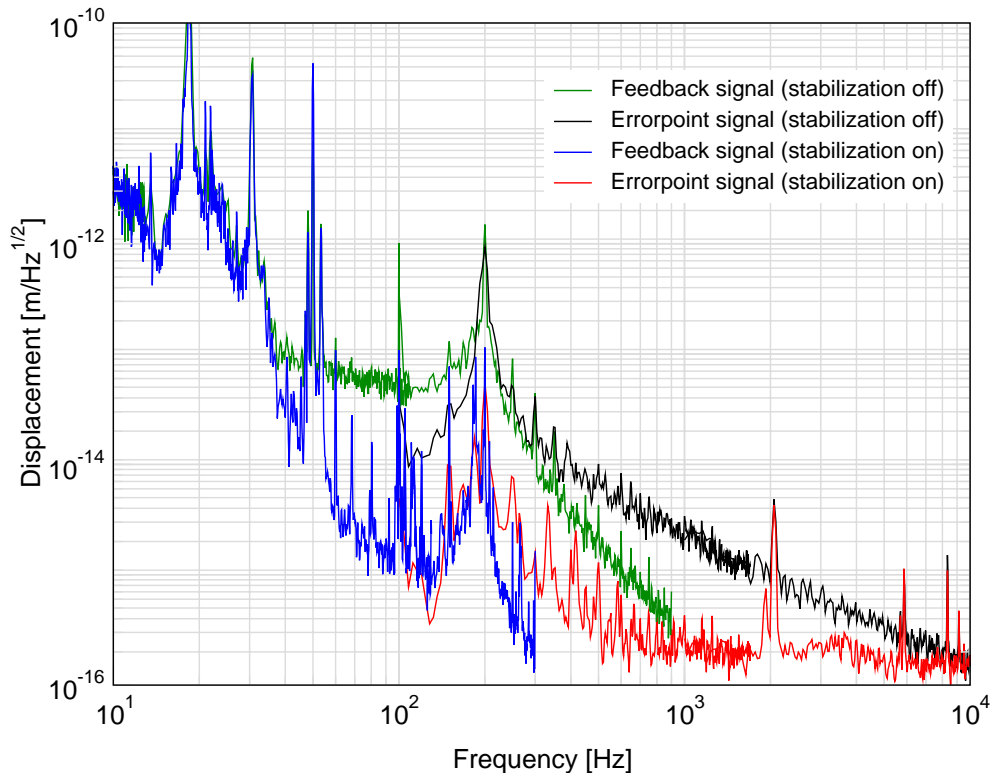


Figure 5.2.: *The frequency noise of the unstabilized laser dominates the sensitivity above 30Hz. Below the unity gain frequency of 200Hz, the feedback signal carries the information, at higher frequencies the error point signal has to be monitored.*

frequency fluctuations of the laser beam, because even if the laser system is stable enough by itself, the beam might pick up additional frequency noise on the way to the suspended cavity. This could originate from changes in the optical path length via changes of the refractive index of the air and perhaps more significantly from acoustically excited vibrations of the optical components. To confirm that this has no influence on the spectrum, we tried to reduce this noise by covering the beam path and the optical components, and we tried to enhance it by strongly increasing the acoustic noise by adding white noise to the system with a loudspeaker. No change in the sensitivity could be observed and the noise at the loudspeaker showed no coherence with the measured spectrum (see figure 5.3).

A coherence measurement combines two input signals to a normalized output signal with a phase that is equal to the phase difference of the two input signals. After averaging over a few output signals, the result will be close to zero in the case of a random phase relationship of the two input signals. Only if the phase relationship between the signals is constant, the signals do not cancel out each other and the result will remain close to one. A constant phase relationship is usually present if one of the two signals is caused by the other. That is why coherence measurements can be used to search for a limiting noise source of a sensitivity curve. Such a noise source should

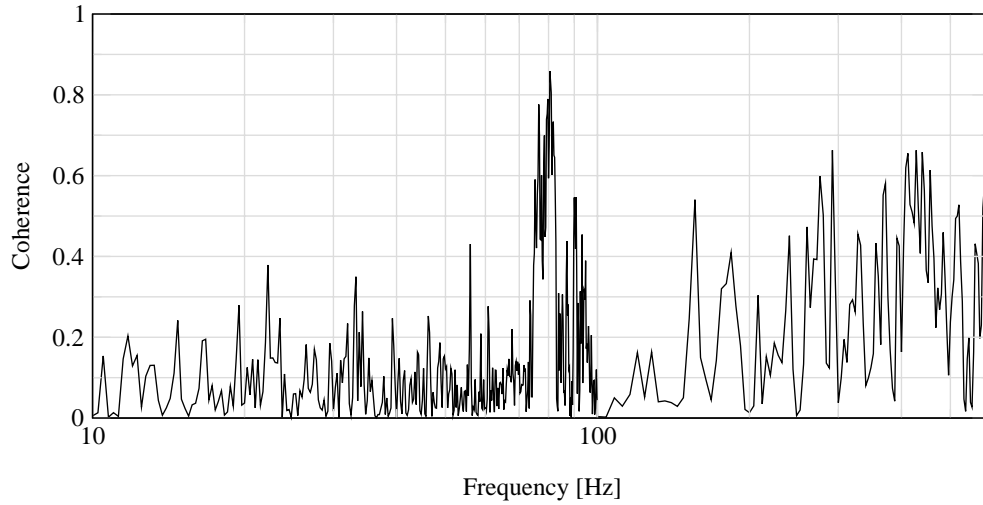


Figure 5.3.: *Coherence measurement between acoustic excitations of the optical components via white noise at a loudspeaker and the spectrum. No significant coherence between the two signals was observed below 80 Hz.*

show a strong coherence with the measured sensitivity curve.

The optical components might not only be excited by acoustic noise, but also by seismic noise. To reduce this, the optical components are placed on a seismically isolated optical table that provides a factor of 10 isolation at the measurement frequencies. Without this seismic isolation, the sensitivity curves sometimes show a higher noise floor, especially in the presence of strong seismic activity, but the sensitivity of a good measurement without this isolation matches the measurements that included the isolation of the optical table. No additional improvement was achieved.

Additional noise to the laser frequency is introduced by the Doppler shift of the laser system on the optical table against the suspended resonator. Because of the seismic isolation of the suspended mirrors, the movement of the optical table will be dominant above the pendulum resonances. The laser system shakes with the seismic in the laboratory (see figure 4.2), reduced by the factor of 10 isolation produced by the optical table. This results in a Doppler noise of

$$\begin{aligned}
 S_d(\omega) &= \left(\frac{l\omega}{c}\right)^2 \Delta x_{\text{seis}}^2(\omega) \\
 \Delta x_{\text{seis}}(\omega) &= \frac{1}{10} \frac{10^{-8}}{1 + \left(\frac{\omega}{2\pi 10\text{Hz}}\right)^2}
 \end{aligned} \tag{5.1}$$

ω is the laser frequency, l is the cavity length, c is the speed of light and Δx_{seis} is the amplitude of the seismic motion. Doppler noise and frequency noise of the laser system itself are well below the current sensitivity (see figure 5.4).

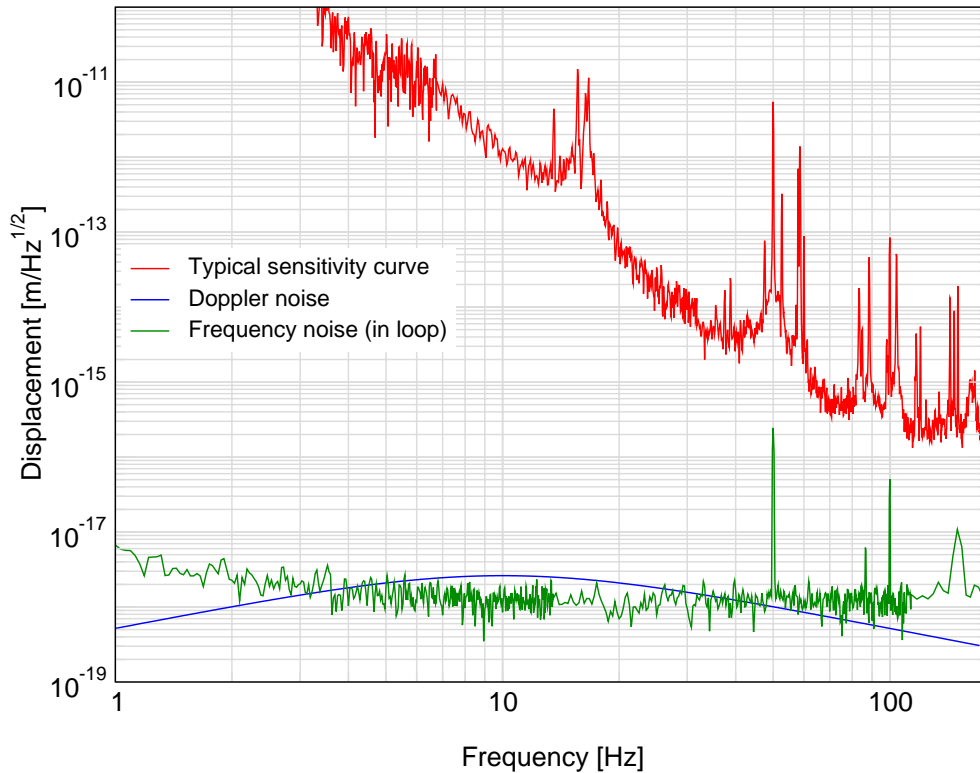


Figure 5.4.: Frequency noise of the stabilized laser and Doppler noise from the movement of the optical table in comparison with the sensitivity.

5.3. Intensity noise

Fluctuations in the laser beam intensity can also lead to noise in the experiment. Power fluctuations not only manifest as an error during the detection process, they also move the suspended mirrors directly. This effect is called radiation pressure noise and it has its origin in the fact that a laser beam of the power P_m that is reflected from a mirror acts with a force on this mirror that is given by

$$F_{rp} = \frac{2P_m}{c} \quad (5.2)$$

The factor of two has to be included, because the light is reflected and not absorbed. The radiation pressure force was first detected in 1901 [43][49]. It leads to a DC shift in the mirror position. If the light power fluctuates, an additional mirror movement will be generated at the frequency of the fluctuation.

5. Sensitivity of the experiment

A laser beam consists of discrete independent photons. If such a beam is detected by a photo diode, the number of photons N that is detected during the time interval τ will not be identical to the number of photons detected during the following time interval. If the mean number of photons \bar{N} is much bigger than one, the standard deviation from this number will be $\sqrt{\bar{N}}$. This results in a frequency independent noise in the spectral density of the light power. It is given by

$$S_P = 2\hbar\omega_L P_m \quad (5.3)$$

The light power at the mirror surface is much bigger than the output power of the laser P . It is increased inside the resonant optical cavity and is given by

$$P_{\text{mir}} = \frac{F}{\pi} P M V_0 \quad (5.4)$$

F is the finesse of the cavity, M is the fraction of the input light power that is matched to the resonator mode and V_0 is the visibility of the resonator in reflection, given by $(P_{\text{max}} - P_{\text{min}})/P_{\text{max}}$ with P_{max} being the reflected power away from the resonance and P_{min} the reflected power at the resonance in the absence of a phase modulation. If we neglect the damping of the mirror, the spectral density of the mirror movement due to radiation pressure is given by

$$S_{\text{rp}} = \frac{4}{c^2} S_P \frac{1}{m^2(\omega^2 - \omega_{\text{res}}^2)^2} = \frac{8F\omega_L\hbar P M V_0}{\pi c^2 m^2(\omega^2 - \omega_{\text{res}}^2)^2} \quad (5.5)$$

The laser power fluctuations will also disturb the detection process. If we assume that the carrier light is mainly transmitted and only the sidebands are reflected from the resonator, the average light power at the photo diode P_{refl} according to equation 3.6 will be

$$P_{\text{refl}} = 2P \frac{m^2}{4} \quad (5.6)$$

m is the modulation index. After the demodulation in the mixer, half of this power, together with half of the noise, is upconverted to twice the modulation frequency and electronically filtered out. The remaining power produces a shot noise that is equivalent to a cavity length noise, which can be calculated using equation 3.10 and 3.11.

$$S_{\text{shot}} = \left(\frac{l}{f_L} \frac{\delta_{\text{FWHM}}}{2Pm} \right)^2 2\hbar\omega_L \frac{m^2}{4} P = \frac{c^2\hbar\pi^2}{8PF^2\omega_L} \quad (5.7)$$

A more detailed analysis of this effect should also include the alignment of the laser beam to the resonator mode and the decrease in sensitivity above the cavity corner frequency. The shot noise is then given by [34]

$$\mathcal{S}_{\text{shot}}(\omega) = \left(\frac{c\pi}{F}\right)^2 \frac{\hbar(1 - J_0^2(m)MV_0)}{16\omega_L \eta P} \left(\frac{1}{MJ_0(m)J_1(m)[1 \pm \sqrt{1 - V_0}]}\right)^2 \times \left[1 + \left(\frac{2f}{\delta_{\text{FWHM}}}\right)^2\right] \quad (5.8)$$

η is the quantum efficiency of the photo diode and $J_0(m)$ and $J_1(m)$ are the first two Bessel functions. If $m \ll 1$, they can be approximated as

$$\begin{aligned} J_0(m) &= 1 - \frac{m^2}{4} \\ J_1(m) &= \frac{m}{2} \end{aligned} \quad (5.9)$$

If only a fraction d ($d < 1$) of the reflected light is detected by the photo diode, the incoming light power must be replaced by $d \times P$, because only that fraction of the incoming light is relevant for the detected shot noise. If the high frequency behaviour is ignored and with the assumptions $M = V_0 = \eta = 1$ and $m \ll 1$, the equations 5.7 and 5.8 are identical. In that case, the magnitude of the modulation index is not relevant for the shot noise. On the other hand in the presence of a bad modematching where the fraction $1 - M$ of the incoming light is directly reflected without carrying any information about the cavity, the shot noise increases significantly with a small modulation index.

A comparison of shot noise and radiation pressure noise with the spectrum of the pendulum displacement is shown in figure 5.5. Both are well below the current sensitivity, but this does not mean that amplitude fluctuations do not appear in the spectrum. The laser is shot noise limited only above a few MHz. At the measurement frequencies, the laser intensity noise due to technical noises is far bigger than what a shot noise calculation indicates. This directly increases the radiation pressure noise at the suspended mirror.

The detection sensitivity is not affected in the same way. Because of the demodulation scheme, only the amplitude fluctuations at the modulation frequency are relevant, and these are shot noise limited. An amplitude fluctuation at low frequencies does not result in a significant signal. If a mirror motion Δx_{mir} results in an output signal P_{out} , a fluctuation of the laser power by a fraction g of the total power ($g \ll 1$) will only cause a change in the output signal of $g \times P_{\text{out}} \ll P_{\text{out}}$. In theory, the detection process is thereby insensitive to low frequency power fluctuations.

5. Sensitivity of the experiment

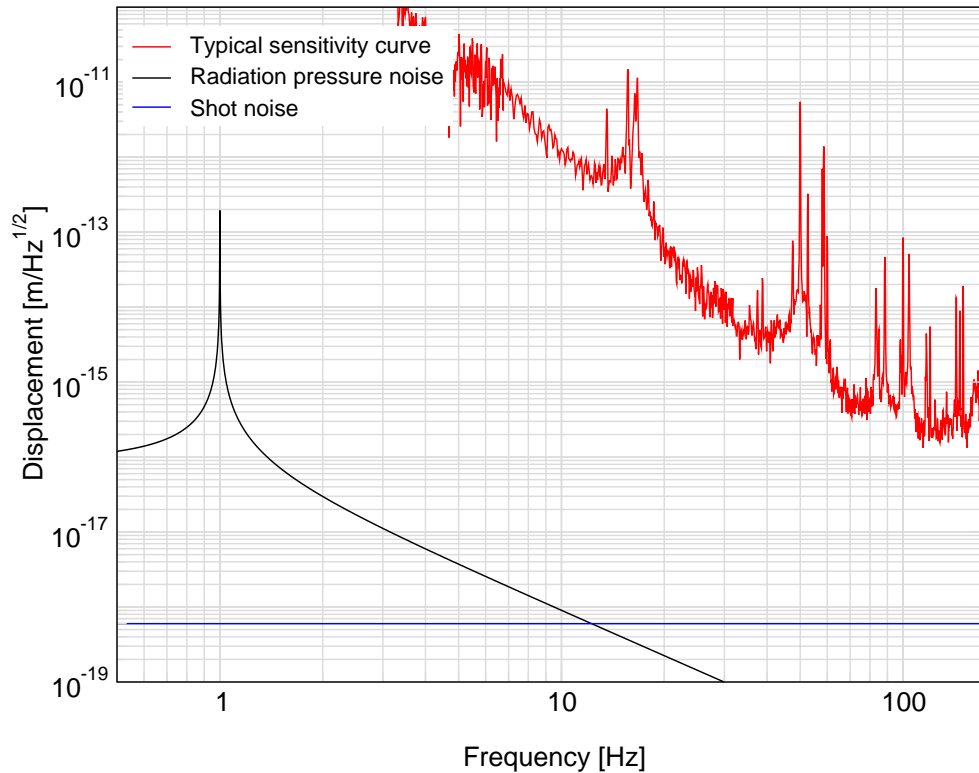


Figure 5.5.: Comparison between the experimental sensitivity, shot noise and radiation pressure noise of a shot noise limited laser.

In the real experiment, that is no longer the case. The EOM that is needed to modulate the sidebands to the laser will always produce a small amplitude modulation and additional polarization modulation that is turned into amplitude modulation after the next polarizing beam splitter. This results in a small offset of the Pound-Drever-Hall signal. In addition, small electronic offsets might be produced in the photo diode or in the mixer itself. These offsets shift the zero crossing of the Pound-Drever-Hall signal and by this the operating point to which the system is locked. Amplitude fluctuations will change the slope of the Pound-Drever-Hall signal and the resulting fluctuations of the operating point lead to a noise in the spectrum.

The amplitude noise can be decreased by reducing the amplitude modulation induced by the EOM. This can be done by a better alignment of the polarization of the laser beam with the electric field inside the EOM. For this a half wave plate is used, but a small amplitude modulation will always remain if the crystal axis is not in perfect alignment with the electric field and the electronic offset still remains. Another alternative would be to add a low noise DC voltage to compensate for the offset, but even that would only optimize the system for a short period of time. The half wave plate in front of the EOM is temperature dependent, and temperature drifts of the environment will increase the amplitude modulation and once again produce an offset.

To evaluate the effects of the laser amplitude fluctuations, an acousto-optic modulator (AOM) was included in the beam path to the suspended cavity. The AOM transfers a fraction of the main laser beam into a frequency shifted first order beam that leaves the AOM under a small angle. By adding a sine wave at a modulation frequency f_m to the AOM, the light power in the two beams is amplitude modulated at the applied modulation frequency. The first order beam can be blocked after it has spatially separated from the main beam, and only an amplitude modulated beam remains.

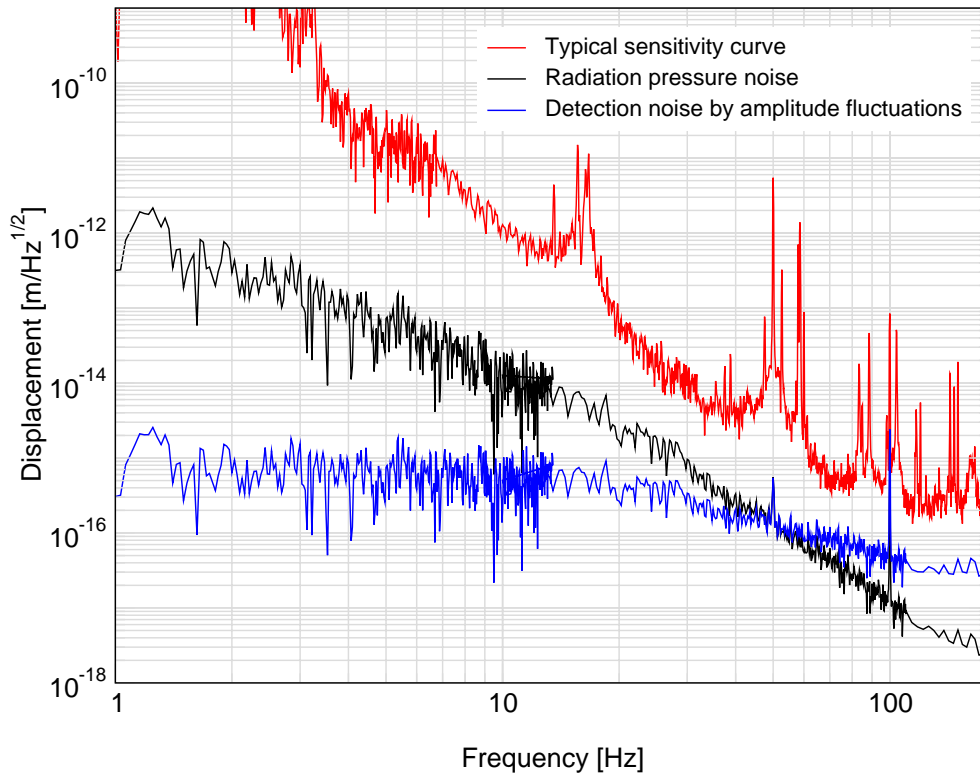


Figure 5.6.: *Strength of the radiation pressure fluctuations and the detection noise, produced by the amplitude fluctuations of the laser.*

The amplitude modulation will appear as a peak at the modulation frequency in the sensitivity curve. If the modulation frequency is changed, the peak decreases with f^{-2} in the low frequency region where the effect of radiation pressure is bigger than the detection noise due to amplitude fluctuations. At higher frequencies the magnitude of the modulation peaks remains constant. If a fraction of the laser beam is given to a separate photo diode, the laser amplitude fluctuations can be monitored. The modulation peak will also appear at this photo diode. By comparing the magnitude of the peak at this diode with the peak in the sensitivity curve, the necessary calibration factor to translate the detected amplitude noise into radiation pressure noise can be found if the modulation frequency is in the low frequency region where the radiation pressure dominates. The f^{-2} behaviour of the pendulum also enters the calibration. At higher frequencies the calibration

factor for detection noise induced by amplitude fluctuations can be found. Both noises are at least an order of magnitude below the achieved sensitivity (see figure 5.6), but to have an additional confirmation that they do not limit the spectrum, an amplitude stabilization was built to reduce the laser amplitude noise by at least one order of magnitude at the interesting frequencies. No change in the sensitivity was observed. Also an increase of the amplitude noise by adding noise to the laser pump diodes, as well as increasing the amplitude modulation induced by the EOM, did not change the spectrum.

The laser amplitude noise at the relaxation frequency of ~ 450 kHz is much greater than the amplitude noise at all other frequencies. To make sure that these high frequency oscillations do not disturb the measurements by some downconversion process, we temporarily used a laser with an included amplitude stabilization that suppresses these fluctuations. However no difference in the sensitivity was observed.

5.4. Additional noise sources

Many other noise sources that might influence the experiment in one way or the other were investigated. Fluctuations of the magnetic field of the environment might act on the magnets attached to the pendulum, but coherence measurements between a magnetic field sensor at the vacuum tank and the spectrum showed no coherence between the two.

We also investigated the effect of a misalignment of the optical beam against the resonator. To do so, we replaced one of the mirrors that was used to spatially match the optical beam to the resonator mode by a mirror mounted on a piezoelectric crystal. This piezo crystal shifted the beam in the vertical direction, and white noise added to it also appeared in the spectrum as a white noise floor (see figure 5.7). In addition we aligned and locked the system to higher order modes that should be more sensitive to alignment fluctuations of the laser beam. Some of these modes showed additional noise at high frequencies. Additional measurements were done with a deliberately bad modematching and by locking to the sidebands of the Pound-Drever-Hall signal, however it was inconclusive if alignment noise already limited the achieved sensitivity. Only after the automatic alignment system was included, which optimises the alignment up to ~ 1 kHz, and no difference in the sensitivity was observed with and without this automatic alignment, we were able to conclude that we are not limited by alignment noise at the moment.

5.4.1. Residual gas

The gas molecules inside the vacuum tank produce additional noise. They move the mirror (see equation 2.4 and 2.7) and they change the refractive index inside the optical resonator, which is equivalent to a change of the optical path length. The latter noise is described by [33]

$$S_{\text{refr}} = \frac{2\sqrt{2}(n_0 - 1)^2 l}{N_0 v_0 \bar{w}} \frac{p}{p_0} \quad (5.10)$$

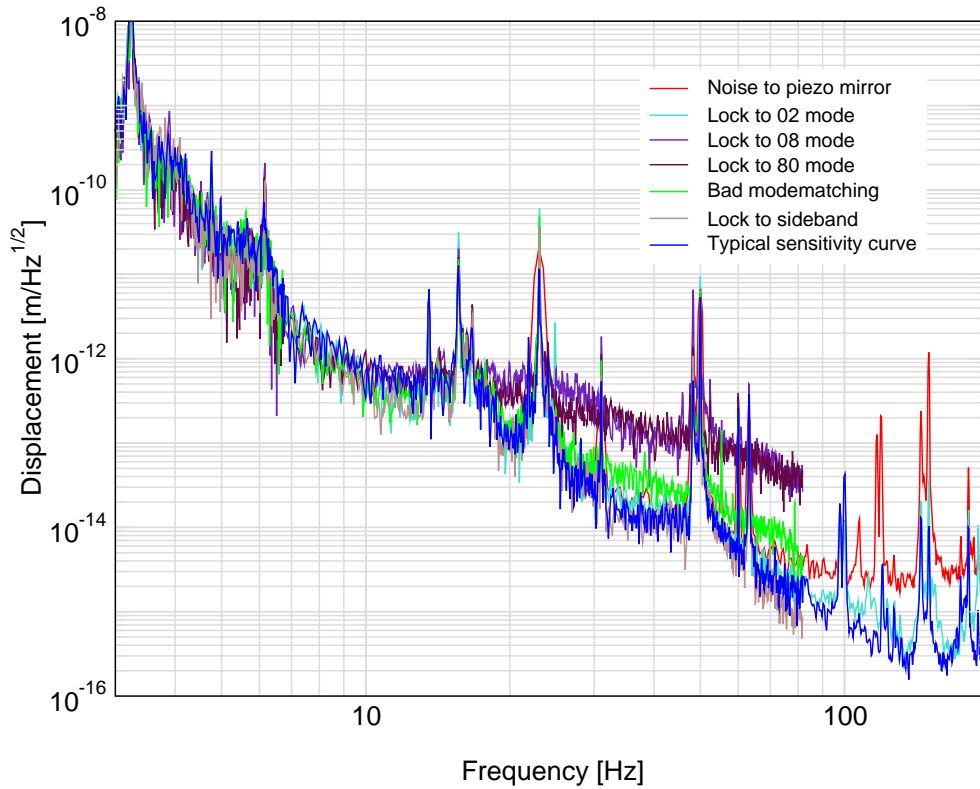


Figure 5.7.: Influence of alignment noise introduced by a mirror on a piezoelectric crystal and performance of the system when it was aligned and locked to higher order modes.

where p is the pressure of the gas, $N_0 = 2.7 \times 10^{25} / \text{m}^3$ is the number of molecules per unit volume at the standard pressure p_0 , n_0 and v_0 are the refractive index of the gas and the velocity of the gas molecules at the standard pressure, l is the cavity length and \bar{w} is the mean radius of the laser beam inside the resonator.

To reduce the noise from gas molecules and to avoid acoustic excitation of the pendulums, the mechanical part of the experiment is located inside a vacuum tank where a pressure of $\sim 10^{-7} \text{ mbar} = 10^{-5} \text{ Pa}$ is achieved. The remaining noises from residual gas are shown in figure 5.8. These noises are far below the current sensitivity, and in agreement with that, measurements at higher pressures inside the vacuum tank did not produce different results.

5.4.2. Electronic noise

The electronic noise of all components of the feedback has to be considered as well. When comparing these noises with the spectrum, one has to remember how they enter the system. For example the white current driver noise that is added to the feedback point results in a noise that

5. Sensitivity of the experiment

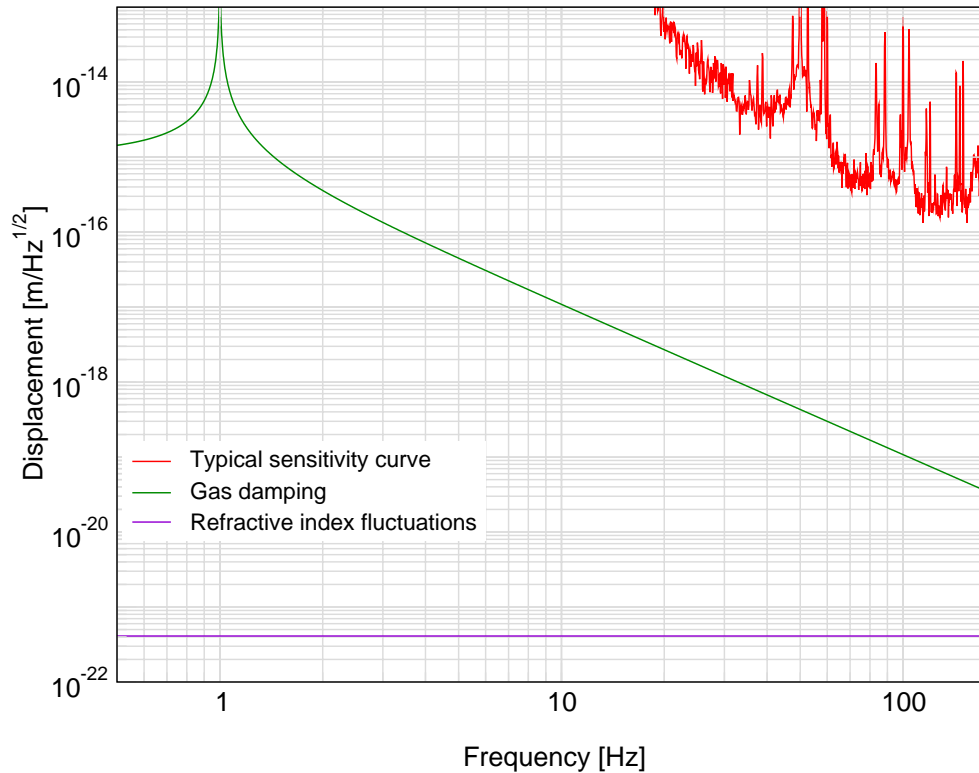


Figure 5.8.: *Noise contributions from the residual gas. The molecules shake the mirror and change the refractive index inside the optical resonator.*

decreases with f^{-2} , while the white noise of the photo diode and mixer combination that enters at the error point results in a white noise in the spectrum (see figure 5.9). Up to 100 Hz, all electronic noises seem to be below the current sensitivity.

Each of the electronic components was replaced or improved to change its noise behaviour, but at low frequencies no effect was observed. On the other hand, measurements taken at the error point above the unity gain frequency were limited by the white electronic noise of the diode and the mixer, and a reduction of the electronic noise immediately enhanced the performance of the system in this region. However some noise from the operational amplifiers will always be present.

To achieve a better performance in the kHz region, we decided to increase the signal to noise ratio by using mirrors with higher reflectivities. The mirrors with a transmission of 1000 ppm that were previously used, were replaced by mirrors with a transmission of only 100 ppm. This results in a steeper slope of the Pound-Drever-Hall signal and bigger electronic signals for the same mirror displacement. The system became more sensitive at high frequencies and was no longer limited by electronic noise, but by several resonances ranging from mechanical resonances of the mirror and power lines to the vibrations of the optical components on the optical table (see figure 5.10).

A disadvantage of this scheme is the very small catching range of the new Pound-Drever-Hall

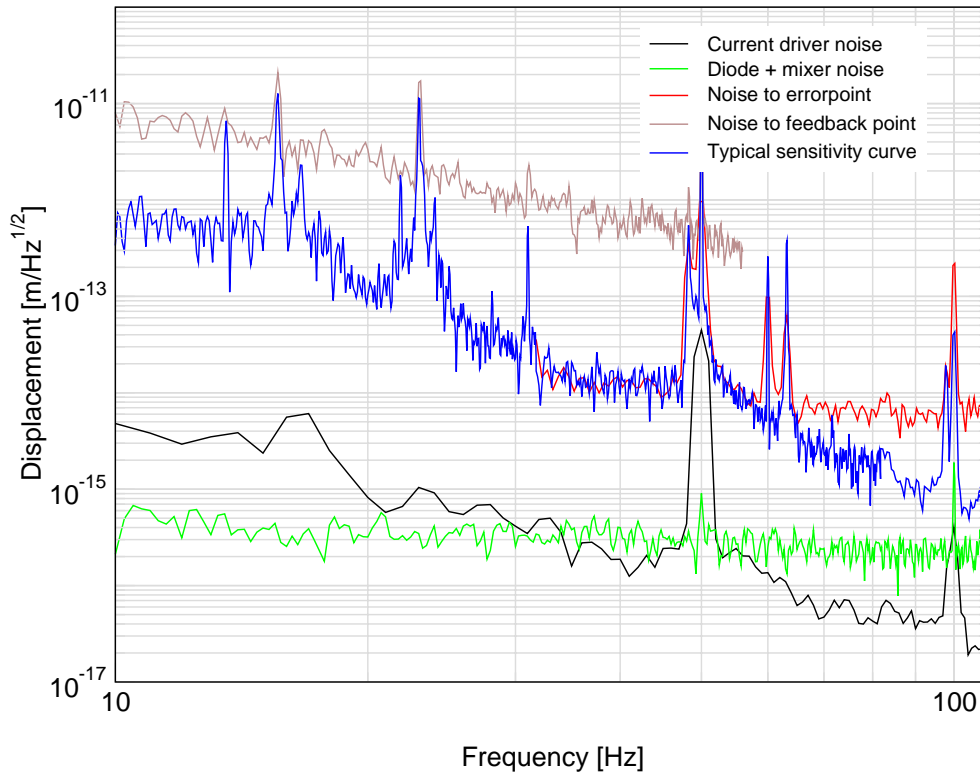


Figure 5.9.: *Electronic noise of the current driver and of the diode and mixer. Also the effect of adding white noise at the feedback point and at the error point is shown.*

signal. When the system is not yet in lock and the mirror swings through a resonance, the time to slow down the mirror and to act on the laser frequency to match it to the resonator length is very short (typically $\sim 10\mu\text{s}$). We were only able to lock the system a few times, usually when the mirror was moving slowly, because it was at a turning point of its pendulum movement. Small oscillations could already exceed the region where the Pound-Drever-Hall signal can be used for locking and only very short locking times were achieved because of that. This made measurements at low frequencies almost impossible, and we decided to return to the old mirrors for further measurements below unity gain.

5.5. Seismic noise

A lot of effort went into the reduction of the seismic excitations of the suspended mirrors. As described in chapter 4, we have build a multiple stage seismic isolation system that consists of a suspended frame structure with the two pendulums inside. The suspension of the frame structure includes vertical isolation by blades.

Originally, the frame structure was suspended as only one pendulum stage and only one ver-

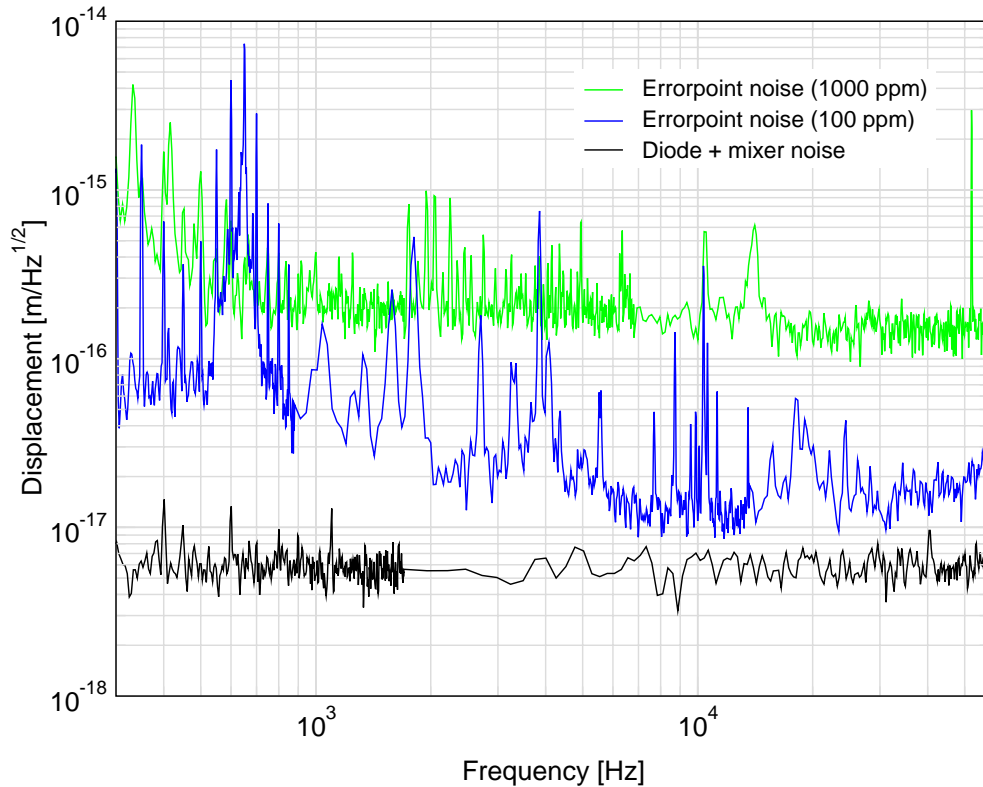


Figure 5.10.: Sensitivity in the kHz region measured at the error point. Mirrors with a transmission of only 100ppm and electronic improvements enhanced the sensitivity.

tical isolation stage was present. To reduce both the horizontal and the vertical seismic excitation of the frame, we changed this to a two stage suspension by adding an additional mass with blades attached to it. No improvement of the sensitivity was observed and we concluded that seismic motion entering through the pendulum chain was no longer a limiting noise source, but after excluding all other reasonable noises from effecting the sensitivity in the region of 10 Hz, we investigated the seismic motion even further.

Coherence measurements between the geophones in one of the stacks and the spectrum are shown in figure 5.11. Below 10 Hz there is a clear coherence between horizontal motion and the spectrum. It is interesting to note that the motion parallel to the propagating axis dominates the movement only up to ~ 2.5 Hz. At higher frequencies the longitudinal motion is suppressed strongly by the different pendulum stages and other degrees of freedom that couple into the longitudinal motion are dominant. For the frequencies above 10 Hz, the result of the coherence measurement is not fully conclusive.

At high frequencies where we would expect a strong filtering of the seismic from the pendulum stages, mechanical short-circuit of some of the pendulum stages would drastically reduce the performance of the seismic isolation. We have taken great care that none of the damping flags

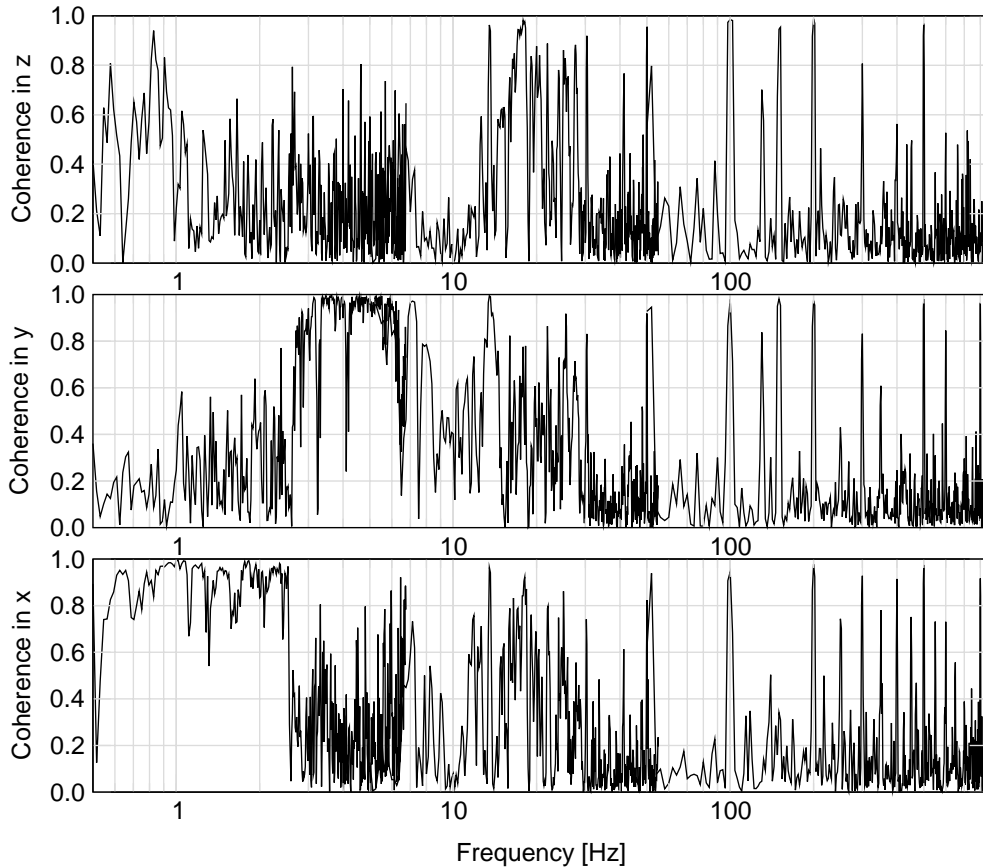


Figure 5.11.: *Coherence measurements between the three geophones in one of the stacks and the spectrum. The upper graph was measured with the vertical geophone (z direction), the other two with the two horizontal geophones. The orientation of the geophone in the lowest graph (x direction) is parallel to the propagation axis of the laser. The horizontal geophones show a clear coherence with the spectrum below 10Hz.*

touches the glass cylinders that surround them, but the active damping itself might be such a seismic short-circuit. Up to the unity gain frequency it damps the pendulum movement against the frame, and up to this frequency the motion of the seismically less isolated frame is added to the pendulums. Ideally this would be a common mode motion of both pendulums, but due to differences in the phase of the transfer functions of the two pendulums and of the damping feedback loops, a differential motion is produced at some frequencies. To reduce this additional noise at the frequencies of interest, a unity gain frequency that is as low as possible is therefore desirable for the local damping. On the other hand some gain is always needed at the pendulum resonances to achieve enough reduction of the resonant movement to be able to lock the system at all.

In order to avoid adding the seismic motion of the environment to the frame, the unity gain frequency of the damping for the resonances of the frame suspension should also be as small as

5. Sensitivity of the experiment

possible. In some set-ups where the differential movement of the pendulums at their resonance frequencies was not too strongly excited by frame motion, we were even able to avoid the damping of the frame completely. However no difference was observed between small damping of the frame and no damping at all.

The damping might also add noise to the pendulum that originates in the electronic noise of the shadow sensor or in circuit noise of the feedback electronic. To suppress this noise, a fifth stage was added to the pendulum chain between the damped masses and the mirrors, but no improvement in the sensitivity was observed.

There is one other possible seismic short-circuit that is associated with the damping. It comes from the wires that carry the electronic signals to the coils. These wires have to be unstretched and as thin as possible, but even reducing the wire diameter and attaching them to an intermediate isolated stage before they reach the frame did not improve the performance of the system.

To determine which frequencies are limited by seismic noise, we placed a fixed cavity inside the vacuum tank at the location of the suspended mirrors. This cavity had the same length and identical optical properties compared to the suspended resonator. The length of the fixed cavity was locked to the laser frequency by a piezo crystal that was placed between the two mirrors. The calibration scheme for this resonator was identical to that of the suspended resonator.

With the fixed resonator on the ground, the achieved sensitivity especially at high frequencies was not very good. The seismic motion of the ground excited its internal resonances. When the cavity was suspended to the full seismic isolation scheme, the noise was reduced a lot at high frequencies (see figure 5.12). A clear improvement in the spectrum was also achieved below 10 Hz when the automatic alignment system was switched on. This gives some indication of the magnitude of the alignment noise caused by pendulum movement in the absence of the automatic alignment system.

All seismic noise that results in a differential movement of two independently suspended mirrors was practically eliminated for the fixed cavity, while all other noises associated with the laser and with the detection scheme were still present. Compared to the usual sensitivity, there was a clear improvement for all frequencies below 50 Hz. From this we concluded that up to this frequency the usual set-up was still limited by seismic noise.

A simulation of the seismic motion was developed to model the contributions of the different degrees of freedom to the seismic noise. The only unknowns in this simulation were the coupling coefficients between the different degrees of freedom and the longitudinal. We evaluated these parameters by matching the simulation with the achieved sensitivity under the assumption that the sensitivity is dominated by seismic noise (see figure 5.13). We also assumed that the small mirror dominates the differential motion, because the prediction of the seismic noise for the big mirror with identical coupling coefficients are almost an order of magnitude lower above 1 Hz.

Using the simulation we developed suspension designs with improved seismic attenuation. The longitudinal isolation in our set-up was already sufficient to reach a much better sensitivity, the angular degrees of freedom had to be improved instead. This could be done by moving the suspension points closer together, but that makes the pendulum very hard to handle. A better

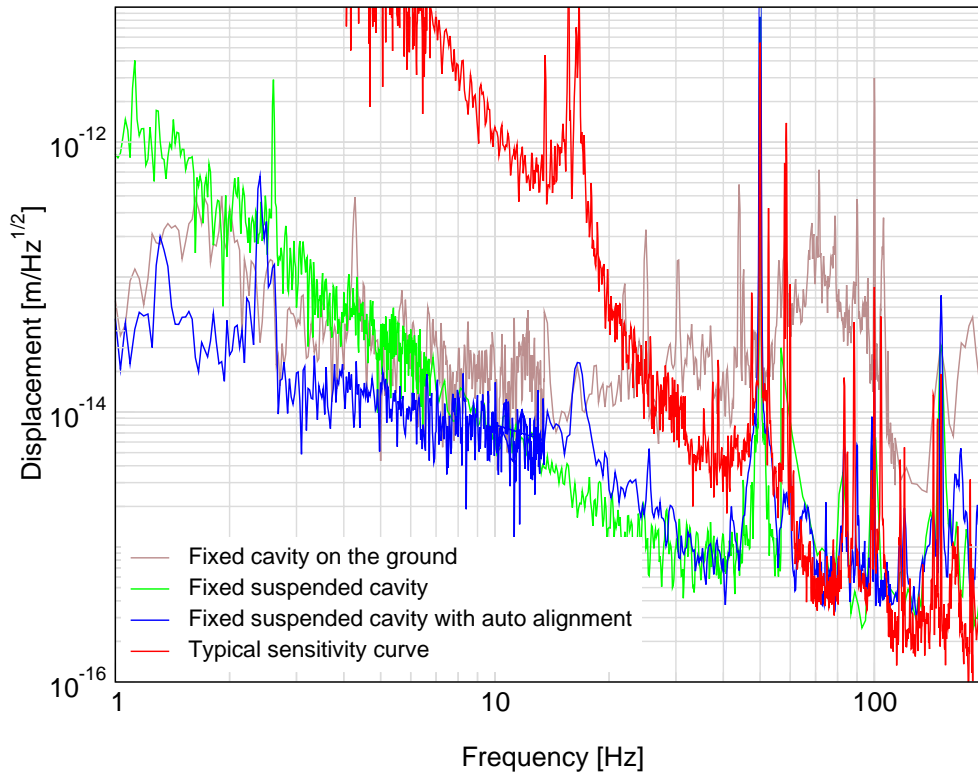


Figure 5.12.: Sensitivity of a fixed cavity inside the vacuum tank that is locked to the laser with a piezo. Measurements were taken with the cavity on the ground and with the cavity suspended to the pendulum chain with and without automatic alignment. Below 50 Hz the fixed cavity is more sensitive than two independently suspended mirrors.

alternative is to increase the moment of inertia of the pendulum stages. This reduces the resonance frequencies and achieves stronger isolation at high frequencies.

In a first attempt, we added an X-shaped structure with heavy masses at the four ends to the small mirror. These four arms increased the moments of inertia for all three rotational degrees of freedom and the predicted noise level was clearly reduced. However we were not able to lock this system due to very big movement at the new low resonance frequencies. Although the damping electronic was changed to act at the new frequencies, the damping became very ineffective because the resonance frequencies of the pendulum stages were no longer matched to each other to produce coupled resonances. Instead, a resonant movement of the new mirror did not produce big oscillations at the damped mass and could thereby not be damped effectively. A second attempt with an X-shaped structure attached to the mass between the damped mass and the mirror failed for the same reason.

Only when we attached smaller arms to both stages below the damped mass, a lock could be achieved. The sensitivity was improved above 10 Hz by almost an order of magnitude and the

5. Sensitivity of the experiment

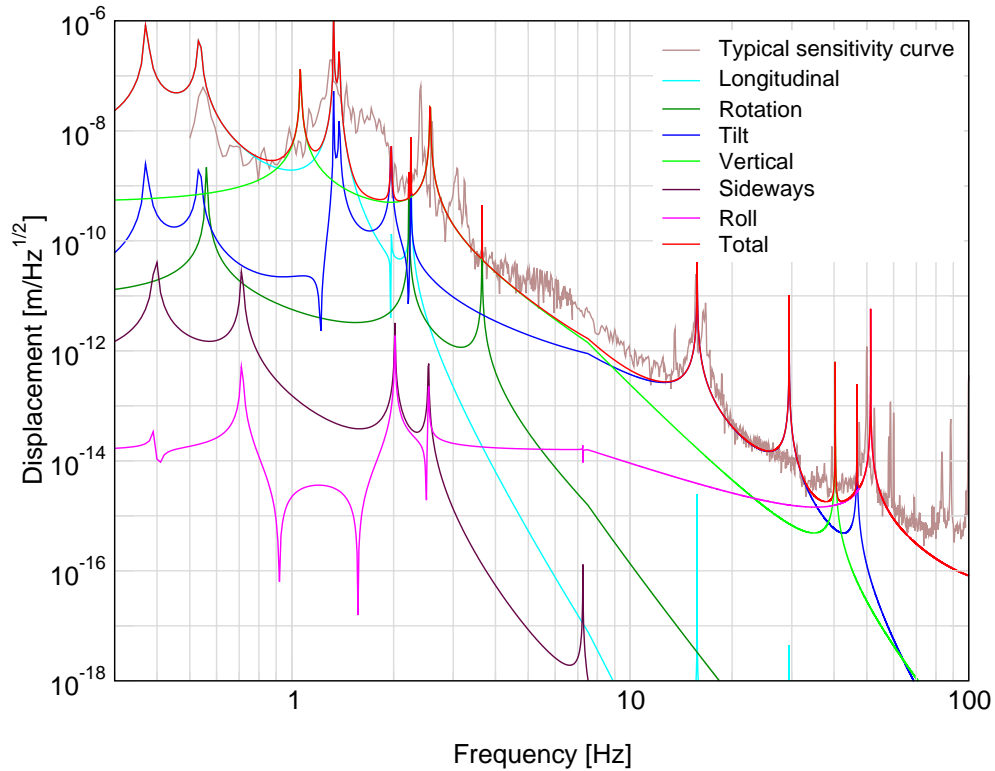


Figure 5.13.: Simulation of the contribution of the different degrees of freedom to the overall seismic motion of the small mirror.

improvement matches the prediction by the simulation (see figure 5.14). This prediction no longer includes a free parameter, because the coupling coefficients were already fixed in the previous measurement. Increasing the gain of the local damping immediately decreased the sensitivity, so the locking had to take place with the lowest gain possible.

To attach bigger arms and still retain good coupling to the damped mass, it was necessary to attach similar arms also to the damped mass. This meant we had to move the positions of the damping coils to make room for these arms. In addition we decided to add a third blade stage to the seismic isolation to reduce the vertical contribution to the spectrum. These new blades were placed within the frame and the two pendulums were suspended to them. The new vertical stage required two new damping coils for each pendulum to reduce the vertical and roll resonances. The pendulum stages with the new arms and the changes to the frame can be seen in figure 5.15. The new aluminium arms have a T-shape with stainless steel cylinders at the end.

The resonant movement of the pendulums was very big for this new set-up, so that the coil-magnet actuator was only able to lock the resonator when the damping gain was very high. This resulted in a spectrum that was not only much higher than the prediction from the simulation of the seismic, it was also higher than the previously achieved sensitivity (see figure 5.16). Besides

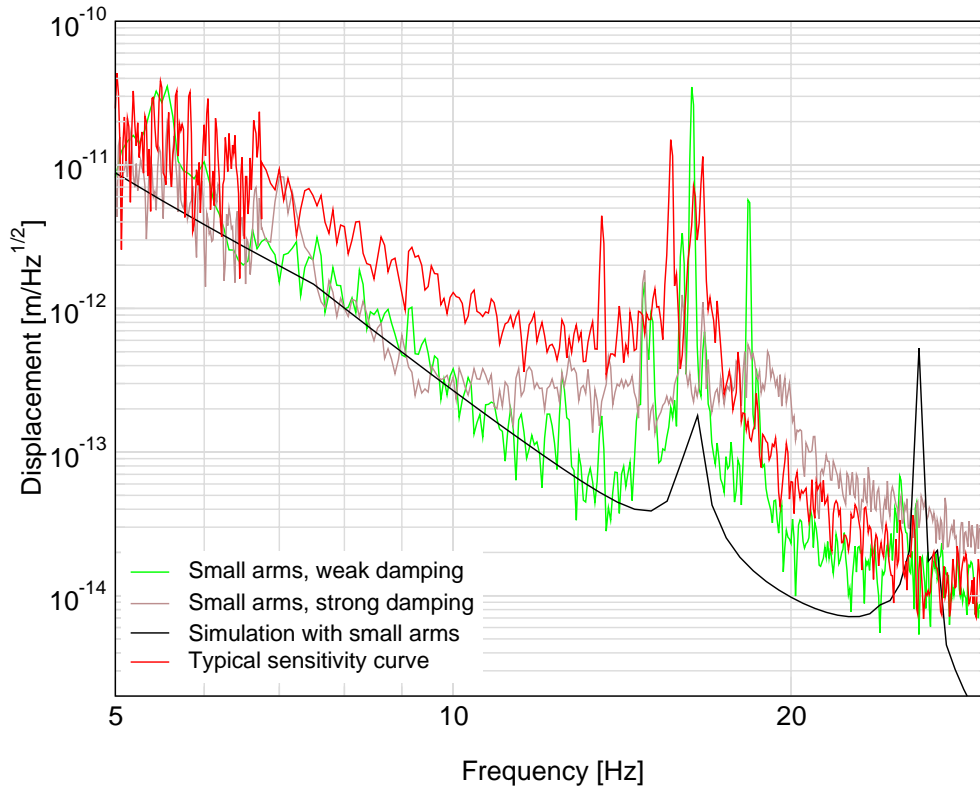


Figure 5.14.: Sensitivity improvement from small arms attached to the last two stages of the small mirror suspension. Increasing the damping gain adds noise to the spectrum.

the damping, internal resonances of the complicated structure of the new masses probably also contributed to the noise at high frequencies. An additional problem for this set-up was that the magnets used for the damping of the pendulums introduced a coupling between the two pendulums by acting on each other. We tried to improve the sensitivity by using the piezo actuator instead of the coils to avoid the excitation of angular resonances and to be able to reduce the damping gain, but we were unable to achieve a better spectrum.

After returning to the old set-up, we included two big mirrors and an active isolation system. A sensitivity improvement near 10 Hz was achieved. On the other hand the new active isolation is so soft that the mechanical adjustment of the pendulums is made very complicated by the excitation of big pendulum oscillations, and even movements at a few meters distance are shaking the tank so much at 1 Hz, that the locking process is disturbed. Although an improvement of an order of magnitude was achieved and a very high sensitivity is reached, the prediction for the thermal noise is still well below the achieved sensitivity (see figure 5.17). This holds even if velocity damping is assumed or if the pendulum Q or the mass are reduced within reasonable values.

5. Sensitivity of the experiment

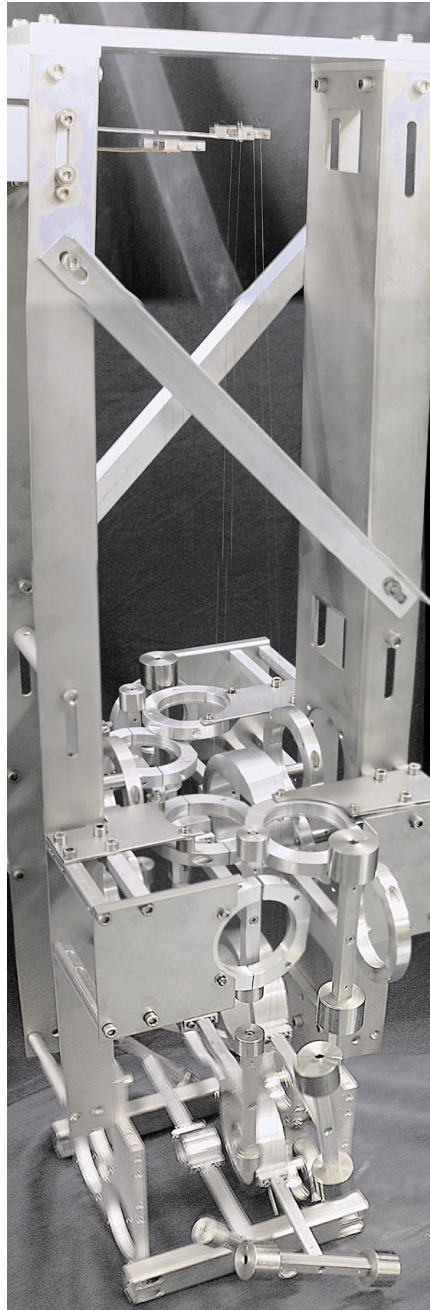


Figure 5.15.: *Frame structure with two pendulums consisting of three stages with high moment of inertia. The damping coils are not yet attached, but the new blades are also visible at the top.*

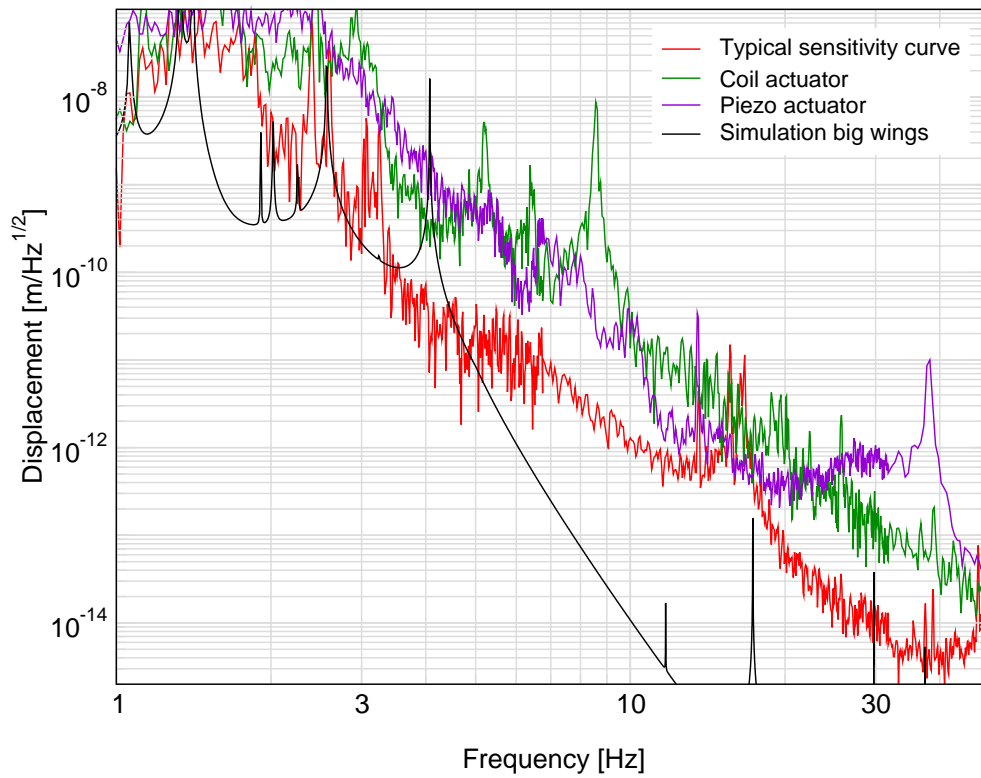


Figure 5.16.: *In contrast to the result expected from the simulation, the noise of the pendulums with very high moment of inertia is increased for both actuators.*

5. Sensitivity of the experiment

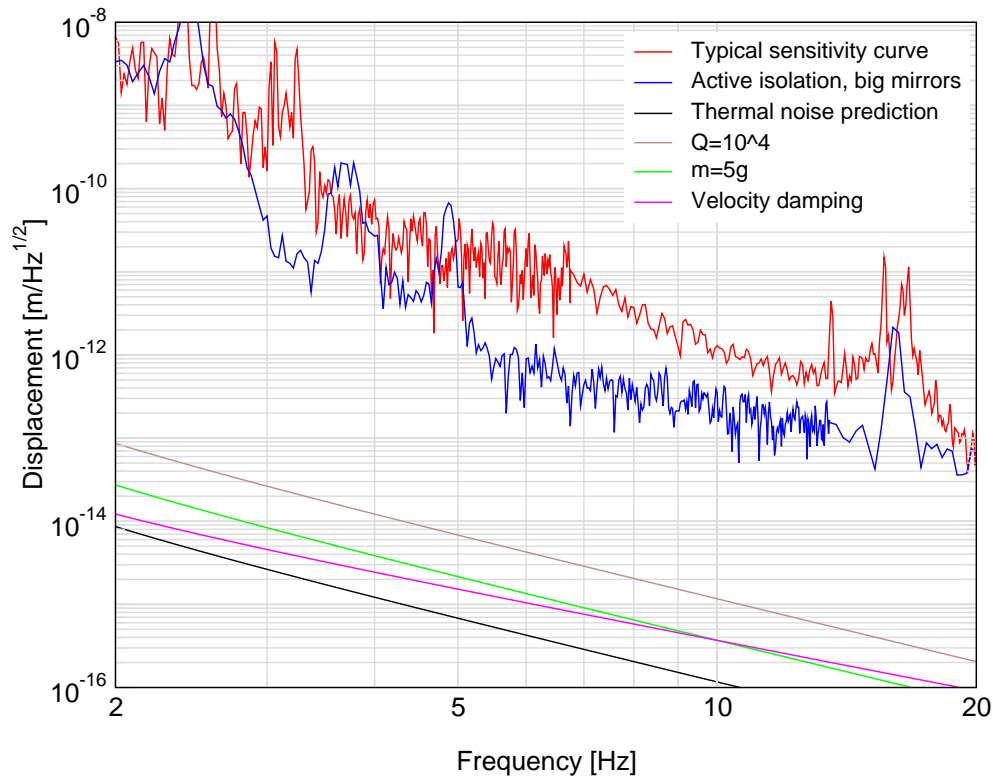


Figure 5.17.: Sensitivity improvement from switching to two big mirrors and actively isolating the vacuum tank. For comparison, the thermal noise prediction of the pendulum mode, the prediction for a reduced Q , for a reduced mass and for velocity damping are also shown.

Conclusion

It was the goal of this work to build an experiment that allows very sensitive measurements of the differential length changes of a Fabry-Perot resonator, which consists of two independently suspended mirrors. These measurements were done in the frequency range between 10 Hz and 100 Hz with the target to reach the off-resonant thermal noise of the pendulum mode. In order to achieve this, the laser frequency was stabilized to a reference resonator. An automatic alignment system overlaps the input beam with the eigenmode of the suspended resonator. To isolate the mirrors from seismic motion of the ground, an isolation system that consists of multiple stages for all degrees of freedom of the pendulum movement was designed. This pendulum chain was suspended inside a vacuum tank to isolate the mirrors from excitations by the air and to minimize refractive index fluctuations inside the optical resonator.

Several noise sources that affect the sensitivity were investigated. This includes optical noises that are caused by laser frequency fluctuations, laser amplitude fluctuations and beam position fluctuations. All of these were reduced sufficiently. Environmental noise from acoustic or seismic excitations of the optical components and the beam path were investigated. Electronic noises were measured and could be reduced by improved electronic designs. However the electronic noise was still a limiting factor in the kHz region. A higher finesse of the optical resonator improved the performance at these frequencies.

Although up to five pendulum stages were used for seismic isolation, a careful investigation revealed that this noise still remained the major obstacle at the frequencies of interest. It changes the length of the Fabry-Perot resonator by coupling of the other degrees of freedom of the pendulum motion into the longitudinal movement. New pendulum designs were developed to reduce this effect, and some improvement was achieved. However, the seismic noise and the noise introduced by the necessary damping of the pendulum movement at the resonance frequencies still prevent a significantly better performance around 10 Hz and the pendulum thermal noise cannot be reached. It seems that only a completely new design of the whole suspension system could improve the situation.



Appendix A

Material parameters

Steel

α	$14 \times 10^{-6} \frac{1}{K}$
κ	$50 \frac{W}{mK}$
ρ	$7.8 \frac{g}{cm^3}$
C	$502 \frac{J}{kgK}$
σ	0.3
Y	$21 \times 10^{10} Pa$

BK7

α	$7.1 \times 10^{-6} \frac{1}{K}$
κ	$1.114 \frac{W}{mK}$
ρ	$2.2 \frac{g}{cm^3}$
C	$8.58 \times 10^2 \frac{J}{kgK}$
σ	0.206
Y	$8.1 \times 10^{10} Pa$
n	1.5

Fused silica (SiO₂)

α	$5.5 \times 10^{-7} \frac{1}{K}$
$\alpha(10 K, 1 K)$	$-2.6 \times 10^{-7} \frac{1}{K}, -2.6 \times 10^{-7} \frac{1}{K}$
κ	$1.4 \frac{W}{mK}$

A. Material parameters

$\kappa(10\text{ K}, 1\text{ K})$	$0.1 \frac{\text{W}}{\text{mK}}, 2 \times 10^{-2} \frac{\text{W}}{\text{mK}}$
ρ	$2.2 \frac{\text{g}}{\text{cm}^3}$
C	$6.7 \times 10^2 \frac{\text{J}}{\text{kgK}}$
$C(10\text{ K}, 1\text{ K})$	$3 \frac{\text{J}}{\text{kgK}}, 3 \times 10^{-3} \frac{\text{J}}{\text{kgK}}$
σ	0.17
Y	$7.2 \times 10^{10} \text{ Pa}$
$\frac{dY}{dT}$	$1.5 \times 10^7 \frac{\text{Pa}}{\text{K}}$
n	1.45
$\frac{dn}{dT}$	$1.5 \times 10^{-5} \frac{1}{\text{K}}$

Sapphire (Al_2O_3)

α	$5 \times 10^{-6} \frac{1}{\text{K}}$
$\alpha(10\text{ K}, 1\text{ K})$	$5.8 \times 10^{-10} \frac{1}{\text{K}}, 5.8 \times 10^{-13} \frac{1}{\text{K}}$
κ	$40 \frac{\text{W}}{\text{mK}}$
$\kappa(10\text{ K}, 1\text{ K})$	$4.3 \times 10^3 \frac{\text{W}}{\text{mK}}, 4.3 \frac{\text{W}}{\text{mK}}$
ρ	$4 \frac{\text{g}}{\text{cm}^3}$
C	$7.9 \times 10^2 \frac{\text{J}}{\text{kgK}}$
$C(10\text{ K}, 1\text{ K})$	$8.9 \times 10^{-2} \frac{\text{J}}{\text{kgK}}, 8.9 \times 10^{-5} \frac{\text{J}}{\text{kgK}}$
σ	0.29
Y	$40 \times 10^{10} \text{ Pa}$
$\frac{dY}{dT}$	$-4 \times 10^7 \frac{\text{Pa}}{\text{K}}$

Tantala (Ta_2O_5)¹

α	$\sim 5 \times 10^{-6} \frac{1}{\text{K}}$
Y	$14 \times 10^{10} \text{ Pa}$
n	2.1
$\frac{dn}{dT}$	$\sim 5 \times 10^{-6} \frac{1}{\text{K}}$

$\text{Ta}_2\text{O}_5/\text{SiO}_2$ coating

α	$\sim 2 \times 10^{-6} \frac{1}{\text{K}}$
----------	--

¹ Values for Ta_2O_5 vary strongly, depending on the manufacturing process.

Appendix B

The linear spectral density

Throughout this thesis we use the spectral density S to describe noise at different frequencies. It is defined as the fourier transform of the auto correlation function $g(\tau)$.

$$S \equiv 2 \int_{-\infty}^{\infty} g(\tau) e^{-i\omega\tau} d\omega \quad (\text{B.1})$$

The factor of two originates from the fact that we use the one sided spectral density, which is defined only for positive frequencies. The auto correlation function is given by¹

$$g(\tau) \equiv \lim_{T \rightarrow \infty} \frac{1}{2T} \int_{-T}^T x(t+\tau)x(t) dt = \langle x(t+\tau)x(t) \rangle_t \quad (\text{B.2})$$

Usually we plot the square root of the spectral density \sqrt{S} , which is called linear spectral density. To get a more instructive picture for this linear spectral density, we should remember that we want to describe how much a system with an average position $\langle x(f, t) \rangle_t$ fluctuates in a given frequency interval ranging from f to $f + \Delta f$. The deviation from the mean position

$$\Delta x(f, t) \equiv x(f, t) - \langle x(f, t) \rangle_t \quad (\text{B.3})$$

would not be a good parameter to express the position fluctuations. The system oscillates around its mean value and if we average over the deviation, we get $\langle \Delta x(f, t) \rangle_t = 0$.

A better choice to describe the fluctuations at the frequency f is the mean square deviation $\langle \Delta x(f, t)^2 \rangle_t$. The remaining problem with this is that the result depends on the measurement

¹ $\langle f(t) \rangle_t$ is the time average over a function $f(t)$.

B. The linear spectral density

bandwidth Δf if we integrate the fluctuations from f to $f + \Delta f$. We will pick up fewer fluctuations if we decrease the frequency spacing between the measurement points and by this the frequency interval per point. To be independent of the measurement process, we divide by the frequency interval.

$$S = \frac{\langle \Delta x(f, t)^2 \rangle_t}{\Delta f} \quad (\text{B.4})$$

This can also be evaluated if we take the backtransformation of equation B.1

$$g(\tau) = \frac{1}{2} \int_{-\infty}^{\infty} S e^{-i\omega\tau} \frac{d\omega}{2\pi} = \int_0^{\infty} S e^{-i\omega\tau} \frac{d\omega}{2\pi} \quad (\text{B.5})$$

and assume $\tau = 0$. If we set $\langle x(f, t) \rangle_t = 0$, which we can always do by a coordinate transformation, and integrate only over the frequency interval of interest, we get

$$\langle \Delta x(f, t)^2 \rangle_t = \int_f^{f+\Delta f} S df \quad (\text{B.6})$$

Equation B.4 results from this if the spectral density does not change strongly with frequency. The unit of the spectral density in a displacement measurement is m^2/Hz . Usually we plot the linear spectral density with the unit $\text{m}/\sqrt{\text{Hz}}$. The advantage of this is that we can multiply the linear spectral density with the transfer functions we have implemented in the experiment to calculate the noise spectrum at different points of the experiment. For the spectral density we would have to multiply with the square of the transfer function, which sometimes can be less obvious.

Bibliography

- [1] A. Y. AGEEV, I. A. BILENKO and V. B. BRAGINSKY: *Excess noise in the steel suspension wires for the laser gravitational wave detector*. Phys. Lett. A, 246:479–484, 1998.
- [2] B. W. BARR, G. CAGNOLI, M. M. CASEY, D. CLUBLEY, D. R. M. CROOKS, K. DANZMANN, E. J. ELLIFE, S. GOSSLER, A. GRANT, H. GROTE, A. HEPTONSTALL, J. HOUGH, O. JENNRICH, H. LÜCK, S. A. MCINTOSH, G. P. NEWTON, D. A. PALMER, M. V. PLISSI, D. I. ROBERTSON, N. A. ROBERTSON, S. ROWAN, K. D. SKELDON, P. SNEDDON, K. A. STRAIN, C. I. TORRIE, H. WARD, P. A. WILLEMS, B. WILLKE and W. WINKLER: *Silica research in Glasgow*. Class. Quant. Grav., 19:1655–1662, 2002.
- [3] E. BLACK: *An introduction to Pound-Drever-Hall laser frequency stabilization*. Am. J. Phys, 69:79–87, 2001.
- [4] F. BONDU, P. HELLO and J. Y. VINET: *Thermal noise in mirrors of interferometric gravitational wave antennas*. Phys. Lett. A, 246:227–236, 1998.
- [5] L. BRACCI ET AL.: *Status of the low frequency facility experiment*. Class. Quant. Grav., 19:1675–1682, 2002.
- [6] V. B. BRAGINSKY, M. L. GORODETSKY and S. P. VYATCHANIN: *Thermodynamical fluctuations and photo-thermal shot noise in gravitational wave antenna*. Phys. Lett. A, 264:1–10, 1999.
- [7] V. B. BRAGINSKY, M. L. GORODETSKY and S. P. VYATCHANIN: *Thermo-refractive noise in gravitational wave antenna*. Phys. Lett. A, 271:303–307, 2000.
- [8] V. B. BRAGINSKY, V. P. MITROFANOV and K. V. TOKMAKOV: *Energy dissipation in the pendulum mode of the test mass suspension of a gravitational wave antenna*. Phys. Lett. A, 218:164–166, 1996.
- [9] V. B. BRAGINSKY and S. P. VYATCHANIN: *Thermodynamical fluctuations in optical mirror coatings*. Phys. Lett. A, 312:244–255, 2003.
- [10] O. S. BROZEK: *Frequenzstabilisierung eines Nd:YAG-Hochleistungs-Laser-Systems für den Gravitationswellendetektor GEO 600*. Doktorarbeit, 1999.

- [11] G. CAGNOLI, L. GAMMAITONI, J. KOVALIK, F. MARCHESONI and M. PUNTURO: *Low-frequency internal friction in clamped-free thin wires*. Phys. Lett. A, 255:230–235, 1999.
- [12] G. CAGNOLI, L. GAMMAITONI, J. KOVALIK, F. MARCHESONI, M. PUNTURO, S. BRACCINI, R. DESALVO, F. FIDECARO and G. LOSURDO: *Mechanical shot noise induced by creep in suspension devices*. Phys. Lett. A, 237:21–27, 1997.
- [13] G. P. CAGNOLI and P. A. WILLEMS: *The effects of nonlinear thermoelastic damping in highly stressed fibres*. Phys. Lett. B, 65:1741111–9, 2002.
- [14] R. R. CALDWELL, M. P. KAMIONKOWSKI and L. WADLEY: *The first space-based gravitational-wave detectors*. Phys. Rev. D, 59:27101–8, 1999.
- [15] H. B. CALLEN and R. F. GREENE: *On a theorem of irreversible thermodynamics*. Phys. Rev., 86:702–710, 1952.
- [16] H. B. CALLEN and T. A. WELTON: *Irreversibility and generalized noise*. Phys. Rev., 83:34–40, 1951.
- [17] D. R. M. CROOKS, P. SNEDDON, G. CAGNOLI, J. HOUGH, S. ROWAN, M. M. FEJER, E. GUSTAFSON, R. ROUTE, N. NAKAGAWA, D. COYNE, G. M. HARRY and A. M. GRETTARSSON: *Excess mechanical loss associated with dielectric mirror coatings on test masses in interferometric gravitational wave detectors*. Class. Quant. Grav., 19:883–896, 2002.
- [18] K. DANZMANN FOR THE LISA STUDY TEAM: *LISA - an ESA cornerstone mission for a gravitational wave observatory*. Class. Quant. Grav., 14:1399–1404, 1997.
- [19] M. DEROSA, L. CONTI, M. CERDONIO, M. PINARD and F. MARIN: *Experimental measurement of the dynamic photothermal effect in Fabry-Perot cavities for gravitational wave detectors*. Phys. Rev. Lett., 89:2374021–4, 2002.
- [20] R. DREVER, J. HALL, F. KOWALSKI, J. HOUGH, G. FORD, A. MUNLEY and H. WARD: *Laser phase and frequency stabilization using an optical resonator*. Appl. Phys., B 31:97–105, 1983.
- [21] A. EINSTEIN: *Über die von der molekularkinetischen Theorie der Wärme geforderte Bewegung von in ruhenden Flüssigkeiten suspendierten Teilchen*. Ann. Phys., 17:549–560, 1905.
- [22] A. EINSTEIN: *Zur Theorie der Brownschen Bewegung*. Ann. Phys., 19:371–381, 1906.
- [23] G. F. FRANKLIN, J. D. POWELL and A. E. NAENI: *Feedback Control of Dynamic Systems*. Addison Wesley Publishing Company, 1994.
- [24] A. GILLESPIE and F. RAAB: *Thermal noise in the test mass suspensions of a laser interferometer gravitational-wave prototype*. Phys. Lett. A, 178:357–363, 1993.
- [25] A. GILLESPIE and F. RAAB: *Suspension losses in the pendula of laser interferometer gravitational-wave detectors*. Phys. Lett. A, 190:213–220, 1994.

-
- [26] G. I. GONZÁLEZ and P. R. SAULSON: *Brownian motion of a torsion pendulum with internal friction*. Phys. Lett. A, 201:12–18, 1995.
- [27] S. GOSSLER, G. CAGNOLI, D. R. M. CROOKS, H. LÜCK, S. ROWAN, J. R. SMITH, K. A. STRAIN, J. HOUGH and K. DANZMANN: *Damping and tuning of the fiber violin modes in monolithic silica suspensions*. submitted to Class. Quant. Grav.
- [28] S. GOSSLER, M. M. CASEY, A. FREISE, A. GRANT, H. GROTE, G. HEINZEL, M. HEURS, M. E. HUSMAN, K. KÖTTER, V. LEONHARDT, H. LÜCK, M. MALEC, K. MOSSAVI, S. NAGANO, P. W. MCNAMARA, M. V. PLISSI, V. QUETSCHKE, D. I. ROBERTSON, N. A. ROBERTSON, A. RÜDIGER, R. SCHILLING, K. D. SKELDON, K. A. STRAIN, C. I. TORRIE, H. WARD, U. WEILAND, B. WILLKE, W. WINKLER, J. HOUGH and K. DANZMANN: *Mode-cleaning and injection optics of the gravitational-wave detector GEO600*. Rev. Sci. Inst., 74:3787–3795, 2003.
- [29] A. M. GREARSSON and G. M. HARRY: *Dissipation of mechanical energy in fused silica fibers*. Rev. Sci. Inst., 70:4081–4087, 1999.
- [30] H. GROTE: *Autoalignment am GEO 600-Modecleaner*. Diplomarbeit, 1999.
- [31] G. M. HARRY, A. M. GREARSSON, P. R. SAULSON, S. E. KITTELBERGER, S. D. PENN, W. J. STARTIN, S. ROWAN, M. M. FEJER, D. R. M. CROOKS, G. CAGNOLI, J. HOUGH and N. NAKAGAWA: *Thermal noise in gravitational wave detectors due to dielectric optical coatings*. Class. Quant. Grav., 19:897–917, 2002.
- [32] G. HEINZEL, A. RÜDIGER, R. SCHILLING, K. STRAIN, W. WINKLER, J. MIZUNO and K. DANZMANN: *Automatic beam alignment in the Garching 30-m prototype of a laser-interferometric gravitational wave detector*. Opt. Comm., 160:321–334, 1999.
- [33] J. HOUGH, B. J. MEERS, G. P. NEWTON, N. A. ROBERTSON, H. WARD, G. LEUCHS, T. M. NIEBAUER, A. RÜDIGER, R. SCHILLING, L. SCHNUPP, H. WALTHER, W. WINKLER, B. F. SCHUTZ, J. EHLERS, P. KAFKA, G. SCHÄFER, M. W. HAMILTON, I. SCHÜTZ, H. WELLING, J. R. J. BENNET, I. F. CORBETT, B. W. H. EDWARDS, R. J. S. GREENHALGH and V. KOSE: *Proposal for a joint German-British interferometric gravitational wave detector*. MPQ 147, GWD/137/JH(89), 1989.
- [34] J. HOUGH, H. WARD, G. A. KERR, N. L. MACKENZIE, B. J. MEERS, G. P. NEWTON, D. I. ROBERTSON, N. A. ROBERTSON and R. SCHILLING: *The stabilization of lasers for interferometric gravitational wave detectors*. The detection of gravitational waves, Cambridge University Press, 329 - 345, 1991.
- [35] Y. HUANG and P. R. SAULSON: *Dissipation mechanisms in pendulums and their implications for gravitational wave detection*. Rev. Sci. Inst., 69:544–553, 1998.
- [36] R. A. HULSE: *The discovery of the binary pulsar*. Rev. Mod. Phys., 66:699–710, 1994.
- [37] O. JENNRICH: *Das Quantenlimit der Interferometrie*. Doktorarbeit, 1998.

- [38] M. KAJIMA, N. KUSUMI, S. MORIWAKI and N. MIO: *Wide-band measurement of mechanical thermal noise using a laser interferometer*. Phys. Lett. A, 264:251–256, 1999.
- [39] V. M. KASPI, J. H. TAYLOR and M. F. RYBA: *High-precision timing of millisecond pulsars. 3: Long-term monitoring of PSRs B1855+09 and B1937+21*. Astrophys. Journ., 428:713–728, 1994.
- [40] H. KOGELNIK and T. LI: *Laser Beams and Resonators*. Appl. Opt., 5:1550–1567, 1965.
- [41] K. KÖTTER: *Aktive seismische Isolation eines Experiments zum Standardquantenlimit der Interferometrie*. Diplomarbeit, 1999.
- [42] K. KURODA, M. OHASHI, S. MIYOKI, D. TATSUMI, S. SATO, H. ISHIZUKA, M. K. FUJIMOTO, S. SEIJI, R. TAKAHASHI, T. YAMAZAKI, K. ARAI, M. FUKUSHIMA, K. WASEDA, S. TELADA, A. UEDA, T. SHINTOMI, A. YAMAMOTO, T. SUZUKI, Y. SAITO, T. HARUYAMA, N. SATO, K. TSUBONO, K. KAWABE, M. ANDO, K. I. UEDA, H. YONEDA, M. MUSHA, N. MIO, S. MORIWAKI, A. ARAYA, N. KANDA and M. E. TOBAR: *Large-scale cryogenic gravitational wave telescope*. Int. Journ. Mod. Phys. D, 8:557 – 579, 1999.
- [43] P. LEBEDEV: *Untersuchungen über die Druckkräfte des Lichtes*. An. d. Phys., 4:433–458, 1901.
- [44] J. E. LOGAN, J. HOUGH and N. A. ROBERTSON: *Aspects of the thermal motion of a mass suspended as a pendulum by wires*. Phys. Lett. A, 183:145–152, 1993.
- [45] E. MAJORA and Y. OGAWA: *Mechanical thermal noise in coupled oscillators*. Phys. Lett. A, 233:162–168, 1997.
- [46] E. MORRISON, B. MEERS, D. ROBERTSON and H. WARD: *Automatic alignment of optical interferometers*. Appl. Opt., 33:5041–5049, 1994.
- [47] M. MUSHA, S. TELADA, K. NAKAGAWA, M. OHASHI and K. UEDA: *Measurement of frequency noise spectra of frequency-stabilized LD-pumped Nd:Yag laser by using a cavity with separately suspended mirrors*. Opt. Comm., 140:323 – 330, 1997.
- [48] K. NAKAGAWA, A. S. SHELKOVNIKOV, T. KATSUDA and M. OHTSU: *Fast frequency stabilization of a diode-laser-pumped monolithic Nd:YAG laser with an extra-cavity electro-optic modulator*. Opt. Comm., 109:446–450, 1994.
- [49] E. NICHOLS and P. HULL: *A preliminary communication on the pressure of heat and light radiation*. Phys. Rev., 13:307–320, 1901.
- [50] K. NUMATA: *Direct measurement of mirror thermal noise*. Ph.D. thesis, 2002.
- [51] M. OHASHI, K. KURODA, S. MIYOKI, T. UCHIYAMA, K. YAMAMOTO, K. KASAHARA, T. SHINTOMI, A. YAMAMOTO, T. HARUYAMA, Y. SAITO, Y. HIGASHI, T. SUZUKI, N. SATO, T. TOMARU, D. TATSUMI, S. TELADA, M. ANDO, A. ARAYA, S. TAKEMOTO,

-
- T. HIGASHI, H. MOMOSE, J. AKAMATSU and W. MORII: *Design and construction status of CLIO*. *Class. Quant. Grav.*, 20:599–607, 2003.
- [52] N. OHISHI, S. OTSUKA, K. KAWABE and K. TSUBONO: *Estimation of thermal noise by a direct measurement of the mechanical conductance*. *Phys. Lett. A*, 266:228–233, 2000.
- [53] S. D. PENN, G. M. HARRY, A. M. GRETARSSON, S. E. KITTELBERGER, P. R. SAULSON, J. J. SCHILLER, J. R. SMITH and S. O. SWORDS: *High quality factor measured in fused silica*. *Rev. Sci. Inst.*, 72:3670–3673, 2001.
- [54] S. D. PENN, P. H. SNEDDON, H. ARMANDULA, J. C. BETZWIESER, G. CAGNOLI, J. CAMP, D. R. M. CROOKS, M. M. FEJER, A. M. GRETARSSON, G. M. HARRY, J. HOUGH, S. E. KITTELBERGER, M. J. MORTONSON, R. ROUTE, S. ROWAN and C. C. VASSILIOU: *Mechanical loss in tantala/silica dielectric mirror coatings*. *Class. Quant. Grav.*, 20:2917–2928, 2003.
- [55] M. V. PLISSI, C. I. TORRIE, M. E. HUSMAN, N. A. ROBERTSON, K. A. STRAIN, H. WARD, H. LÜCK and J. HOUGH: *GEO 600 triple pendulum suspension system: Seismic isolation and control*. *Rev. Sci. Inst.*, 71:2539 – 2545, 2000.
- [56] G. A. PRODI ET AL.: *Initial operation of the international gravitational event collaboration*. *Int. Journ. Mod. Phys. D*, 9:237–245, 2000.
- [57] L. RIBICHINI, V. LEONHARDT, H. LÜCK and K. DANZMANN: *An algorithm to compute the transfer function of a mechanical system*. submitted to *Class. Quant. Grav.*
- [58] S. ROWAN, G. CAGNOLI, P. SNEDDON, J. HOUGH, R. ROUTE, E. K. GUSTAFSON, M. M. FEJER and V. MITROFANOV: *Investigation of mechanical loss factors of some candidate materials for the test masses of gravitational wave detectors*. *Phys. Lett. A*, 265:5–11, 2000.
- [59] S. ROWAN, R. HUTCHINS, A. MCLAREN, N. A. ROBERTSON, S. M. TWYFORD and J. HOUGH: *The quality factor of natural fused quartz ribbons over a frequency range from 6 to 600 Hz*. *Phys. Lett. A*, 227:153–158, 1997.
- [60] A. RÜDIGER, R. SCHILLING, L. SCHNUPP, W. WINKLER, H. BILLING and K. MAISCHBERGER: *A mode selector to suppress fluctuations in laser beam geometry*. *Optica Acta*, 28:641–658, 1981.
- [61] P. R. SAULSEN: *Thermal noise in mechanical experiments*. *Phys. Rev. D*, 42:2437–2445, 1990.
- [62] P. R. SAULSON: *Fundamentals of interferometric gravitational wave detectors*. World Scientific Publishing, 1994.
- [63] P. S. SHAWHAN: *The search for gravitational waves with LIGO: Status and plans*. *Int. Journ. Mod. Phys. A*, 16:1028–1030, 2001.

- [64] J. R. SMITH, G. M. HARRY, J. C. BETZWIESER, A. M. GRETARSSON, D. A. GUILD, S. E. KITTELBERGER, M. J. MORTONSON, S. D. PENN and P. R. SAULSON: *Mechanical loss associated with silicate bonding of fused silica*. *Class. Quant. Grav.*, 20:5039–5047, 2003.
- [65] TAMA COLLABORATION: *Stable operation of a 300-m laser interferometer with sufficient sensitivity to detect gravitational-wave events within our galaxy*. *Phys. Rev. Lett.*, 86:3950–3954, 2001.
- [66] J. H. TAYLOR: *Binary pulsars and relativistic gravity*. *Rev. Mod. Phys.*, 66:711–719, 1994.
- [67] M. TINTO: *The Cassini Ka-band gravitational wave experiments*. *Class. Quant. Grav.*, 19:1767–1773, 2002.
- [68] C. I. E. TORRIE: *Development of suspensions for the GEO 600 gravitational wave detector*. Ph.D. thesis, 2000.
- [69] S. TRÄGER: *Thermisches Rauschen - Eine Empfindlichkeitsgrenze der Interferometrie*. Doktorarbeit, 1998.
- [70] A. VICERÈ: *Introduction to the mechanical simulation of seismic isolation systems*. *Experimental Physics of gravitational waves*, World Scientific, 349 - 378, 2000.
- [71] VIRGO COLLABORATION: *The present status of the VIRGO central interferometer*. *Class. Quant. Grav.*, 19:1421–1428, 2002.
- [72] J. WEBER: *Observations of the thermal fluctuations of a gravitational-wave detector*. *Phys. Rev. Lett.*, 17:1228–1230, 1966.
- [73] P. WILLEMS, C. LAMB, A. HEPTONSTALL and J. HOUGH: *Search for stress dependence in the internal friction of fused silica*. submitted to *Phys. Lett. A*.
- [74] P. WILLEMS, V. SANNIBALE, J. WEEL and V. MITROFANOV: *Investigations of the dynamics and mechanical dissipations of a fused silica suspension*. *Phys. Lett. A*, 297:37–48, 2002.
- [75] B. WILLKE, S. BROZEK, K. DANZMANN, V. QUETSCHKE and S. GOSSLER: *Frequency stabilization of a monolithic Nd:Yag ring laser by controlling the power of the laser-diode pump source*. *Opt. Lett.*, 25:1019 – 1021, 2000.
- [76] B. WILLKE ET AL.: *The Geo 600 gravitational wave detector*. *Class. Quantum Grav.*, 19:1377–1387, 2002.
- [77] K. YAMAMOTO, S. OTSUKA, M. ANDO, K. KAWABE and K. TSUBONO: *Experimental study of thermal noise caused by an inhomogeneously distributed loss*. *Phys. Lett. A*, 280:289–296, 2001.
- [78] C. ZENER: *Internal friction in solids*. *Phys. Rev.*, 53:90–105, 1938.

Acknowledgements

The search for gravitational waves is certainly one of the most interesting topics in physics today, and only very few scientist are so fortunate to work in such an exciting field. I have to thank Prof. Dr. Karsten Danzmann for giving me the opportunity to work in this field and for providing much help and scientific input whenever it was needed. I will also always remember his ability to create a positive working atmosphere at the institute and to allow young scientists to look beyond the walls of their own laboratory and to participate in a truly international field of research.

Different supervisors have guided me during my experimental work and have provided much help and creative input. I want to mention Stefan Träger, who first introduced me to the task of thermal noise interferometry and helped me in the beginning. It was very nice to work with Patrick Klövekorn, who not only provided a lot of advise, but also created a good atmosphere in the laboratory. I also want to thank Harald Lück, who encouraged me during many discussions and helped me with many problems.

Benno Willke never lost interest in the progress of the experiment and the student meetings under his supervision have been very constructive and sometimes forced me to address problems that otherwise would have been overlooked. It was always possible to ask Gerhard Heinzl for help, and his input was most welcome and directly advanced the progress of the experimental work. In the beginning, a lot of advise also came from Sascha Brozek.

At first I worked with Karsten Kötter, who also accompanied me during my university time, and the experiment was joined later by Uta Weiland. It was nice to have worked with both of them. I have spent a lot of time in the laboratory with Luciano Ribichini and we never seemed to have stopped with our discussions. The progress of the experiment has benefited a lot from his participation.

I enjoyed sharing my office with Mario Müller and later with Stefan Gossler. Michèle Heurs, Volker Quetschke and Michaela Malec should also be mentioned, as well as Hartmut Grote, who played volleyball with me. To all of them I could turn for help and advice.

I thank Harald Lück, Luciano Ribichini, Siong Heng, Gerhard Heinzl and Joshua Smith for proof-reading parts of this thesis.

I also want to thank my parents who always supported and helped me.

This work was supported by the Deutsche Forschungsgemeinschaft within the Sonderforschungsbereich 407.



Curriculum vitae

Volker Leonhardt
Henzeweg 5
30455 Hannover

Born on February 14., 1974 in Hannover, Germany
Marital status: not married, no children

- 01. 2000 - to date Doctoral studies in physics and scientific assistent, Max-Planck-Institute for Gravitational Physics (Albert-Einstein-Institute) and University of Hannover (SFB 407)
- 09 1999 Physik-Diplom, University of Hannover
- 10 1994 - 09 1999 Diploma studies in physics, University of Hannover
- 07 1993 - 06 1994 Compulsory military service, 2. Nachschubbatallion 1
- 06 1993 Abitur, Gymnasium Lutherschule
- 08 1986 - 06 1993 Gymnasium Lutherschule
- 08 1984 - 07 1986 Orientierungsstufe Entenfangweg
- 08 1980 - 07 1984 Grundschule Vinnhorst

Publications

V. Leonhardt: *Aufbau eines Interferometers zur quantenlimitierten Längenmessung*, Diplomarbeit, Universität Hannover, (1999)

V. Leonhardt, L. Ribichini, P. Kloevekorn, B. Willke, H. Lueck and K. Danzmann: *Towards measuring the off-resonant thermal noise of a pendulum mirror*, *Class. Quantum Grav.* 19, 1717 - 1721, (2002)

V. Leonhardt, L. Ribichini, H. Lueck and K. Danzmann: *The Hannover thermal noise experiment*, accepted by *Class. Quant. Grav.*

B. Willke, P. Aufmuth, C. Aulbert, S. Babak, R. Balasubramanian, B. W. Barr, S. Berukoff, S. Bose, G. Cagnoli, M. M. Casey, D. Churches, D. Clubley, C. N. Colacino, D. R. M. Crooks, C. Cutler, K. Danzmann, R. Davies, R. Dupuis, E. Elliffe, C. Fallnich, A. Freise, S. Gossler, A. Grant, H. Grote, G. Heinzel, A. Heptonstall, M. Heurs, M. Hewitson, J. Hough, O. Jenrich, K. Kawabe, K. Koetter, V. Leonhardt, H. Lueck, M. Malec, P. W. McNamara, S. A. McIntosh, K. Mossavi, S. Mohanty, S. Mukherjee, S. Nagano, G. P. Newton, B. J. Owen, D. Palmer, M. A. Papa, M. V. Plissi, V. Quetschke, D. I. Robertson, N. A. Robertson, S. Rowan, A. Ruediger, B. S. Sathyaprakash, R. Schilling, B. F. Schutz, R. Senior, A. M. Sintes, K. D. Skeldon, P. Sneddon, F. Stief, K. A. Strain, I. Taylor, C. I. Torrie, A. Vecchio, H. Ward, U. Weiland, H. Welling, P. Williams, W. Winkler, G. Woan, and I. Zawischa: *The Geo 600 gravitational wave detector*, *Class. Quantum Grav.* 19, 1377 - 1387, (2002)

J. Hough, P. Aufmuth, R. Balasubramanian, B. W. Barr, O. S. Brozec, G. Cagnoli, M. Casey, E. Chassande-Mottin, D. Churches, D. Clubley, D. R. M. Crooks, C. Cutler, K. Danzmann, C. Fallnich, A. Freise, S. Gossler, A. Grado, A. Grant, H. Grote, M. Husman, K. Kawabe, M. Kirchner, P. Kloevekorn, K. Koetter, V. Leonhardt, H. Lueck, P. W. McNamara, S. A. McIntosh, K. Mossavi, S. Nagano, G. P. Newton, B. J. Owen, D. Palmer, M. A. Papa, M. Peterseim, M. V. Plissi, V. Quetschke, D. I. Robertson, N. A. Robertson, S. Rowan, A. Ruediger, B. S. Sathyaprakash, R. Schilling, B. F. Schutz, A. M. Sintes, K. D. Skeldon, P. Sneddon, K. A. Strain, I. Taylor, C. I. Torrie, A. Vecchio, H. Ward, A. Weidner, H. Welling, P. Williams, B. Willke, W. Winkler, I. Zawischa: *GEO 600 – research, progress and prospects*, World Scientific (Proceedings of the Ninth Marcel Grossmann Meeting on General Relativity), 1843 - 1844, (2002)

B. Willke, P. Aufmuth, C. Aulbert, S. Babak, R. Balasubramanian, B. W. Barr, S. Berukoff, S. Bose, G. Cagnoli, M. M. Casey, D. Churches, C. N. Colacino, D. R. Crooks, C. Cutler, K. Danzmann, R. Davies, R. Dupuis, E. Elliffe, C. Fallnich, A. Freise, S. Gossler, A. Grant, H. Grote, J. Harms, G. Heinzel, S. Herden, A. Hepstonstall, M. Heurs, M. Hewitson, J. Hough, O. Jennrich, K. Kawabe, K. Koetter, V. Leonhardt, H. Lueck, M. Malec, P. McNamara, Kasem Mossavi, S. Mohanty, S. Mukherjee, S. Nagano, G. P. Newton, B. J. Owen, M. A. Papa, M. V. Plissi, V. Quetschke, L. Ribichini, D. I. Robertson, N. A. Robertson, S. Rowan, A. Ruediger, B. S. Sathyaprakash, R. Schilling, B. F. Schutz, F. Seifert, A. M. Sintes, K. D. Skeldon, P. Sneddon, K. A. Strain, I. Taylor, C. I. Torrie, A. Vecchio, H. Ward, U. Weiland, H. Welling, P. Williams, W. Winkler, G. Woan, I. Zawischa: *Status of the GEO 600 gravitational wave detector*, Proc. SPIE 4856 (Gravitational-Wave Detection), 238-246, (2003)

S. Gossler, M. M. Casey, A. Freise, A. Grant, H. Grote, G. Heinzel, M. Heurs, M. E. Husman, K. Koetter, V. Leonhardt, H. Lueck, M. Malec, K. Mossavi, S. Nagano, P. W. McNamara, M. V. Plissi, V. Quetschke, D. I. Robertson, N. A. Robertson, A. Ruediger, R. Schilling, K. D. Skeldon, K. A. Strain, C. I. Torrie, H. Ward, U. Weiland, B. Willke, W. Winkler, J. Hough and K. Danzmann: *Mode-cleaning and injection optics of the gravitational-wave detector GEO600*, Rev. Sci. Inst. 74, 3787 - 3795, (2003)

M. Hewitson, P. Aufmuth, C. Aulbert, S. Babak, R. Balasubramanian, B. W. Barr, S. Berukoff, G. Cagnoli, C. A. Cantley, M. M. Casey, S. Chelkowski, D. Churches, C. N. Colacino, D. R. M. Crooks, C. Cutler, K. Danzmann, R. Davies, R. Dupuis, E. Elliffe, C. Fallnich, A. Freise, S. Gossler, A. Grant, H. Grote, S. Grunewald, J. Harms, G. Heinzel, S. Heng, A. Heptonstall, M. Heurs, J. Hough, Y. Itoh, O. Jennrich, R. Jones, S. Hutter, K. Kawabe, C. Killow, K. Koetter, K. Krishnan, V. Leonhardt, H. Lueck, B. Machenschalk, M. Malec, K. Mossavi, S. Mohanty, S. Mukherjee, S. Nagano, G. P. Newton, M. A. Papa, M. Perreur-Lloyd, M. Pitkin, M. V. Plissi, V. Quetschke, S. Reid, L. Ribichini, D. I. Robertson, N. A. Robertson, S. Rowan, A. Ruediger, B. S. Sathyaprakash, R. Schilling, R. Schnabel, B. F. Schutz, F. Seifert, A. M. Sintes, J. Smith, P. Sneddon, K. A. Strain, I. Taylor, C. I. Torrie, A. Vecchio, H. Ward, U. Weiland, H. Welling, P. Williams, B. Willke, W. Winkler, G. Woan, and I. Zawischa: *A report on the status of the GEO 600 gravitational wave detector*, Class. Quantum Grav. 20, 581 - 591, (2003)

A. M. Sintes, P. Aufmuth, C. Aulbert, S. Babak, R. Balasubramanian, B. W. Barr, S. Berukoff, S. Borger, G. Cagnoli, C. A. Cantley, M. M. Casey, S. Chelkowski, D. Churches, C. N. Colacino, D. R. M. Crooks, C. Cutler, K. Danzmann, R. Davies, R. Dupuis, E. Elliffe, C. Fallnich, A. Freise, S. Gossler, A. Grant, H. Grote, S. Grunewald, J. Harms, G. Heinzel, S. Heng, A. Heptonstall, M. Heurs, M. Hewitson, J. Hough, R. Ingley, Y. Itoh, O. Jennrich, R. Jones, S. Hutter, K. Kawabe, C. Killow, K. Koetter, K. Krishnan, V. Leonhardt, H. Lueck, B. Machenschalk, M. Malec, C. Messenger, K. Mossavi, S. Mohanty, S. Mukherjee, S. Nagano, G. P. Newton, M. A. Papa, M. Perreur-Lloyd, M. Pitkin, M. V. Plissi, V. Quetschke, S. Reid, L. Ribichini, D. I. Robertson, N. A. Robertson, S. Rowan, A. Ruediger, B. S. Sathyaprakash, R. Schilling, R. Schnabel, B. F. Schutz, F. Seifert, J. Smith, P. Sneddon, K. A. Strain, I. Taylor, C. I. Torrie, A. Vecchio, H. Ward, U. Weiland, H. Welling, P. Williams, B. Willke, W. Winkler, G. Woan, and

I. Zawischa: *Detector characterization in GEO 600*, Class. Quantum Grav. 20, 731 - 739, (2003)

G. Woan, P. Aufmuth, C. Aulbert, S. Babak, R. Balasubramanian, B.W. Barr, S. Berukoff, S. Bose, G. Cagnoli, M. Casey, D. Churches, C.N. Colacino, D.R.M. Crooks, C. Cutler, K. Danzmann, R. Davis, R.J. Dupuis, E. Elliffe, C. Fallnich, A. Freise, S. Goßler, A. Grant, H. Grote, G. Heinzl, A. Hepstonstall, M. Heurs, M. Hewitson, J. Hough, O. Jennrich, K. Kawabe, K. Koetter, V. Leonhardt, H. Lueck, M. Malec, P. McNamara, K. Mossavi, S. Mohanty, S. Mukherjee, S. Nagano, G.P. Newton, B.J. Owen, M.A. Papa, M.V. Plissi, V. Quetschke, D.I. Robertson, N.A. Robertson, S. Rowan, A. Ruediger, B.S. Sathyaprakash, R. Schilling, B.F. Schutz, R. Senior, A.M. Sintes, K.D. Skeldon, P. Sneddon, F. Stief, K.A. Strain, I. Taylor, C.I. Torrie, A. Vecchio, H. Ward, U. Weiland, H. Welling, P. Williams, W. Winkler, B. Willke, I. Zawischa: *The GEO 600 gravitational wave detector – pulsar prospects*, ASP Conference Series CS-302, (2003)

L. Ribichini, V. Leonhardt, H. Lueck and K. Danzmann: *An algorithm to compute the transfer function of a mechanical system*, submitted to Class. Quant. Grav.

The LIGO Scientific Collaboration: *Setting upper limits on the strength of periodic gravitational waves using the first science data from the GEO600 and LIGO detectors*, to be published

The LIGO Scientific Collaboration: *Analysis of LIGO data for gravitational waves from binary neutron stars*, to be published

The LIGO Scientific Collaboration: *Detector Description and Performance for the First Coincidence Observations between LIGO and GEO*, to be published

